2019

Characterization And Perturbation Of Functional Networks That Support Human Memory

Ethan Andrew Solomon
University of Pennsylvania, esolomon15@gmail.com

Characterization And Perturbation Of Functional Networks That Support Human Memory

Abstract
Episodic memory is essential to our daily lives, as it attaches meaning to the constant stream of sensory inputs to the brain. However, episodic memory often fails in a number of common neurocognitive disorders. Effective therapies remain elusive, owing to the complexity of brain networks and neural processes that support episodic encoding and retrieval. In particular, it is not understood how inter-regional communication within the brain supports memory function, though such communication may be critical to the highly integrative nature of episodic memory. To uncover the patterns of memory-related functional connectivity, we asked a large cohort of neurosurgical patients with indwelling electrodes to perform a verbal free-recall task, in which patients viewed lists of simple nouns and recalled them a short time later. As patients performed this task, we collected intracranial EEG (iEEG) from electrodes placed on the cortical surface and within the medial temporal lobe (MTL). First, we examined whole-brain functional networks that emerged during the encoding and retrieval phases of this task, using spectral methods to correlate frequency-specific signals between brain regions. We identified a dynamic network of regions that exhibited enhanced theta (3-8 Hz) connectivity during successful memory processing, whereas regions tended to desynchronize at high frequencies (30-100 Hz). Next, using only electrodes placed within the MTL, we asked whether functional coupling was also observed among this mesoscale subnetwork of highly specialized regions that play an outsize role in memory. Recapitulating our earlier findings, we noted broadly enhanced theta connectivity within the MTL, centering on the left entorhinal cortex during successful encoding operations. Finally, to determine whether such low-frequency functional connections reflect correlative or causal relations in the brain, we applied direct electrical stimulation via electrodes placed within the MTL. We found that low-frequency connections (5-13 Hz) predicted the emergence of theta activity at distant regions in the brain – particularly when stimulation occurred near white matter – indicating the potential causal relevance of iEEG-based functional connections. Taken together, these studies underscore the importance of low-frequency functional coupling to memory across spatial scales, and suggest this form of coupling indicates a causal relation between brain regions.

Degree Type
Dissertation

Degree Name
Doctor of Philosophy (PhD)

Graduate Group
Bioengineering

First Advisor
Michael J. Kahana

Keywords
hippocampus, iEEG, memory, networks, oscillations

CHARACTERIZATION AND PERTURBATION OF FUNCTIONAL NETWORKS

THAT SUPPORT HUMAN MEMORY

Ethan A. Solomon

A DISSERTATION

in

Bioengineering

Presented to the Faculties of the University of Pennsylvania

in

Partial Fulfillment of the Requirements for the

Degree of Doctor of Philosophy

2019

Supervisor of Dissertation	**Graduate Group Chairperson**
_____	_____
Michael J. Kahana Professor, Psychology	Ravi Radhakrishnan Professor, Bioengineering

Dissertation Committee

Danielle S. Bassett, Eduardo D. Glandt Faculty Fellow and Associate Professor of Bioengineering

Lyle H. Ungar, Professor of Computer and Information Science

Geoffrey K. Aguirre, Associate Professor of Neurology

To the patients who selflessly volunteered to participate
in the studies that made this work possible.

Acknowledgements

There is a very long list of people I have to thank for making my PhD possible. The work in these pages would not have happened without – literally – dozens of people from my personal and professional lives, and they each deserve my deep gratitude (and credit!).

First, I want to thank my mentor, Michael Kahana, for building a lab that I was privileged to be a part of. Mike has spent years creating a fantastic research enterprise, with a laser-like focus on statistical rigor and prolific – yet careful – data collection. His efforts have paid off. There is no place else in the world where I could have been equally as immersed in the electrophysiology of human memory, a subject of which I knew little when I first joined the lab in 2015. Under Mike's mentorship, I published my first manuscript. I attended and presented at conferences around the world. I learned to write grants. And, of course, I learned a lot about how little we understand episodic memory. I think I still don't quite grasp how tirelessly Mike has worked to create an environment where all this is possible. For those efforts, and for his mentorship over the past few years (and hopefully many more to come), he has my sincere thanks.

"It takes a village" might not be a mantra that wins elections, but it certainly makes for successful DARPA grants. I have so many DARPA RAM colleagues and friends to thank for their incredibly hard work over the past four years: Paul Wanda, the best all-in-one scientist/research coordinator/clinical tester/neuroimager/grant writer anyone could ever ask for; Youssef Ezzyat and Jim Kragel, the extraordinary postdocs who showed me the ropes and wrote papers with me; Maciek Swat, Zach Duey, Mike DePalatis, Leon Davis, Stas Busygin, and Henry Solberg, the programmers who debugged stuff so I didn't have to;

Zeinab Helili and Alison Xu, the amazing researchers/clinical site testers; and Dan Rizzuto, who is now trying to turn our research into something people can actually use.

I've been told that Prof. Christoph Weidemann was part of the DARPA RAM project, but I never had the pleasure of seeing him at the biweekly calls. Strange – must have been the days I wasn't there. Regardless, he deserves my deep gratitude for providing wonderful mentorship and friendship since I first joined the lab. Though he's now back in the UK, I'll always remember him, because he left one of his suitcases in my basement.

As the lab moves into a post-DAPRA world, I have even more fantastic scientists to thank for keeping me on my toes, challenging me at lab meetings, and being great friends. I've become a better scientist just by sitting in close spatial proximity to Senior Member of the Main Lab Nora Herweg, and I'm excited to collaborate with her on a number of surely-groundbreaking ideas. My co-graduate students and good friends Rivka Cohen, Logan Fickling, Dan Schonhaut, and Ada Aka have been incredibly supportive and kind, and make for stellar lab meeting questioners. The same goes for Jesse Pazdera and Effie Li, who are also my co-graduate students, as far as I'm concerned. Nicole Kratz and Deb Gaspari are the lab's unsung heroes, making sure the trains run on time, day-in, day-out. All of these people are the reason I never really want to work from home, even if I can.

I also want to acknowledge the wonderful support from the MD/PhD program, particularly Maggie Krall and Skip Brass. They truly run the Best MSTP in the Galaxy®.

Finally, I want to thank my family, for encouraging my interest in science and medicine from a young age. I am confident that I would not be writing these words without their constant love and support. And to Hannah, who even between night shifts in the PICU somehow summoned the will to listen thoughtfully to my practice presentations on theta synchronization in the medial temporal lobe. I don't know how you do it.

ABSTRACT

CHARACTERIZATION AND PERTURBATION OF FUNCTIONAL NETWORKS THAT SUPPORT HUMAN MEMORY

Ethan A. Solomon

Michael J. Kahana

Episodic memory is essential to our daily lives, as it attaches meaning to the constant stream of sensory inputs to the brain. However, episodic memory often fails in a number of common neurocognitive disorders. Effective therapies remain elusive, owing to the complexity of brain networks and neural processes that support episodic encoding and retrieval. In particular, it is not understood how inter-regional communication within the brain supports memory function, though such communication may be critical to the highly integrative nature of episodic memory. To uncover the patterns of memory-related functional connectivity, we asked a large cohort of neurosurgical patients with indwelling electrodes to perform a verbal free-recall task, in which patients viewed lists of simple nouns and recalled them a short time later. As patients performed this task, we collected intracranial EEG (iEEG) from electrodes placed on the cortical surface and within the medial temporal lobe (MTL). First, we examined whole-brain functional networks that emerged during the encoding and retrieval phases of this task, using spectral methods to correlate frequency-specific signals between brain regions. We identified a dynamic network of regions that exhibited enhanced theta (3-8 Hz) connectivity during successful memory

processing, whereas regions tended to desynchronize at high frequencies (30-100 Hz). Next, using only electrodes placed within the MTL, we asked whether functional coupling was also observed among this mesoscale subnetwork of highly specialized regions that play an outsize role in memory. Recapitulating our earlier findings, we noted broadly enhanced theta connectivity within the MTL, centering on the left entorhinal cortex during successful encoding operations. Finally, to determine whether such low-frequency functional connections reflect correlative or causal relations in the brain, we applied direct electrical stimulation via electrodes placed within the MTL. We found that low-frequency connections (5-13 Hz) predicted the emergence of theta activity at distant regions in the brain – particularly when stimulation occurred near white matter – indicating the potential causal relevance of iEEG-based functional connections. Taken together, these studies underscore the importance of low-frequency functional coupling to memory across spatial scales, and suggest this form of coupling indicates a causal relation between brain regions.

Table of Contents

List of Tables

List of Illustrations

Chapter 1:

Introduction

Memory is an ever-present facet of our daily experience. It allows us to effortlessly tune our behaviors to the situation at hand – seeing a labmate's face, for example, releases a flood of associated information: what this person's name is, your prior interactions with them, and whether you should congratulate them on their recently-completed thesis. Memory attaches rich meaning to the stream of sensory information we encounter in every moment of our lives. It is hard to imagine what life would be like without memory entirely, though we know that even the first hints of normal, age-related decline in memory function can be deeply unsettling.

As central as it is to our lives, we do not know how the brain gives rise to human episodic memory. Behavioral assays of memory – starting in earnest more than 125 years ago – have described key features of how we learn and forget, but do not offer a mechanism for how memories are formed and retrieved in the brain. Clinical case studies, neuroimaging, and invasive neurosurgical recordings have begun to unravel that mystery by isolating particular brain structures that exhibit enhanced activity during memory operations. To be sure, we can now confidently declare that regions of the medial temporal lobe (MTL) play a key role in episodic memory[1], but the precise manner in which these structures encode information, and how they communicate with the rest of the brain, remains unanswered.

Understanding memory is not simply a matter of scientific curiosity. Diseases of memory and cognition are among the most devastating for patients and their families, but the

complex neural circuitry that gives rise to these processes pose a serious challenge to effective therapeutic interventions. Nearly 6 million Americans live with memory loss associated with Alzheimer's dementia, including 10% of those over the age of 65. The burden of dementia worldwide stands at 50 million people[2]. Worse yet, there are no effective therapies to restore memory function.

Increasingly, clinicians and scientists have turned to brain stimulation as a tool to better understand – and hopefully improve – human memory[3]. Stimulation techniques come in several forms, but all rely on the general idea that electrical perturbations of brain activity can alter cognition and behavior[4]. Is it possible that stimulation in the right part of the brain, at the right time, can restore the normal operation of dysfunctional memory circuits? Developing such an approach depends on answering two fundamental questions: (1) What is the normal pattern of neural activity that supports episodic memory, and (2) What changes in neural activity are induced by electrical stimulation?

To fully answer these questions, it is insufficient to only characterize where in the brain we observe memory-related activity. Memory involves the integration of information across widespread cortical areas, necessitating rapid, complex patterns of inter-regional communication between brain structures[5]. Functional magnetic resonance imaging (fMRI) has been used to study memory networks in the human brain[6–10], but this method lacks the high temporal resolution necessary to track rapid fluctuations in neural activity that accompany memory formation and retrieval. Intracranial electroencephalography (iEEG), recorded from neurosurgical patients with drug-resistant epilepsy, affords high spatial and temporal resolution and is ideally suited to examine the detailed structure of electrical networks that engage during memory encoding and retrieval[11].

The goal of this dissertation is to characterize the meso- and macro-scale brain networks that support human memory, and to use intracranial stimulation techniques to assess the interaction between exogenous stimulation events and endogenous networks. This was accomplished in the course of three core investigations, all based on assessments of iEEG collected from large cohorts of human neurosurgical patients. This dissertation is organized around these investigations, as follows:

Chapter 2 covers relevant background material, including foundational principles of human memory, EEG recording and analysis, fundamentals of network neuroscience, and a review of recent work in intracranial brain stimulation.

Chapter 3 cover our work to extract memory-related iEEG networks across the whole brain. Here, we ask whether functional connectivity in particular frequency bands, namely theta and gamma, best correlates with memory performance, and whether such networks exhibit structure that varies over time and space. We identified a widespread dynamic network of enhanced theta activity underlying successful episodic encoding and retrieval operations.

Chapter 4 extends the work in Chapter 3 by asking whether low-frequency networks are also observable in the mesoscale. Specifically, we assayed memory-related functional connectivity between subregions of the hippocampus and medial temporal lobe. We found that, during encoding, time-varying theta connectivity centers on the left entorhinal cortex, but this network substantially reorganizes during retrieval.

Chapter 5 describes our efforts to understand how electrical stimulation events may propagate through functional networks, and whether stimulation events have differential effects depending on the network topology of a stimulated node. We confirmed that low-frequency functional connections predict the propagation of stimulation events in the MTL.

Finally, in **Chapter 6** we provide a summary of the thesis work and discuss key open questions in network neuroscience and human memory.

Major Contributions

The major contributions of this work are:

1. Characterizing the whole-brain networks of electrical activity that underlie successful episodic memory encoding and retrieval; determining the most prominent frequency band in which inter-regional connectivity is observed, and describing the spatiotemporal structure of such networks.

2. Describing the functional connectivity networks within the medial temporal lobe; asking whether mesoscale networks between nearby brain regions recapitulate network principles from the whole-brain.

3. Understanding the perturbation of functional networks with intracranial electrical stimulation; asking whether patterns of functional connectivity explain the propagation of stimulation events throughout the brain, and characterizing the patterns of evoked activity in regions distant to the stimulation site.

Chapter 2:
Background

Principles of Human Episodic Memory

"Episodic" memory refers specifically to the ability to recall information about past experiences, and it will be the focus of most of the investigations presented here. Episodic memory has been systematically studied for over 125 years. In the late 19th century, Hermann Ebbinghaus famously conducted memorization studies on himself, characterizing the rate at which he could learn and forget lists of random syllables[12]. The powerful notion at the root of his work – and virtually all subsequent studies until the modern day – was that episodic memory relies on *associations* between stored items. The associative nature of memory is salient in our everyday lives; being in a particular place, seeing an old friend, or smelling a favorite food tends to bring forth information of related events or people. More broadly, we now conceptualize memory as a process that links new information – *content* – with a prevailing *context*, or the combined experience of ambient sensory inputs and internal mental states[13].

Most behavioral research into human episodic memory is essentially an elaborate exercise to characterize how alterations in content or context affect our ability to store and retrieve information. Commonly, subjects will be presented with sequences of items to store in memory – often words or pictures. In *cued recall* paradigms, subjects are explicitly prompted to complete an item, given some component of it; for example, subjects may be

asked to remember pairs of words, and are cued with only one word from each pair. In *free recall* paradigms, subjects are simply asked to recall as many items as possible, in the absence of any explicit cues. Implicitly, however, subjects use two cues. First, the prevailing context, such as sitting in the same testing room where the items were originally learned, serves to spur the retrieval of those memories. Second, memories act as the cues themselves – recalling one prior word will tend to cue the recall of words experienced in close temporal proximity[14], much as reminiscing with old about high school prompts the spontaneous retrieval of childhood family memories (Figure 2.1).

The free recall paradigm is a particularly powerful tool to study human episodic memory. The method has high ecological validity; much of our everyday lives involve the spontaneous retrieval of past experiences or knowledge, cued by nothing more than the current collection of sensory inputs and internal mental states. Relatedly, the retrieval period in free recall constitutes an endogenous cognitive search process, guided by the way in which knowledge is inherently organized in the brain. It is conceivable that cued recall paradigms force subjects to adopt particular strategies that hinge on the presentation of an arbitrary cue stimulus. Conversely, free-recall gains real-world validity at the expense of experimental control – subjects may adopt any number of strategies to support successful encoding or retrieval, potentially reducing the ability to detect statistically consistent effects across subjects. Furthermore, the absence of an explicit cue stimulus during retrieval presents challenges to rigorously studying the neural substrates of retrieval events.

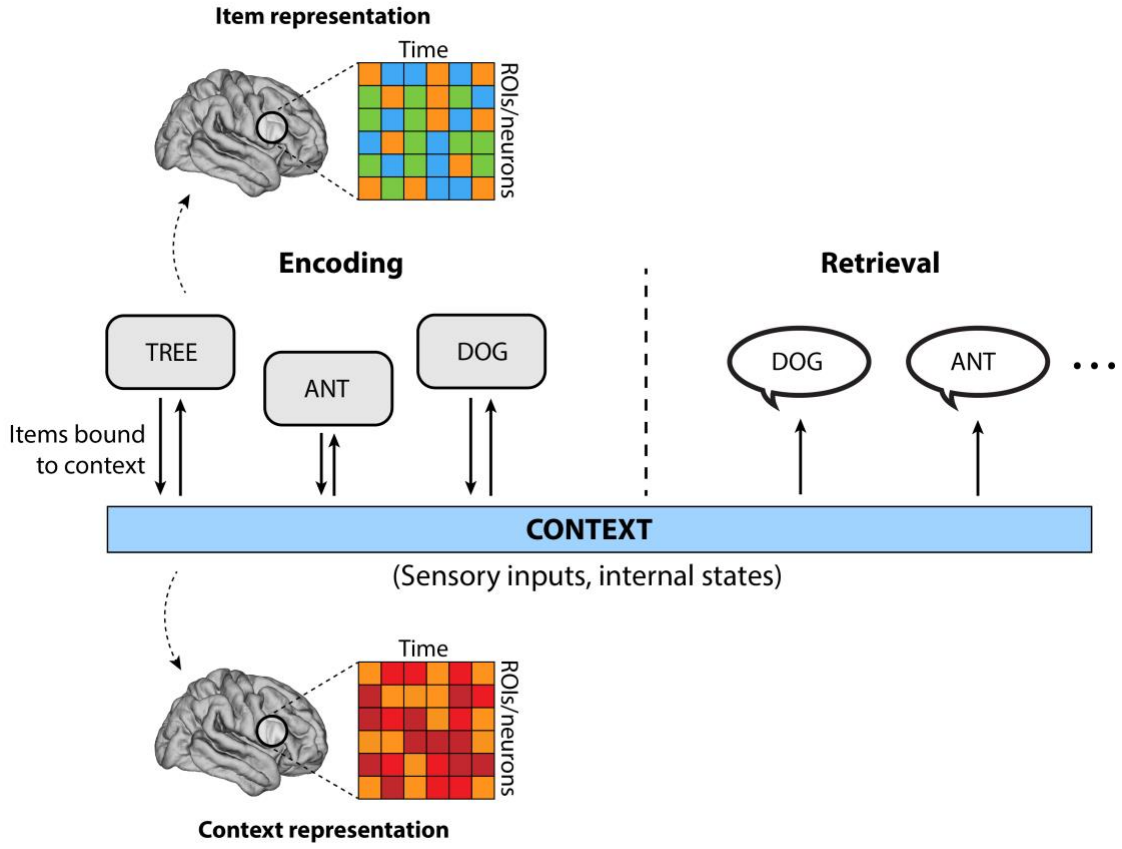

Figure 2.1. Processes of episodic memory encoding and retrieval. Episodic memory can be conceptualized as a linking of new items and the prevailing context. Context reflects the ongoing collection of sensory inputs and internal mental states that occur as new information (items) are encoded into memory. Drifting context forms the basis for later retrieval of past experiences. The cognitive neuroscience of memory seeks to understand the way in which items and context are neurally represented, and the underlying mechanisms that link the two.

Nonetheless, with an eye towards the eventual development of therapeutics to rescue episodic memory, free-recall is a useful episodic memory assay amenable to behavioral and neural observation and perturbation. We therefore relied on free-recall episodic memory for the bulk of the experiments conducted in completion of this dissertation. In particular, we used a verbal free-recall paradigm in which subjects were asked to remember lists of simple words and recall as many as possible after a brief arithmetic distractor task (Figure 2.2).

How can free recall be used to understand the fundamental mechanisms that give rise to human episodic memory? How exactly are associations formed between items and their contexts, and how do we engage those associations to accurately recall prior experiences?

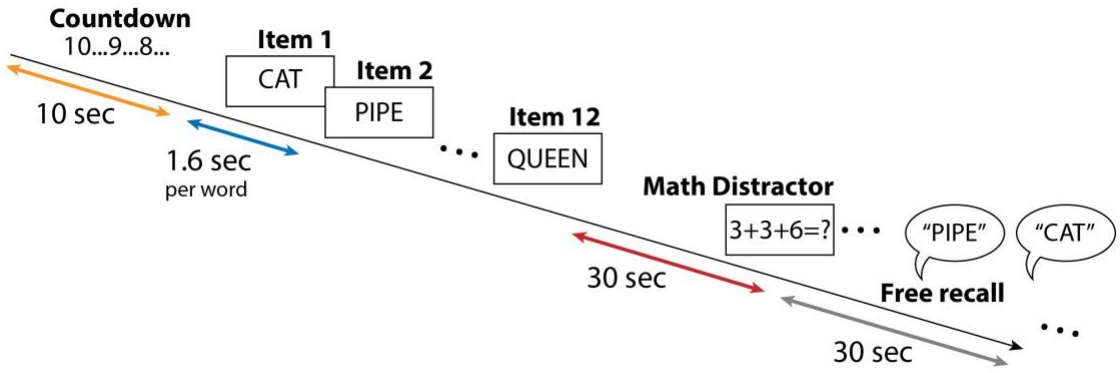

Figure 2.2. Verbal free recall task. In the verbal free recall task, subjects are instructed to remember 12-item lists of simple nouns, each presented successively on a computer screen. After a brief arithmetic distractor task, subjects are asked to freely recall as many words from the prior list as possible.

Recent theoretical and empirical work has combined notions of context-based episodic memory with insights from spatial navigation to conceptualize memory as an embedding of information in a "cognitive space."[15] This space, like physical space, places items with strong associations near each other, such as if two events occurred in a similar context. Items might also be closely associated – and therefore embedded closely in a cognitive space – via pre-existing knowledge like the semantic content of word items. Retrieval therefore constitutes an "exploration" of cognitive spaces, akin to the free exploration of a physical environment. Accordingly, it may be possible to predict behavioral patterns of retrieval events based on an understanding of how these cognitive spaces are constructed. The work described in this thesis establishes a set of neural features associated with verbal free-recall; future work should ask whether such features align across verbal and spatial tasks, to support the notion of a domain-general representational space in the brain.

Intracranial EEG

Noninvasive neuroimaging, in particular functional magnetic resonance imaging (fMRI), has been extensively used to understand the brain activity that correlates with behavior and cognition[8,16–18]. However, fMRI's poor temporal resolution limits its utility to tease apart neural mechanisms that support rapid computations occurring on millisecond timescales. Indwelling electrodes placed directly in brain tissue can capture activity at this timescale, reflecting electric field changes induced by the aggregated activity of thousands of neurons near the electrode[11,19]. This local field potential (LFP) can be safely recorded in human neurosurgical patients undergoing clinical monitoring for medication-resistant epilepsy. Patients are typically implanted with dozens or hundreds of such electrodes to help clinicians identify epileptogenic tissue for resection and eloquent areas to surgically avoid (Figure 2.3). During their hospital stay, patients are asked to participate in research studies and neural activity is recorded as subjects perform cognitive tasks (such as verbal free recall).

iEEG's superior temporal resolution revealed that – as was known from animal studies – human cognition is correlated with rhythmic fluctuations in the LFP, called *oscillations*[20,21]. Neural oscillations have been observed in every part of the brain and occur at timescales ranging from 1 Hz to 100 Hz (and potentially beyond). The exact purpose and generation of neural oscillations is the subject of intense research, though current thinking suggests that the functional role of oscillations is differentiated by their rate. Low-frequency oscillations, including the theta (4-8 Hz), alpha (9-13 Hz), and beta (15-25 Hz) ranges, have been observed in diverse cortical areas as humans behave and perform cognitive tasks[22–24]. Gamma frequencies, between 30 and 100 Hz, also correlate with cognition and behavior, but it is not clear to what extent iEEG recordings in this range reflect rhythmic oscillatory activity versus overall changes in the firing rate of neurons proximal to the recording electrode[25–29].

Studies of intracranial EEG seek to correlate modulations of oscillatory activity with cognitive or behavioral events. Experimentalists typically use Fourier methods to

decompose iEEG signals – a voltage measure – into component parts within particular frequency bands of interest. The exact decomposition method differs in accordance with the hypothesis at hand and experimental constraints, but common methods include the Hilbert transform, Morlet wavelet convolution, and multitapers. The subsequent frequency-filtered signals are usually next analyzed to extract spectral power, reflecting the overall energy contained in a given frequency. Filtered signals can also be analyzed for spectral phase, or the position (i.e. angle) of a sinusoidal wave at a given point in time. Together, the collection of power and phase measurements at a set of frequencies are the fundamental unit of analysis in any iEEG study.

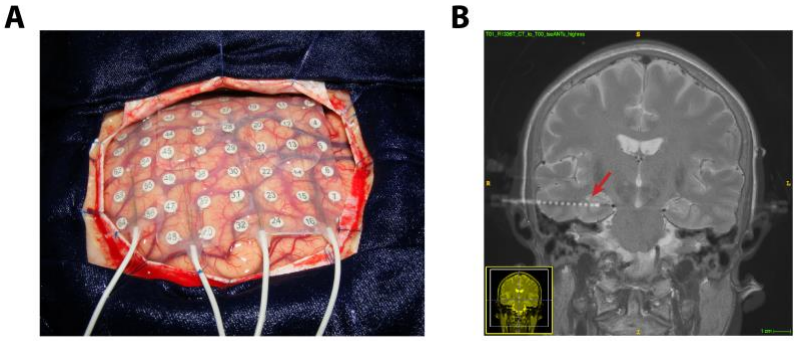

Figure 2.3. Intracranial EEG. A. Surgical placement of a grid electrode in a patient with medication-resistant epilepsy. Grid electrodes are placed subdurally, allowing direct recording of electrical potentials from the cortical surface (electrocorticography; ECoG). **B.** Post-operative CT scan coregistered to pre-operative T1 MRI, highlighting the placement of a linear depth electrode in the right temporal lobe (red arrow). Depth electrodes enable the recording of LFPs from the medial temporal lobe. Image in (a) reproduced from https://mnepilepsy.org/services/ .

Despite excellent temporal resolution, iEEG is not without its pitfalls. Though the method also affords precise spatial resolution – electrodes are typically only a few millimeters in diameter – electrodes are only placed in the brain according to clinical considerations, not research agendas. Accordingly, placement differs drastically from patient-to-patient, and structures believed critical to a particular cognitive process may not be sampled at all. Moreover, it is only ethical to perform invasive brain surgery in people with a dire clinical need – usually medication-resistant epilepsy. Though it is likely that the general neural mechanisms supporting cognition and behavior are the same in epileptic brains as compared to neurotypical brains, it is also clear that brain tissue in an epilepsy patient can

exhibit highly pathologic activity even outside the seizure focus[30–33]. It remains an open question as to how much these pathologies affect our measurements and judgments of human neural function.

Network Neuroscience

Since the early 20th century, neuroscience has sought to correlate brain structure and function with the generation of behavior. The most straightforward way to do this is make a measurement of activity within the brain (e.g. scalp/intracranial EEG, microwire recordings, fMRI, calcium imaging, etc.), measure an interesting behavioral output, and ask whether the two are correlated. This approach has yielded key insights into brain function and consequent Nobel prizes. Indeed, this approach largely defines the common understanding of neuroscience among the general public; a part of the brain lights up when a mouse or a person does something interesting.

But even since the earliest days of modern neuroscience, it has been clear that the brain does not function through the isolated activity of particular regions[34]. Rather, the brain is a highly interconnected organ, with each neuron or chunk of cortex receiving thousands of axonal inputs from other places, and sending out thousands more. The brain's inherent structure suggests *connectivity* is a critical piece of the puzzle to understanding how collections of neurons generate movement, language, memory, thought, and emotion.

Until recently, connectivity was largely the domain of anatomists studying white matter tracts in cadaveric brains. Starting in the 1980s and accelerating in the 1990s, neuroscientist began to use new tools to uncover *functional* correlations in brain activity. Instead of asking, "are these two brain regions physically connected?", fMRI and intracranial recordings enabled us to ask, "do these two brain regions behave in concert?"[16] The idea of *functional connectivity* has evolved into one of neuroscience's most prolific and exciting subfields.

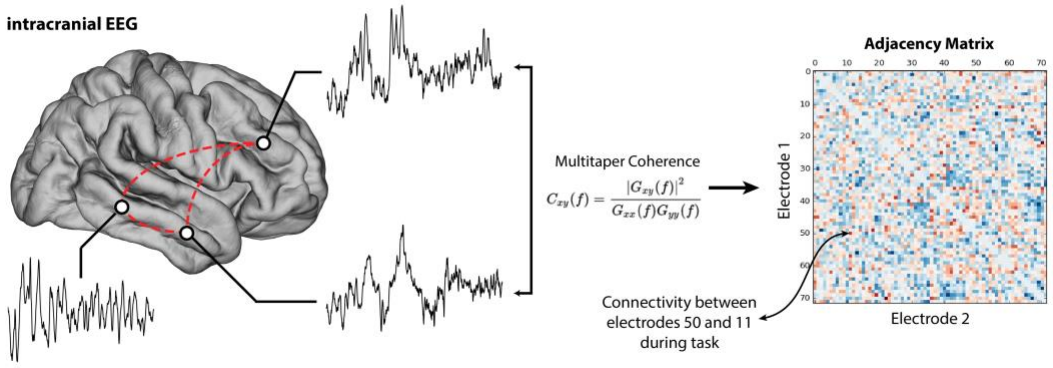

Figure 2.4. Intracranial measures of functional connectivity. Intracranial function connectivity can be computed by several methods, including multitaper coherence. Coherence reflects the normalized cross-spectral density between iEEG recordings from disparate brain regions, at a given frequency. The coherence between all possible pairs of electrodes is given by an adjacency matrix (right), which represents a whole-brain network and can be subject to further graph-theoretic analysis.

Functional connectivity is essentially a measure of timeseries correlations. Whether these timeseries are fluctuations in the BOLD signal recorded through fMRI, or the theta-filtered signal from iEEG electrodes, we can ask whether up-and-down fluctuations of these signals co-occur (with or without lags) between distant brain regions (Figure 2.4). We now know that functional connectivity, like measures of local neural activity, is correlated with cognitive and behavioral events. The activity of the prefrontal cortex and hippocampus, for example, becomes correlated as human subjects engage in episodic memory tasks[10,35]. Critically, it bears emphasizing that functional connectivity is *not* a measure of causal relations; inter-regional correlations do not imply that that one region directly influences another, or that information directly flows from one to the next[36]. Experimental perturbations (see "Brain Stimulation") remain the only gold-standard way to assess the causal role of brain activity in generating behavior.

Moving beyond pairwise correlations, more recent work in neural connectivity conceptualizes the brain as a *network* of interconnected regions. In this framework, it is the coordinated activity among all regions of the brain that ultimately supports complex behaviors[37,38]. Neuroscientists have borrowed tools from the mathematical field of graph theory to understand these networks. Brain regions are equated to network *nodes*,

connected to other nodes by *edges*. In real brains, edges reflect structural or functional connections, depending on a researcher's particular hypothesis or exploratory question. Edges are often given weights in accordance with the magnitude of functional correlations or structural connections, though it is also possible to threshold weights and simply analyze a network of binary, connected-or-not network.

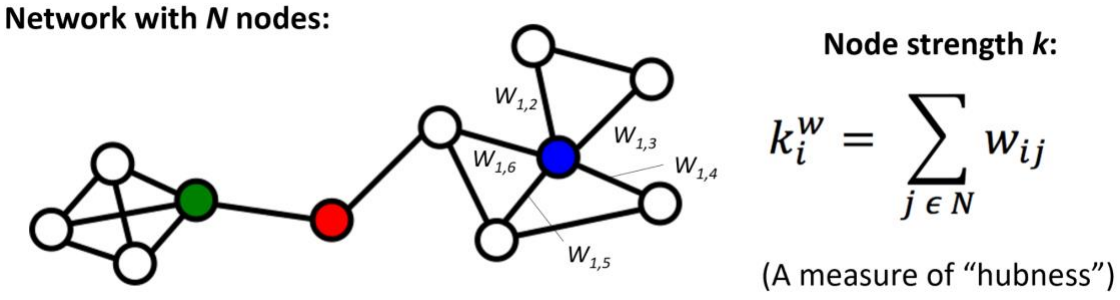

Figure 2.5. General network structure and the node strength statistic. *Left*: Schematic network with circles representing nodes and lines representing edges. The node strength is given by the sum of connection weights to a given node, indicated on the blue colored node.

It is now routine to use graph-theoretic measures to assess the higher-order structure of these functional/structural brain networks. Higher-order structure reflects the complex topology of brain networks – certain recurring patterns (or *motifs*) of nodes and edges have been observed in naturally-occurring networks, including the brain[39]. The node strength statistic, for example, measures the sum total of all connection weights to a given node. Nodes with high node strengths are called "hubs," which in the brain may indicate regions that strongly influence or orchestrate the activity of many others (Figure 2.5). Other statistics, such as the clustering and betweenness coefficients, capture more complex patterns of interconnectedness and serve as useful summaries of the role a particular node plays in a broader network. Taken together, graph-theoretic analysis of brain networks is a new and powerful tool for linking features of network topology with interesting cognitive or behavioral variables.

The ensuing studies in this dissertation seek to use simple graph-theoretic analysis to relate changes in iEEG-based functional brain networks with episodic memory. The bulk of the

analyses presented here are fundamentally correlational; functional connectivity is measured as correlated changes in iEEG signals across space, and connectivity itself is further correlated with behavioral variables relating to episodic memory. However, the last study presented here leverages another innovation: the use of intracranial brain stimulation to assess the *causal* role of brain activity.

Brain Stimulation

Electrical brain stimulation is not a fundamentally new technique. In fact, neurologists and psychiatrists have been delivering electrical pulses to human brain tissue for almost 100 years, both as clinical and research endeavors[40]. These efforts have been instrumental to understanding the causal role of certain brain structures in behavior; as early as 1937, it became apparent that particular areas of the cortex were responsible for speech or sensation, which became altered upon electrical stimulation of the area[41]. Electroconvulsive therapy, in which a current is passed through the brain noninvasively, has for over 50 years been used as a last-resort therapy for refractive psychiatric illness, particularly depression[42]. More recently, deep brain stimulation (DBS) through indwelling electrodes has been used to effectively treat Parkinson's and related disorders[43].

Today, a variety of stimulation methods are approved for research use in humans. Transcranial magnetic stimulation (TMS) has become particularly popular, owing to its noninvasiveness, low-risk, and ease of use. Transcranial electrical stimulation (TES) is also commonly deployed. In neurosurgical patients fitted with indwelling electrodes, electrical current can be applied to brain tissue directly, called direct electrical stimulation (DES). DES provides a means of providing spatially-focused stimulation even to deep brain structures, including the MTL (Figure 2.6).

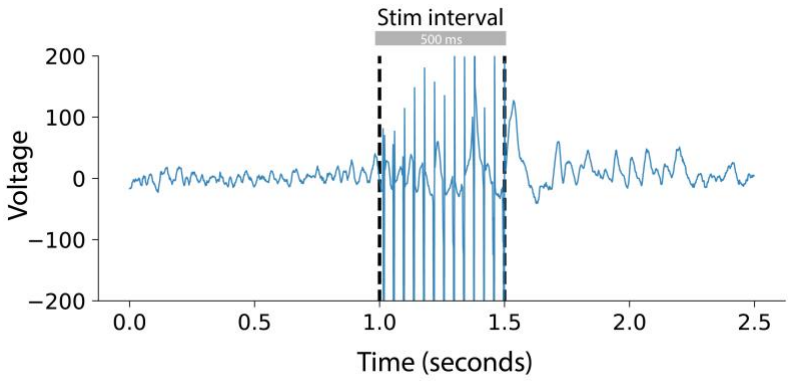

Figure 2.6. Example trace of an intracranial stimulation event. iEEG recording from a depth electrode before, during, and after a 500 ms square pulse stimulation event. Stimulation itself elicits a recording artifact (visible as high-amplitude spikes during the stimulation interval) and ensuing change in neural activity in the post-stimulation period.

Despite its relatively long history, the way in which electrical stimulation affects neural activity is largely unknown. Depending on parameters and methods, stimulation can enhance or decrease neural excitability and firing rate local to the targeted area, but it is unclear whether such modulations are facilitating ongoing neural processes or merely injecting noise[40]. Even more mysterious is the way in which stimulation events are propagated through the brain via endogenous mechanisms. In monkeys, it has been shown that direct electrical stimulation propagates through known anatomical connections in the visual system[44]. In humans, stimulation events were also noted to move through structural *and* functional connections, as measured via fMRI[45,46]. Beyond these basic studies, it is not understood (1) precisely how ensembles of neurons react to applied currents, (2) how neurons transmit the perturbation to distant regions, and (3) how exogenous stimulation manifests as alterations in behavior or cognition.

The mysteriousness of brain/stimulation interactions has not stopped experimentalists and clinicians from asking whether stimulation can be used for therapeutic benefit. Beyond the well-established use of DBS in Parkinson's patients, recent studies have asked whether stimulation can be used to ameliorate deficits in memory or psychiatric illness, to name a few[47,48]. Results have so far been inconsistent; for example, some studies show electrical

stimulation can be used to enhance memory, while others suggest it decreases memory performance[49–53]. Notably, these studies span a wide range of stimulation amplitudes, frequencies, anatomical targets, and task-related timing. Indeed, there is now a consensus that stimulation for therapeutic benefit must optimize (1) the time at which stimulation is delivered, relative to ongoing neural activity, and (2) the location of stimulation given a desired change in behavior. Unfortunately, solving this optimization problem requires a far more advanced understanding of (1) how the brain generates behavior, and (2) how stimulation alters neural activity.

In pursuit of this heightened understanding, this dissertation sought to establish the underlying patterns of neural activity that manifest during episodic encoding and retrieval, with a focus on functional connectivity. Additionally, the effects of intracranial stimulation were examined through the lens of functional connectivity (FC), establishing whether FC explains the propagation of stimulation events through the brain.

CHAPTER 3:

Whole-Brain Electrical Networks

Solomon, E. A., et al. "Widespread theta synchrony and high-frequency desynchronization underlies enhanced cognition." *Nature communications* 8.1 (2017): 1704.

Abstract

The idea that synchronous neural activity underlies cognition has driven an extensive body of research in human and animal neuroscience. Yet, insufficient data on intracranial electrical connectivity has precluded a direct test of this hypothesis in a whole-brain setting. Through the lens of memory encoding and retrieval processes, we construct whole-brain connectivity maps of fast gamma (30-100 Hz) and slow theta (3-8 Hz) spectral neural activity, in a dataset of 294 neurosurgical patients fitted with indwelling electrodes. Here we report that gamma networks desynchronize and theta networks synchronize during encoding and retrieval. Further, for nearly all brain regions we studied, gamma power rises as that region desynchronizes with gamma activity elsewhere in the brain, establishing gamma as a largely asynchronous phenomenon. The abundant phenomenon of theta synchrony is positively correlated with a brain region's gamma power, suggesting a predominant low-frequency mechanism for interregional communication.

Introduction

The brain gives rise to behavior and thought through the coordinated activity and transfer of information between disparate regions[5]. Despite over a century of investigation into the brain's interconnectedness[34] however, the nature of these inter-regional interactions remains unknown. Our understanding of connectivity in the brain originates from studies that use indirect measures of neural activity, like blood-oxygen-level dependent (BOLD) functional MRI, extracranial electroencephalography (EEG), and magnetoencephalography (MEG)[54]. While these techniques provide a useful picture of how distant brain regions act in concert during cognition, they lack the spatial or temporal precision of direct electrical recordings in the brain[37]. Until recently, the limited availability of such intracranial data made it difficult to assess the connectivity dynamics of the whole brain as it performs cognitive tasks.

Recent studies using direct brain recordings in neurosurgical patients have made it possible to robustly investigate neural synchronization, the coordinated activity of ensembles of neurons in different parts of the brain. Synchronization is an appealing mechanism for explaining how the brain stores memories, processes sensory inputs, or performs any operation that involves interlinking representations of the outside world[54], and it generally occurs on different timescales - or frequencies - of neural activity. In particular, gamma-band (30-100 Hz) synchronization is frequently invoked as a means for the brain to communicate between regions, since the fast nature of an oscillatory gamma signal is timed appropriately for rapid perceptual operations or induction of synaptic strengthening[21,25,55,56]. Support for this idea comes mostly from animal studies[25,56–58], though some human EEG studies also report cognitively induced low-gamma and short-range synchronicity[59–61]. However, others have argued that this body of work is conceptually and empirically deficient to defend the broad notion that high-frequency activity supports a meaningful neural connection[29,62–65]. Notably, conduction delays between cortical areas would make the precise synchronization of gamma oscillations difficult, and overall power at high frequencies may be too weak to support neuronal synchrony. Furthermore, the literature on this subject is mixed - even some of the most influential studies of gamma

synchrony in humans report significant periods of desynchronization[59,60,66] and steep drop-offs in synchrony at higher frequencies[61]. These critiques raise the possibility that gamma does not serve to support communication between cortical regions, though this hypothesis has not been directly tested.

If activity in the gamma range is not synchronous, it may instead reflect the aggregation of rapid, stochastic firing in a population of neurons near an electrode, not an oscillatory modulation of activity that indicates coordinated activity across space[27,67]. Were this true, the general neural activation of a brain region – captured by the spectral power recorded at a cortical electrode – would rise as the synchronicity of that region with others would tend to fall. However, this form of broadband asynchronous activity may coexist with narrowband synchronous oscillations,[68,69] and both may contribute to spectral changes at frequencies in the gamma band. In this case, it remains untested whether the oscillatory component of a gamma-band signal underlies long-range synchronization, and to what extent high-frequency activity during cognition reflects synchronous oscillations versus asynchronous broadband activity.

If high-frequency activity is not the principal mediator of inter-regional synchronization, low-frequency interactions may be a promising alternative. Synchrony in the slower theta-band (3-8 Hz) has been reliably found to correlate with cognition in humans and animals[70–73], and theta oscillations are also linked to modulations of gamma activity[74,75]. However, low-frequency networks have not been characterized on a brain-wide scale, making it difficult to differentiate general principles of brain function from dynamics that may be particular to specific structures. It is possible that canonical regions such as the medial temporal lobe and prefrontal cortex participate in low-frequency networks while less well-studied regions break from this trend. Moreover, low-frequency interactions have not yet been directly related to modulations of spectral power on a brain-wide scale, though probing these interactions may reveal the relationship between a region's functional connectivity and local processing.

In this study, our goal is to determine what principles underlie how neural activity is coordinated across the brain during memory processing, and to answer how spectral power

and synchrony are related: To what extent is inter-regional communication mediated by low- versus high-frequency interactions? As the local high-frequency activity of a region increases, does its synchrony concomitantly decrease? How often do we observe high-frequency oscillations during cognition, and are they associated with long-range connectivity? While 294 subjects perform memory encoding and retrieval tasks – processes which rely on the integration and binding of information – we record iEEG and construct whole-brain networks of high- and low-frequency phase interactions. To determine how synchrony changes over time and space, we parse these networks with graph-theoretic tools that identify hubs of the network, and then correlate the spatio-temporal pattern of synchrony at these hubs with simultaneously-measured spectral power. Though our focus is on gamma- and theta-band synchrony, we consider whether connectivity dynamics in these bands are better captured by broader frequency ranges, such as broadband low (< 30 Hz) and broadband high (> 30 Hz) . We observe widespread desynchronization of high-frequency activity and synchronized low-frequency activity during memory processes, which correlate with regions of enhanced high-frequency power. Our findings support the notion that macroelectrode-scale recordings largely reflect asynchronous neural firing at high frequencies, but also suggest a low-frequency mechanism for interregional communication.

Results

Quantification of brain-wide connectivity phenomena

To assess connectivity between brain regions, we collected intracranial electroencephalographic (iEEG) data from 294 patients undergoing clinical monitoring for seizures while they performed a verbal free-recall memory task (Figure 3.1a; see Figure 3.S1 for behavioral results). In this task, patients saw a series of words, each presented briefly on a screen, and were instructed to recall as many as possible. To construct networks of activity, we adopted a common spectral phase-synchronization approach to measure connectivity between pairs of electrodes, called the phase-locking value, which quantifies the consistency of phase differences at a given frequency across trials of the experiment[76] (Fig. 3.1b, 3.1c; Methods). In this paper, we primarily focus on regularly-

spaced frequencies in the 45-100 Hz range, referred to collectively as "high gamma," though we make no prior assumption as to whether these frequencies capture predominantly broadband asynchronous or oscillatory synchronous effects. Some analyses are extended to the 30-60 Hz range, referred to as "low gamma."

We first sought to quantify the grand-average modulation in high gamma (HG) and theta connectivity during item encoding that correlates with subsequent successful recall of that item – in other words, the relative level of synchronization comparing successful to unsuccessful encoding events. To measure this, we averaged the modulation in HG or theta connectivity across all possible electrode pairs that spanned every pair of anatomically-defined regions of interest (ROIs) in all subjects (ROIs are based on automated Talairach atlas labeling[77], e.g. superior frontal gyrus, middle temporal gyrus, etc. See Methods for details, Table 3.T1 for ROI abbreviations used in this paper). Connection weights are then z-scored against a null distribution, obtained by permuting remembered/not-remembered trial labels, to reflect the connection strength between ROIs relative to that expected by chance. The result of this procedure in the gamma and theta bands are adjacency matrices, which represent the pairwise connectivity between all ROIs (Figure 3.1d), and which can be rendered as brain maps (Figure 3.1e).

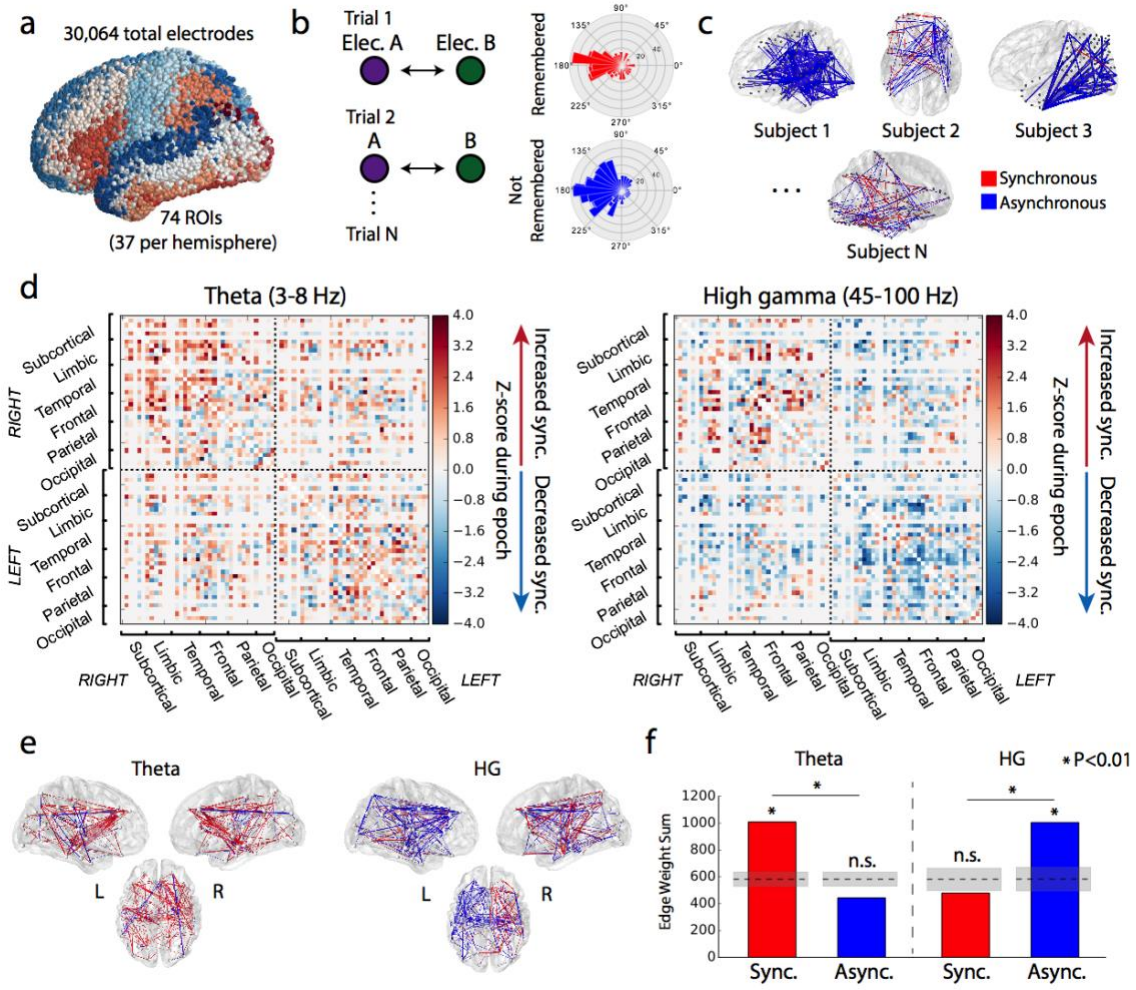

Figure 3.1. Network construction and basic analysis. (a) 3D visualization of all surface electrodes included in our dataset, colored by the Talairach atlas labels used in this article's analysis. **(b)** Schematic of spectral phase approach that compares the distributions of phase differences between electrodes across all trials of the verbal free-recall task. Significantly tighter distributions indicate greater synchronization. **(c)** Connectivity maps were extracted for each of 294 neurosurgical patients, reflecting the connectivity change associated with successful item recall. Effects were pooled across subjects and ROIs to construct the final network. Blue indicates decreased phase synchrony associated with successful encoding, red indicates increased synchrony. **(d)** 74x74 ROI adjacency matrices representing the z-scored time- and frequency-averaged connection weights during the item presentation interval (0-1600ms). The high gamma network is constructed from frequencies between 45-100 Hz, and theta from 3-8 Hz. Node indices are organized by lobe per the indicators on the axes. Grey areas represent connections between ROIs with fewer than 7 subjects' worth of data. **(e)** 3D visualizations of the whole-brain HG and theta networks. **(f)** Summed positive and negative connection weights in each frequency band. In a remembered versus not-remembered contrast, the total level of synchronous theta connections and asynchronous HG connections were

significantly greater than chance (P<0.01), and there was a significant frequency-synchrony interaction (P<0.01, chi-square test). Dotted lines indicate mean chance level, shaded area +/- 1 STD.

Encoding networks showed markedly different properties between HG- and theta-band frequencies. As measured by the summed connection weights across the entire network, HG asynchrony and theta-band synchrony significantly correlated with successful encoding (Figure 3.1f; $P < 0.01$ via permutation test of summed connection weights; see Methods). And though the network-wide level of synchronous activity in HG was not significant (permutation $P = 0.892$), this does not preclude the possibility that specific connections among ROIs are associated with successful memory encoding. Similarly, the overall level of theta-asynchronous interactions was not greater than chance (permutation $P >0.99$). Extending this analysis to higher and lower frequencies revealed significant asynchrony (Figure 3.2a; permutation $P < 0.05$) in frequencies between 30 Hz and 120 Hz, including the typical 30-60 Hz low gamma band. Significant synchrony in frequencies between 3 Hz and 28 Hz – theta, alpha, and beta bands – was also observed (permutation $P < 0.01$). The brainwide connectivity z-score is given as a heatmap for each assessed frequency and timepoint in Figure 2b.

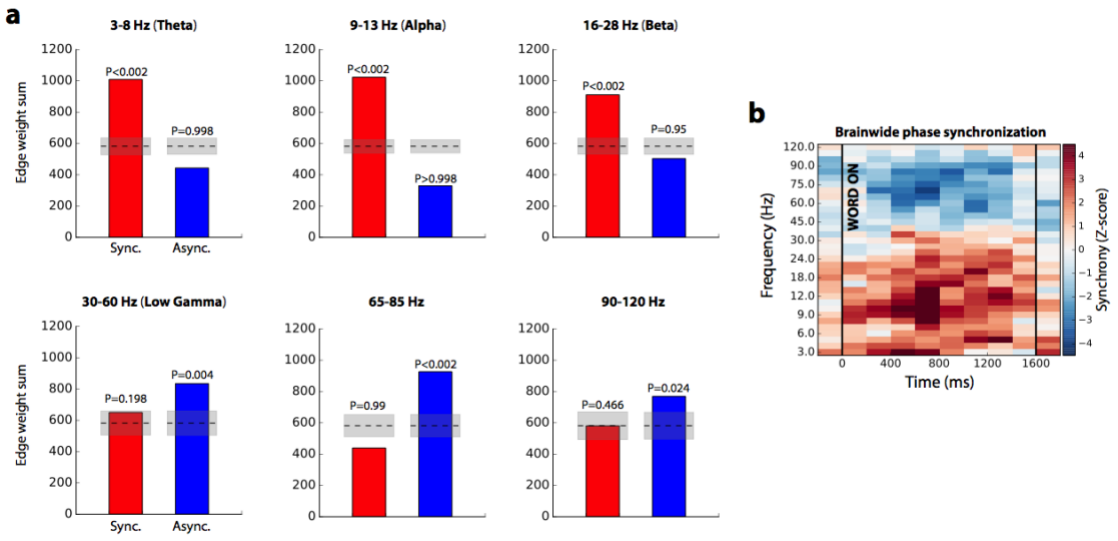

Figure 3.2. Synchrony effects from 3-120 Hz. (a) Overall level of SME synchrony/asynchrony in six frequency bands spanning 3 Hz to 120 Hz, measured as in Figure 3.1f (edge weight sum). Shaded gray areas represent chance mean +/- 1 STD. **(b)** Z-scored brainwide phase synchronization subsequent memory effect (SME) in the memory encoding interval, measured by summing all

connection weights in the network, compared to the sum expected by chance. This analysis is performed in successive 200ms windows spanning the encoding interval. Red reflects increased synchrony associated with successful memory encoding, blue reflects decreased synchrony (see Methods for details). Vertical black lines indicate word onset and offset.

Our findings of brain-wide HG asynchrony and theta synchrony during successful memory encoding suggest that it is low-frequency connections which support information integration or coordinated brain activity during memory formation. However, we must first answer two deeper questions to determine whether there is a relationship between the neural activity of a region and the state of its connections to the rest of the brain: First, what is the brain-wide spatiotemporal pattern of synchrony/asynchrony during memory processing, and how does it relate to the pattern of local spectral power? Second, are there differing fundamental sources of neural activity that may have different power-synchrony relationships?

Identification of network hubs

Given that we observed significant levels of synchrony or asynchrony in low and high frequency ranges, we next asked whether there is anatomic specificity to these phenomena. Are positive and negative connections homogenously distributed throughout the brain, or are there specific regions that exhibit greater modulation of connectivity during successful memory encoding?

To determine the most highly-connected (or highly-disconnected) ROIs, we turned to basic principles of graph theory. We used the node strength statistic (the sum of the unthresholded weights of every connection to a given node, here defined as an ROI) to identify which brain regions act as highly-connected "hubs" in the memory network during the word presentation interval (0-1600 ms), the epoch with the greatest task-related modulation[78]. We defined hubs as ROIs with significantly greater node strength than expected by chance ($P < 0.05$ via permutation test of node strengths, Benjamini-Hochberg corrected for multiple comparisons across ROIs), and we performed this analysis to identify hubs from all synchronous and asynchronous connections separately (see Methods). In HG, we found 3 synchronous-hubs and 19 asynchronous-hubs, which reflect brain regions that

significantly increase or decrease their overall connectivity when a word is successfully encoded ($0.006 < P < 0.033$, FDR corrected). The theta-network exhibits 32 synchronous hubs widely dispersed across the cortex ($0.005 < P < 0.049$, FDR corrected), but no hubs of asynchronous activity. Theta and HG hubs are depicted in Figure 3.3, along with their strongest connections ($Z > 2.5$).

Taken together, these findings demonstrate that frontal, temporal, and medial temporal lobe (MTL) cortical regions became desynchronized from each other in HG during memory encoding. A smaller subset of right mesial frontal regions expressed synchronous activity with each other and functionally connect to temporal and parietal cortex. In the slower theta rhythm, the brain exhibited generally correlated activity, with numerous fronto-temporal, temporal-parietal, and interhemispheric functional connections.

Our finding that there is widespread theta-synchronization during memory encoding follows from prior scalp and intracranial studies, which have shown that low-frequency entrainment is associated with cognition[70–73,79]. These findings also mirror findings in the fMRI literature of low-frequency networks that converge on the MTL in memory tasks[10]. The emergence of bilateral MTL as asynchronous hubs in HG is more surprising – this observation suggests, in a general sense, that structures such as the hippocampus do not synchronize at high frequencies with many other brain regions during successful encoding.

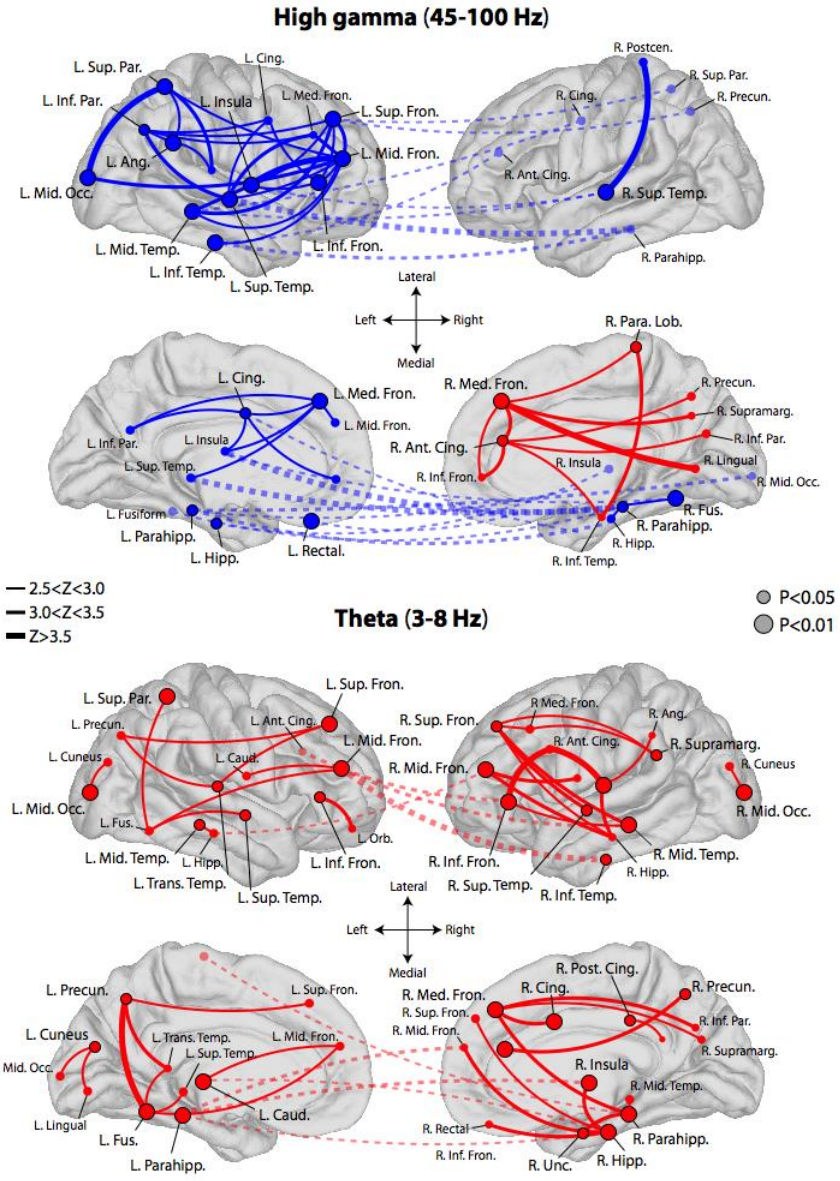

Figure 3.3 **Network hubs.** Depiction of hub ROIs identified in the brainwide theta and high gamma memory encoding networks. The analysis was performed separately for all positive connection weights (red) and all negative connection weights (blue), yielding "synchronous hubs" and "asynchronous hubs," which respectively increase or decrease their connectivity with the network during successful memory encoding. Significant synchronous and asynchronous hubs for the item-presentation interval are displayed according to their approximate localization on an average brain surface, with red circles indicating synchronous hubs and blue indicating asynchronous hubs (larger circles, FDR-corrected $P < 0.01$; smaller circles, $P < 0.05$). For each hub, the top 5 connections between that hub and any other part of the brain is plotted, if the connection weight z-score was greater than 2.5. Line thickness indicates absolute z-score value, according to the figure legend.

Dashed lines indicate cross-hemispheric connections. Some labels are excluded from certain views to maintain readability. To aid visualization, hemispheres are reflected from their true position in the skull.

Temporal modulation of connectivity effects

To better characterize the role of these hubs in memory encoding, we asked whether a hub's participation in the HG or theta network changes over time. We assessed this by computing the node strength statistic at each 200 ms non-overlapping time window spanning 200 ms prior to 200 ms after the word presentation interval (see Methods). ROIs exhibited their strongest modulation of network participation between 400 ms and 1200 ms after onset of a word, with a particularly robust decrease in HG connectivity of left MTL structures between 800-1000 ms (significant hippocampus, parahippocampus, and uncus ROIs, $P < 0.05$ via permutation test of node strengths; see Methods for details). Correspondingly, the right MTL exhibited an increase in theta synchrony between 800-1200 ms (permutation $P < 0.05$). Theta synchrony in the right frontal lobe (significant middle, medial, inferior, and superior frontal cortices, permutation $P < 0.05$) peaked earlier, between 600-800 ms, while right temporal (significant middle, transverse, superior, and inferior temporal cortices, permutation $P < 0.05$) synchrony peaked between 1000-1200 ms (left cortical areas follow a similar pattern, see Figure 3.S2). In Figure 3.4, we show timecourses of node strength for ROIs in a subset of broader brain regions that contained hubs as identified previously (see Figure 3.S2 for additional timecourses).

It is not surprising that we observed strong modulation of connectivity in both frequency bands during the item presentation interval, since this time period is also known to feature the greatest change in spectral power[78]. What is not known, however, is how the directionality of connectivity changes relates to that change in spectral power – does enhanced theta-synchrony or decreased HG-synchrony in a brain region predict its HG or theta power?

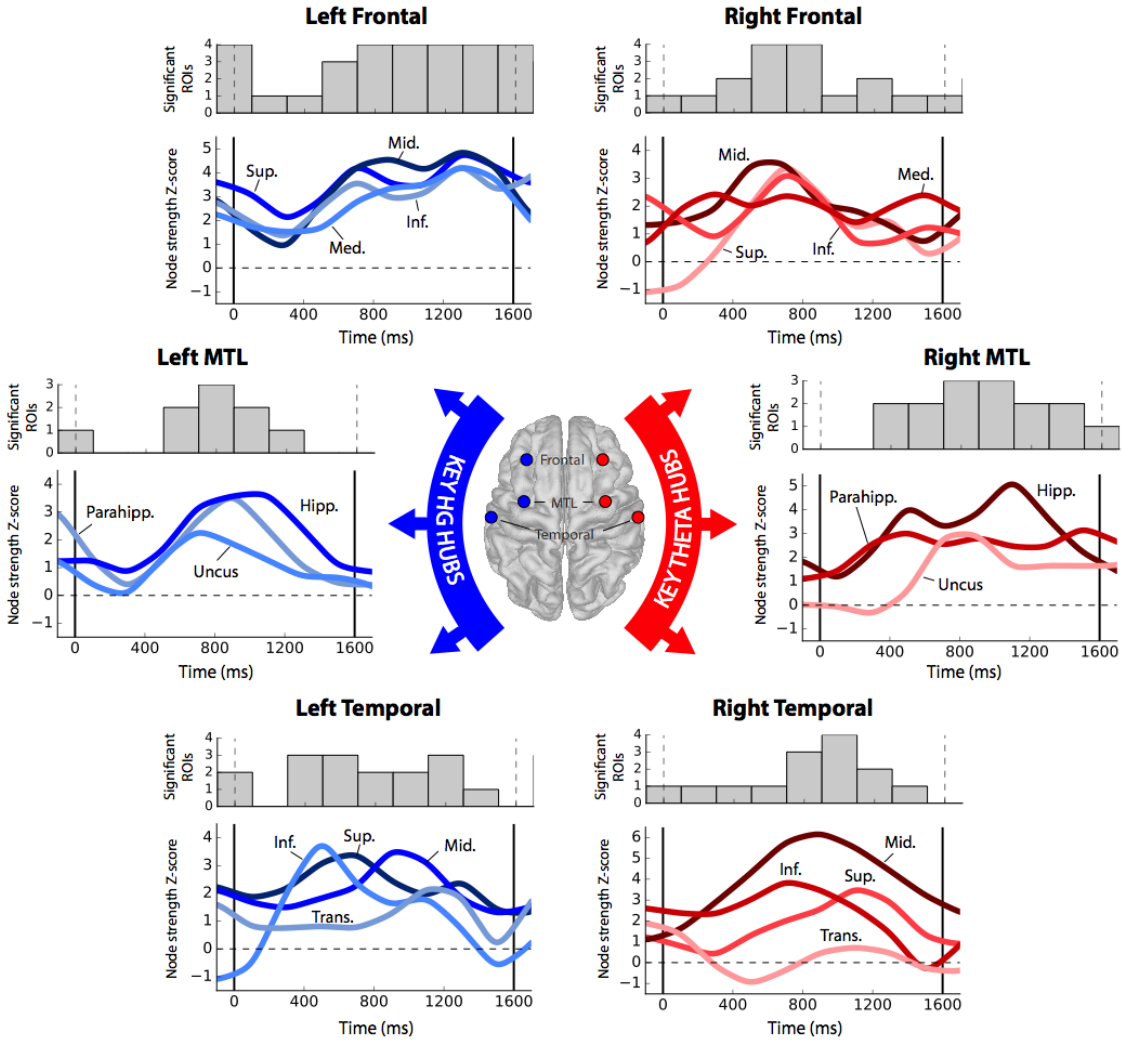

Figure 3.4. Timecourse of ROI participation in memory networks. Node strength as a function of time for 6 key regions that contain hubs in the theta or high gamma networks: right and left MTL, frontal lobe, and temporal lobe. Blue-shaded lines indicate asynchronous hub strength over time, while red indicates synchronous hub strength. Vertical lines indicate word onset and offset at 0 ms and 1600 ms. Above the z-scored timecourses are plotted the total count of specific ROIs within each broader region that reach significance at a given timepoint ($P < 0.05$). For visualization only, timecourses were smoothed with a 2-point moving average and radial basis filter.

Relationship between connectivity and spectral power

Having established the spatio-temporal dynamics of synchrony during performance of a memory task – noting the presence of MTL hubs that peak in their activity during the item presentation interval, for instance – we are now equipped to ask how these connectivity dynamics relate to spectral power, or the general neural activation of a region. Answering this question fills an important gap in knowledge about the nature of connectivity in the brain, by showing how connectivity and power relate across a diverse array of cortical regions during memory processing.

We used the node strength of each ROI as a basis for a spectral power-synchrony correlation, asking whether a region's overall participation in the whole-brain network correlates with that region's modulation of spectral power. For each ROI, we computed the power-synchrony (node strength) correlation across time and frequency in HG. We further asked how power and synchrony correlate across all ROIs and time after averaging effects within frequency band, enabling cross-band correlations.

We found that only one ROI exhibited a significant positive correlation between HG power and synchrony – the left transverse temporal gyrus - after Benjamini-Hochberg correction for multiple comparisons (Figure 3.5a; Pearson correlation, $r = 0.27$, corrected $P = 0.017$). Twenty-four regions exhibited a significant negative correlation (Figure 3.5a; Pearson correlation, $-0.48 < r < -0.23$, $4.6 \times 10^{-6} < P < 0.037$). Example power-synchrony heatmaps are given for four regions in Figure 3.5b, depicting significant (corrected $P < 0.05$) negative correlations in the right parahippocampus, left medial temporal lobe, and left frontal cortex.

Across all ROIs (74) and timepoints (10) together, the HG power-synchrony Pearson correlation was -0.339 , $P = 0.002$ via a permutation test of synchrony and power correlation (Figure 3.5c; see Methods for details). In theta, within-ROI correlations showed 3 ROIs each of positive and negative power-synchrony relationships (corrected $P < 0.05$; Figure 3.S3), but the general effect across all time and ROIs together was negative though not significant (Pearson correlation, $r = -0.12$, permutation $P = 0.23$; Figure 3.5c). Additionally, theta synchrony was weakly - but not significantly - correlated with HG power

(Pearson correlation, r = 0.11, permutation P = 0.2; Figure 3.5c). The brainwide spectral power and synchrony at all frequencies from 3 Hz to 120 Hz are shown in Figure 3.S4.

Measuring correlations across all ROIs together may obscure meaningful relationships within the subset of ROIs that actively participate in memory processing. We therefore sought to assess whether regions of the "core" memory network – those ROIs that significantly modulate their neural activity during successful memory encoding – exhibit power-synchrony dynamics that are different from the rest of the brain. These regions are said to exhibit a subsequent memory effect (SME)[80]. We found a total of 37 ROIs with no significant difference between HG power during successful versus unsuccessful encoding, and classified these as outside the core memory network. Next, we matched these ROIs against the 37 ROIs with the largest SMEs, representing the core memory network (see Table 3.T1 for ROI classifications and z-scores). Among these two ROI subsets, we again computed power-synchrony correlations across all regions and all timepoints during the word encoding interval. In both groups, HG power and synchrony were inversely correlated (Figure 3.6; Pearson correlation, r = -0.38 in-network and r = -0.158 out-of-network, P < 0.001 and P < 0.05 via permutation test; see Methods). However, only in the core memory network was theta synchrony significantly predictive of HG power (Pearson correlation, r = 0.25, permutation P = 0.003; see Methods). The difference in correlation between in-network and out-of-network does not reach significance (permutation P = 0.20).

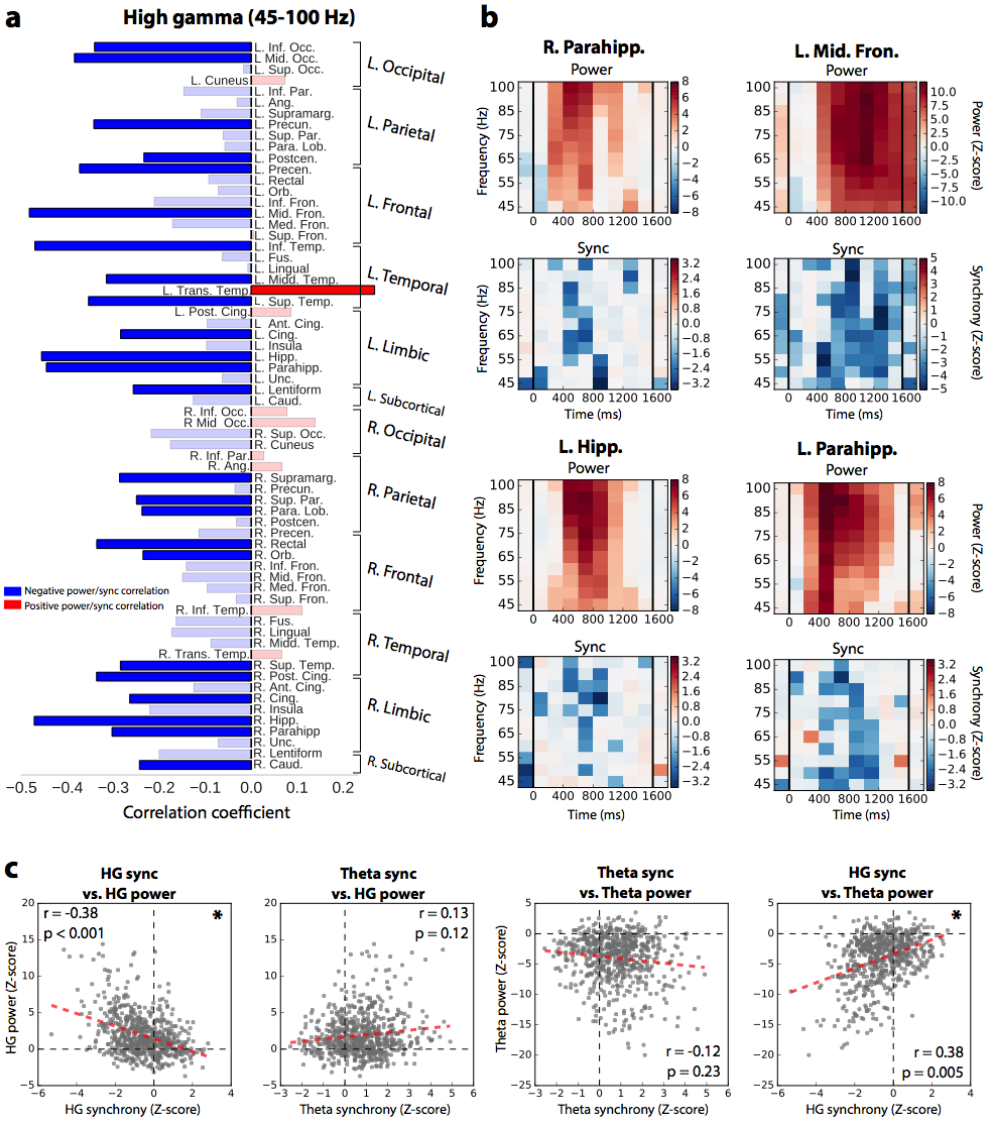

Figure 3.5. Power-synchrony correlations across the whole brain. (a) Pearson correlation of the modulation of high gamma node strength and power across time and frequency for each ROI, during the word encoding interval. Bar plots show the power-synchrony correlation for each ROI, with blue indicating negative and red indicating positive correlations. Faded bars are not significant after FDR correction for multiple comparisons (α = 0.05). **(b)** For four example ROIs we depict time-frequency heatmaps of that ROI's z-scored spectral power (top) and z-scored node strength (bottom). Red colors indicate a relative increase of power/synchrony when an item is successfully encoded, while blue indicates a relative decrease. For visualization only, absolute z-scores less than 1.5 are faded, and vertical bars indicate word onset and offset. **(c)** Pearson correlation of z-scored power and z-scored node strength (synchrony) against each other for all timepoints and all ROIs, after averaging

within frequency band. HG power and HG synchrony are significantly inversely related ($P < 0.001$, permutation test), HG synchrony is positively correlated with theta power ($P = 0.005$), while other tested relationships do not meet significance.

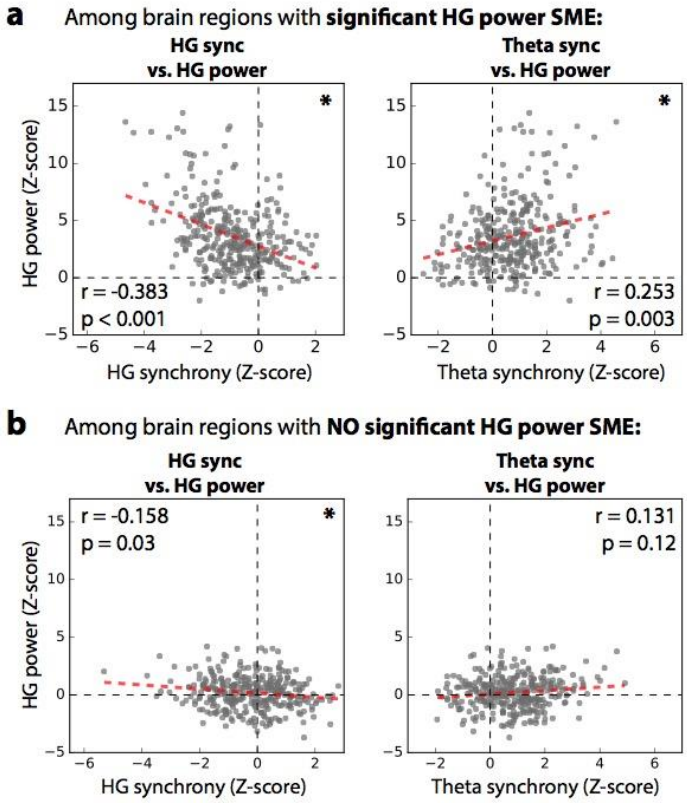

Figure 3.6. Correlations in core memory network. (a) Power-synchrony correlations in the core memory network: the 37 ROIs with significant HG-power subsequent memory effect (SME). (b) Power-synchrony correlations across the 37 ROIs with the no significant HG-power effects. Among the core memory network – consisting mostly of left frontal, temporal, and MTL cortex – z-scored gamma power and z-scored synchrony were significantly anticorrelated, while theta synchrony and gamma power were significantly positively correlated (top row; $P < 0.001$ and $P < 0.01$ via permutation test, respectively). Among regions that did not exhibit strongly modulated HG activity in successful memory encoding, HG power and synchrony were still inversely correlated (Pearson correlation, $\boldsymbol{r} = -0.158$, $P < 0.05$), but theta synchrony was not significantly predictive of HG power ($\boldsymbol{r} = 0.131$, $P = 0.12$).

Generalization of network phenomena to memory retrieval

To establish whether memory retrieval is also characterized by desynchronized HG activity and synchronized theta-band activity, we identified all of the 500 ms time windows in each subject's recall period that precede onset of a response vocalization, and compared connectivity dynamics against 500 ms time windows that are not followed by any vocalization for at least 2 seconds ("unsuccessful memory search"). Procedures are otherwise identical to those described in Figure 3.1 and Methods – phase locking values in successful retrieval are compared to unsuccessful memory search, and these differences are pooled across subjects and ROIs. The result is a whole-brain connectivity map that reflects how phase synchrony is correlated with successful memory retrieval versus unsuccessful memory search (Figure 3.7a, 3.7c).

We found that the same network-level patterns of connectivity held true in the retrieval contrast compared to the encoding contrast. The HG retrieval network is characterized by a significant degree of asynchronous activity (Figure 3.7b; $P < 0.01$ via permutation test of edge weight sum; see Methods) and an insignificant overall level of synchronous activity (permutation $P > 0.99$). In theta-band, there is a greater degree of synchronous activity compared to asynchronous (permutation $P < 0.01$; Figure 3.7b). The relationship between power and synchrony also holds true in the analysis of recall. Even without sub-selecting for a core memory network as in Figure 6, we find an inverse HG power-synchrony correlation (Pearson correlation, $r = -0.67$, permutation $P < 0.01$; Figure 3.7d), although theta synchrony was positively but not significantly correlated with HG power (Pearson correlation, $r = 0.11$, permutation $P = 0.36$; Figure 3.7d).

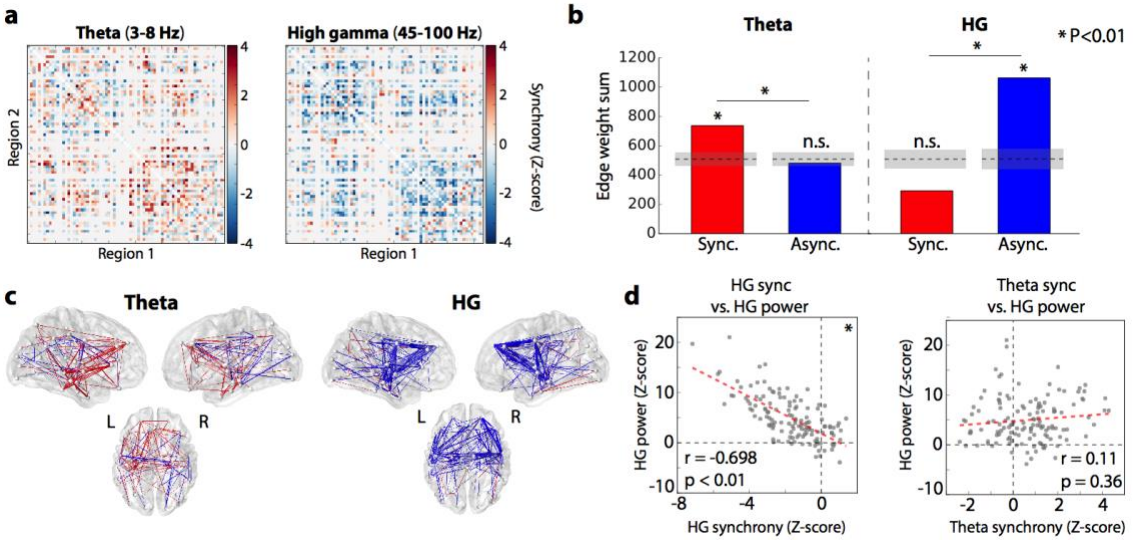

Figure 3.7. Generalization to memory retrieval processes. (a) Adjacency matrices, reflecting relative recall vs. baseline synchronization, organized as in Figure 3.1d. (b) Summed positive and negative connection weights in each network, showing a strong desynchronization effect in gamma-band and a synchronization in theta ($P < 0.01$ for both). There was a significant frequency-synchrony interaction ($P < 0.01$, chi-square test). (c) 3D representation of gamma (top) and theta (bottom) retrieval networks, organized as in Figure 3.1e. (d) Correlation of spectral power and phase synchronization across all regions (74) and timepoints spanning a retrieval trial (2). HG power and synchrony were significantly inversely correlated (Pearson correlation, $\boldsymbol{r} = -0.698$, $P < 0.01$ via permutation test), while an ROI's theta synchrony was positively but not significantly predictive of HG power ($\boldsymbol{r} = 0.11$, $P = 0.36$)

Filtering for oscillatory activity

Findings of HG desynchronization associated with successful memory encoding and retrieval suggest stochastic, non-oscillatory neural activity. However, it is possible that a mixture of two fundamental signals that occupy the same frequency band: some components may be oscillatory, facilitating inter-regional communication, while others reflect asynchronous neural spiking activity. If the asynchronous component is much stronger or more commonplace than the oscillatory component, our results may be unable to capture true high-frequency synchronization that correlates with successful memory operations.

To answer whether high-frequency synchronization is driven by oscillatory dynamics, we examined which electrodes exhibit oscillations in the low gamma band ("LG," 30-60 Hz),

utilizing a validated oscillation-detection routine ("Better Oscillation Detection" method, see Methods for details; see Figure 8a for an example)[81]. We identified the specific frequency and time at which a given electrode showed reliably increased oscillatory activity associated with trials that were later remembered, as compared to those forgotten ("oscillatory SME"; Fig. 3.8b for an example). Among the subset of electrodes with oscillatory SMEs, we reconstructed our phase-synchronization networks to determine whether enhanced oscillatory activity was associated with increased inter-regional synchronization.

261 electrodes in our dataset exhibited increased oscillatory activity associated with successful memory, maximally occurring at 52 Hz, between 400 and 600 ms after word onset (Fig. 3.8c). This is 1% of the total electrodes assessed; 5.6% of electrodes exhibited a 30-60 Hz SME and 10.4% of electrodes that exhibited a 65-100 Hz power SME in the same time window (Figure 3.8d). In the phase synchronization subnetwork that can be constructed from these 261 electrodes, we observed more synchronous ROI pairs than asynchronous pairs, when examining the network at the specific time (400-600 ms) and approximate frequencies (50-55 Hz) of maximal oscillatory SME (Figure 3.8e; $P = 0.068$ via permutation test of edge count sum; see Methods). Examining this subnetwork at the same time but at higher frequencies (65-85 Hz) reveals a return to the typical preponderance of asynchronous activity (Figure 3.8e; permutation $P = 0.046$). This same trend can be observed in Figure 3.8f, where maximal subnetwork-wide synchrony occurs in the same frequency range as that of maximal oscillatory SME (maximal $Z = 1.2$ at 55 Hz).

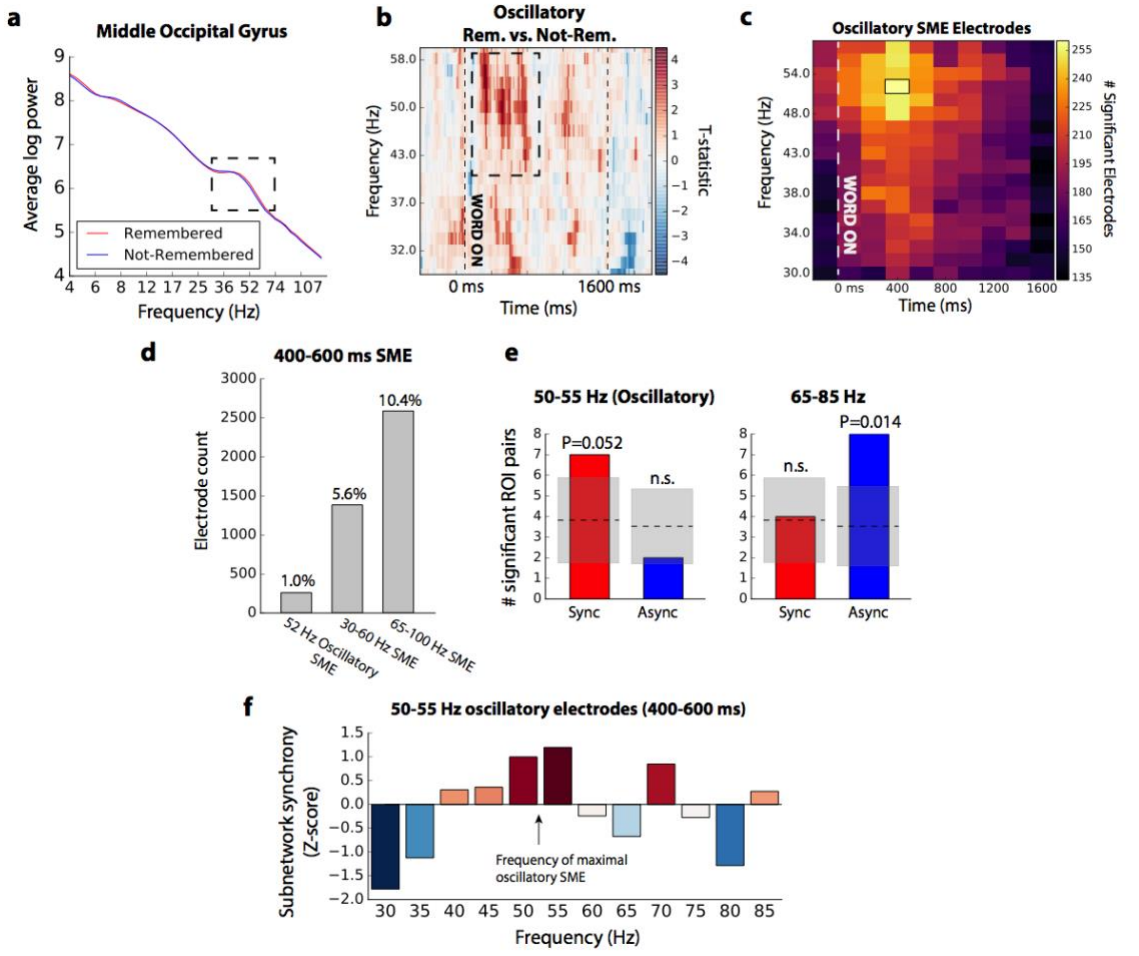

Figure 3.8. Synchronization of low gamma (30-60 Hz) oscillatory activity. (a) Example of an electrode exhibiting a gamma oscillation in the middle occipital gyrus, as detected by BOSC (see Methods for details). Red line reflects average log power across all remembered events, blue line reflects average log power across not-remembered events. An isolated peak in the power spectrum is indicated, between approximately 36 and 74 Hz. (b) For the electrode in (a), heatmap of the t-statistic reflecting the relative frequency of oscillations detected in remembered versus not-remembered trials. Red colors indicate more oscillations detected at given frequency and timepoint in trials that were later remembered correctly. Vertical lines indicate word onset and offset (0 and 1600 ms). T-statistics less than 2 are faded, for visualization only. Increased oscillatory power from 43 Hz to 58 Hz, coincident with the oscillatory peak in (a), is indicated. (c) Count of all electrodes in the 294-subject dataset that exhibit an oscillatory subsequent memory effect (SME) between 30 and 58 Hz, at each 200ms epoch spanning the word presentation interval (see Methods). The most electrodes exhibit oscillatory SMEs at 52 Hz, between 400 and 600 ms after onset of a word (black box). (d) Count of electrodes in the dataset that exhibit different kinds of SMEs between 400 and 600 ms: 52 Hz oscillation, 30-60 Hz average power, or 65-100 Hz average power. (e) Count of significant synchronous or asynchronous network connections using only the subset of electrodes exhibiting 52 Hz oscillatory SME at 400-600ms. Synchronization effects were deemed significant at $P < 0.05$, with

the chance mean and standard deviation at this significance level indicated in the gray shaded area. Left: Counts observed at 50-55 Hz, near the frequency of maximal oscillatory SMEs (52 Hz). Right: Counts observed in the 65-85 Hz range among the same electrode subset. The frequency/synchrony interaction is not significant ($P = 0.11$). (f) Average network synchrony (z-score) for the subnetwork of regions sampled in the 52 Hz oscillatory electrode subset, measured by summing the subnetwork connection weights at each frequency in the 400-600 ms window, and comparing to the sum expected by chance.

Discussion

We set out to uncover fundamental principles that govern the electrophysiological networks of activity in the human brain. As 294 subjects performed a verbal free-recall memory task, we analyzed three frequency bands that have been strongly implicated in neural synchronization[24]: theta (3-8 Hz), low gamma (30-60 Hz), and high gamma (45-100 Hz). Gamma networks exhibited strong desynchronizations between brain regions, especially those that saw an increase in gamma power. Theta networks were characterized by enhanced synchrony, especially among regions with strong increases in HG power. Moreover, hubs of theta network activity tend to localize in frontal, temporal, and medial temporal cortices – regions that are known to play a strong role in memory encoding and retrieval[82].

Here we report findings that address whether theta or gamma band neural activity drives synchronization during memory processing. Gamma activity as a general biological mechanism of information transmission[25,54,55,70] is not backed by many compelling observations in the human brain. We found a profound decrease in HG synchronization that is associated with successful memory encoding and retrieval, especially among regions that see heightened overall HG activation. This relation is consistent with the hypothesis that broadband high-frequency activity in the human brain – as detected by macroelectrodes on the cortical surface – largely reflects the aggregation of fast, stochastic spiking activity of a population of neurons[29]. It refutes the notion that this kind of broadband signal synchronizes across long distances during cognitive operations, though such interactions may still be at play in visual areas[83] and at smaller spatial scales.

Far from suggesting that brain regions are cut off from their neighbors, the observation that highly-active memory regions significantly increase their theta synchronization offers a low-frequency mechanism by which the brain coordinates its many parts – a brain-wide finding that was suggested by prior studies which could only examine specific interactions[73,84]. Furthermore, our results demonstrate how theta networks exhibit time-varying structure, highlighting frontotemporal hubs that strengthen their connections starting 500 ms after onset of an item to be remembered. The fMRI connectivity literature parallels this, demonstrating broad, low-frequency networks that act to support human memory by convergence on the MTL[7,10,85,86]. The extent to which whole-brain iEEG-based networks overlap with fMRI networks is unexplored territory.

A small subset of electrodes exhibited increased narrowband gamma-oscillatory power associated with successful memory encoding. We observed increased long-range phase synchronization among this subset at the frequency of maximal oscillatory activity. This indicates that, in some instances, gamma-band activity is organized into coherent, oscillatory waves that may serve to coordinate activity between different regions. The rareness of this phenomenon should not be understated; statistically reliable oscillatory SMEs were detected in only 1% of electrodes in our 294-subject dataset.

A prior study by Burke, et al. in 2013 also suggested a general decrease in gamma synchronization and increase in theta during memory encoding in humans, but only at the level of lobe-wise interactions[84]. The findings presented here extend that work in several important ways. First, we establish that decreases in synchrony accompany increases in high-frequency power, and that this fundamental relationship between power and synchrony manifests itself throughout the human brain. Second, we examined synchrony dynamics at a much finer spatial scale, allowing for the possibility that aggregation by lobe obscured synchronous gamma activity between nearby regions. Third, we teased out oscillatory effects in gamma, demonstrating that while synchrony is observed in rare instances, successful human cognition is overwhelmingly associated with a relative increase in asynchronous high-frequency signal.

Our data demonstrate the existence of two forms of gamma: Broadband asynchronicity, more common, and more rarely, narrow-band synchronous oscillations featuring long-range synchronization. Typically, the asynchronous broadband signal overwhelms the rare instances of oscillatory synchronization, explaining the widespread high-frequency desynchronization we found. These findings help reconcile a discrepancy in the synchronization literature: There is an established body of animal work in which cellular-scale recordings document high-frequency synchronization within or between inferotemporal, medial temporal, prefrontal, and occipital cortices during cognition[57,58,87–89]. But a far more tenuous corpus exists for humans at the macroelectrode scale – intracranial reports of synchronous gamma activity are rare and often simultaneously find significant periods of desynchronization[59,60,66]. Here, we quantified the extent to which human cognition is associated with two high-frequency neural dynamics, and found a predominant asynchronous signal at all frequencies above 30 Hz alongside a minority oscillatory synchronous signal. It is likely that more robust oscillatory activity can be detected with microelectrode recordings – as in prior animal work – but the results here speak against the importance of such dynamics at the scale of iEEG.

Whole-brain connectivity patterns still must be characterized in alternative memory paradigms, and other cognitive tasks altogether. Here, we investigated functional connectivity during a free recall task, a prominent technique used to probe contextually-mediated episodic memory. In freely recalling items from a previously studied list, subjects engage in a process of cue-dependent retrieval, wherein the cue for each recalled item includes information about the context of the target list and the previously recalled items. While this procedure disentangles neural activity from the influence of an external stimulus, experimenter-cued memory paradigms – especially cued recall and recognition – can provide additional valuable information about the time-course of item retrieval.

The whole-brain connectivity network we report here extends the active frontier of network neuroscience[39]. By enabling the assessment of networks at different timescales of neural activity, whole-brain iEEG studies provide insights that go beyond non-invasive techniques – for example, the present study identified essentially opposite dynamics

between low and high frequency activity, which cannot be assessed by fMRI. By expanding our understanding of connectivity to the dimension of temporal frequency, this enhanced window into neural communication could reveal new ways in which network dynamics correlate with, or even predict, disease states[90,91]. Connectivity maps also inform the use of direct brain stimulation as a therapeutic intervention – functional connectivity could serve as a model for predicting how stimulation effects propagate from one region to another, influencing activity throughout the brain[92]. If these connectivity-based models of brain function prove to be reliable, they may help clinicians use stimulation to repair the brain activity underlying damaged cognitive processes[51], such as memory deficits in patients with traumatic brain injury or neurodegenerative disease.

Distributed networks of electrical activity in the brain have remained largely uncharacterized despite their critical role in human cognition[25]. During memory encoding and retrieval, we discovered that whole-brain gamma networks were largely asynchronous, while theta networks were synchronous and specifically engaged among regions with a high degree of local processing. Our results lay the foundation for future study of low-frequency electrical networks as the primary driver of interregional communication in the human brain.

Methods

Participants

294 patients with medication-resistant epilepsy underwent a surgical procedure to implant subdural platinum recording contacts on the cortical surface and within brain parenchyma. Contacts were placed so as to best localize epileptic regions. Data reported were collected at 10 hospitals over 14 years (2003-2017). Prior to data collection, our research protocol was approved by the Institutional Review Board at participating hospitals, and informed consent was obtained from the participants and their guardians.

Free-recall task

Each subject participated in a delayed free-recall task in which they studied a list of words with the intention to commit the items to memory. The task was performed at bedside on a laptop, using PyEPL software. Analog pulses were sent to available recording channels to enable alignment of experimental events with the recorded iEEG signal.

The recall task consisted of three distinct phases: encoding, delay, and retrieval. During encoding, lists of 12 words were visually presented in the native language (either English or Spanish) of the subject. Words were selected at random, without replacement, from a pool of nouns (http://memory.psych.upenn.edu/WordPools). Word presentation lasted for a duration of 1600 ms, followed by a blank inter-sitmulus interval of 750 to 1000 ms. Presentation of word lists was followed by a 20 second post-encoding delay. Subjects performed an arithmetic task during the delay in order to disrupt memory for end-of-list items. Math problems of the form A+B+C=?? were presented to the participant, with values of A, B, and C set to random single digit integers. After the delay, a row of asterisks, accompanied by a 60 Hz auditory tone, was presented for a duration of 300 ms to signal the start of the recall period. Subjects were instructed to recall as many words as possible from the most recent list, in any order during the 30 second recall period. Vocal responses were digitally recorded and parsed offline using Penn TotalRecall (http://memory.psych.upenn.edu/TotalRecall). Subjects performed up to 25 recall lists in a single session.

A subset of 92 patients performed a variant of the previously described task. List presentation consisted of a total of 15 items. In addition, a green fixation cross served as a list-cue to signal an upcoming list of words. The list-cue was presented for a duration of 1600 ms, followed by the presentation of a blank screen for 800 to 1200 ms. The ISI in this variant of the task lasted from 800 to 1200 ms in duration. The recall period for this version of the task was 45 seconds in length.

Electrocorticographic recordings

iEEG signal was recorded using subdural grids and strips (contacts placed 10 mm apart) or depth electrodes (contacts spaced 5-10 mm apart) using recording systems at each clinical site. iEEG systems included DeltaMed XlTek (Natus), Grass Telefactor, and Nihon-Kohden EEG systems. Signals were sampled at 500, 512, 1000, 1024, or 2000 Hz, depending on hardware restrictions and considerations of clinical application. Signals recorded at individual electrodes were converted to a bipolar montage by computing the difference in signal between adjacent electrode pairs on each strip, grid, and depth electrode. Bipolar signal was notch filtered at 60 Hz with a fourth order 2 Hz stop-band butterworth notch filter in order to remove the effects of line noise on the iEEG signal.

Anatomical localization

Anatomical localization of electrode placement was accomplished using independent processing pipelines for depth and surface electrode localization. For patients with MTL depth electrodes, hippocampal subfields and MTL cortices were automatically labeled in a pre-implant, T2-weighted MRI using the automatic segmentation of hippocampal subfields (ASHS) multi-atlas segmentation method[42]. Post-implant CT images were coregistered with presurgical T1 and T2 weighted structural scans with Advanced Normalization Tools[93]. MTL depth electrodes that were visible on CT scans were localized within MTL subregions by neuroradiologists with expertise in MTL anatomy[94]. Subdural electrodes were localized by reconstructing whole-brain cortical surfaces from pre-implant T1-weighted MRIs using Freesurfer[95]. Regions of interest (ROI) used for connectivity analyses were given by the Talairach label of a given electrode's position after mapping final contact locations to Talairach space, with the exception of any electrode localized to a hippocampal subfield, which were collectively labeled "hippocampus." We considered 37 possible labels for each hemisphere, or 74 total.

In a subset of 92 patients, contact localization was accomplished by coregistering the postoperative CTs with post- or pre-operative MRIs using FSL (FMRIB Software Library)

BET (Brain Extraction Tool) and FLIRT (FMRIB Linear Image Registration Tool) software packages.

Contacts placed in an epileptogenic area or in non-neural tissue (as determined by a clinician) were excluded from all the analyses in this report.

Data analyses and spectral decomposition

iEEG signals were all treated as bipolar montages (a difference in the raw signals from two adjacent electrodes), with sampling rates varying between 500 Hz and 2000 Hz, depending on the subject. We convolved the signal (downsampled to 500 Hz) from each bipolar electrode in each subject with complex-valued Morlet wavelets (wave number 5) to obtain phase and power information. We used 35 wavelets from 3-120 Hz, though most analyses focus on the 45-100 Hz (high gamma) and 3-8 Hz (theta) ranges (HG: 11 wavelets spaced 5 Hz, except between 90Hz and 100Hz; theta, 6 wavelets space 1 Hz). Each wavelet was convovled with 3600 ms of data surrounding each word presentation (referred to as "trial," 1000 ms before word onset to 2600 ms after word onset), and buffered with 1000ms on either end (clipped after convolution).

For each subject, for all possible pairwise combinations of electrodes, we compared the distributions of phase differences in all remembered trials against all not-remembered trials, asking whether there is a significantly higher concentration, or tightness of the distribution, in one or the other (Fig. 1B). To do this, we found the difference of the mean resultant vector lengths (often called phase-locking value) of the remembered and not-remembered phase difference distributions ($\bar{R}$ values computed with Circular Statistics Toolbox)[96]:

$$D_{pq}(f,t) = \bar{R}_{\mathrm{rem}} - \bar{R}_{\mathrm{nrem}}$$

Where $\bar{R}_{\mathrm{rem}}$ and $\bar{\mathrm{R}}_{\mathrm{nrem}}$ refer to the mean resultant vector lengths of all remembered and not-remembered trials, *pq* is an electrode pair, *f* is a frequency band, and *t* is a window in time.

Intuitively, a higher resultant vector length (which falls between 0 and 1) reflects a tighter distribution of phase differences and greater synchronization between two electrodes. Therefore, higher positive differences (*D*) indicate greater phase-locking for remembered trials, whereas lower negative differences reflect greater phase-locking for not-remembered trials. *D* was computed for each frequency spanning a range from 3 to 120 Hz, and for 18 non-overlapping 200ms time windows spanning the trial, by averaging phase difference values within those windows before computing phase-locking values and their corresponding *D*. Unless stated otherwise, the analyses in this report consider only the eight 200 ms windows between word onset (0 ms) and offset (1600 ms), called the "item presentation interval."

$\bar{R}$ values are biased by the number of vectors in a sample. Since our subjects generally forget more words than they remember (Figure 3.S1), we adopt a nonparametric permutation test of significance. For each subject, and each electrode pair, the phase-synchrony computation described above was repeated 500 times with the trial labels shuffled, generating a distribution of *D* statistics that could be expected by chance for every electrode pair, at each frequency and time window. Since only the trial labels are shuffled, the relative size of the surrogate remembered and not-remembered samples also reflect the same $\bar{R}$ sample size bias. Consequently, the true *D* (D_{true}) can be compared to the distribution of null *D*s to derive a p-value or z-score. Higher z-scores indicate greater synchronization between a pair of electrodes for items that are later recalled.

To construct a network of phase synchrony effects between all brain regions, we pooled synchrony effects across electrode pairs that span a pair of ROIs, and then pooled these ROI-level synchronizations across subjects with that pair of ROIs sampled (ROIs were determined by the Talairach label for each electrode after coregistration). To do this, we first averaged the D_{true} values across all electrode pairs that spanned a given pair of ROIs within a subject. Next, we averaged the corresponding null distributions of these electrode pairs, resulting in a single D_{true} and a single null distribution for each ROI pair in a subject. We then averaged the D_{true} values and null distributions across all subjects with electrodes in a given ROI pair. By comparing the averaged D_{true} to the averaged null distribution, we

computed a z-score at each frequency and temporal epoch that indicates indicating significant phase-synchrony or asynchrony, depending on which tail of the null distribution the true statistic falls. Higher z-scores indicate greater synchronization between a pair of ROIs for items that are later recalled.

Network construction and analyses

Using the population-level statistics described above, a 74-by-74 adjacency matrix was constructed for each of the 18 non-overlapping temporal epochs and for each frequency. This matrix represented every possible interaction between all ROI pairs. The z-score of the true *D* relative to the null distribution was used as the connection weight of each edge in the adjacency matrix. Negative weights indicate ROI pairs that, on average, de-synchronized when a word was recalled successfully, and positive weights indicate ROI pairs that synchronized when a word was recalled successfully. We zeroed-out any ROI pairs in the adjacency matrix represented by less than 7 subjects' worth of data, to limit the likelihood that our population-level matrix is driven by strong effects in a single or very small number of individuals. 1,243 ROI pairs (out of a possible total of 2,701) were excluded due to low subject counts, comprised largely of interhemispheric pairs (795 pairs, or 64% of those excluded) and pairs involving regions where electrodes are less commonly placed, including basal ganglia and occipital cortex.

Since it is possible that collections of weaker connection weights may still account for significant structure in our network, we did not apply a z-score threshold before further analyses. To assess for the significance of phenomena at the network level, we instead used 500 null networks that can be constructed on the basis of *D*s derived from the shuffled trial labels to generate a distribution of chance network-level statistics. True statistics were compared to these null distributions to obtain a p-value or z-score (e.g. network-wide summed connection weights were computed for true and null networks and reported in Figure 3.1f, 3.2a, and 3.6b).

Accordingly, for every operation performed on the true connectivity network, the same was done on each of the 500 null networks that reflect connection strengths expected by chance.

For example, to ask whether a ROI has a significantly increased node strength at a given point in time (see subsection on Hub analysis), node strength was computed for each of the 500 null networks to generate a distribution of strengths expected by chance. The true node strength is compared to the null distribution in order to get a Z-score or p-value.

Adjacency matrices reflect the average connectivity strength during the item presentation interval (0-1600 ms) for each frequency band. To create them, we averaged true connection strengths within frequency bands, then averaged across the eight 200 ms time windows in this interval, and compared the result to the time/frequency average from each of the 500 null networks, resulting in a new Z-score for the time/frequency-averaged network (Figure 3.1d).

Hub analysis

To identify which ROIs are more highly synchronous or asynchronous, we used the node strength statistic from graph theory to identify "hubs" of the network. Node strength reflects the sum of all connection weights to a particular node (or ROI) in the network, and is formalized as:

$$k_i^w = \sum_{j \in N} w_{ij}$$

Where k is the node strength of node i, and w_{ij} refers to the edge weight between nodes i and j. N is the set of all nodes in the network[39].

To identify hubs during the word presentation interval, we first averaged connection weights within a frequency band and across the presentation interval (as done in Figure 3.1). Each ROI's node strength is then computed with these time/frequency-averaged weights, per the equation above. The same procedure was done for each of the 500 null networks generated from shuffled trial labels (see "Network construction and analyses"), creating a null distribution of node strength for each ROI. P-values were obtained by observing where a true node strength falls in its corresponding null distribution. Final p-

values were corrected for multiple comparisons (Benjamini-Hochberg procedure, $\alpha = 0.05$ or 0.01) to yield the final tally of significant hubs. This process was done for all synchronous ($Z > 0$) and asynchronous ($Z < 0$) connections separately, yielding synchronous and asynchronous collections of hub ROIs. For visualization only, connections depicted in Figure 3.3 were derived by ranking the time/frequency averaged connection weights of each hub, and selecting up to the top 5 connections above a Z-score of 2.5.

To construct ROI activation timecourses, we compared the frequency-averaged node strength at each time window against its corresponding null distribution to generate a Z-score and a p-value, done separately for all positive and negative connection weights. Our selection of right and left medial temporal lobe, frontal, and temporal cortices was driven by their implication in memory in prior literature[5,84,97] and the presence of gamma and/or theta-band hubs in each of those broad regions (Figure 3.4).

Power-synchrony analysis

Spectral power was obtained by the same Morlet wavelet convolution as used to extract phase information (see "Data analyses and spectral decomposition"). For all bipolar electrodes in each subject, we log transformed and z-scored power within each session of the free-recall task, which comprises approximately 300 trials. Power values were then averaged into 8 non-overlapping 200 ms windows spanning the entire trial, matching our procedure for phase synchrony.

To assess the statistical relationship between power and later recollection of a trial word (called the subsequent memory effect, or SME), power values for each electrode, trial, time, and frequency were separated into two distributions according to whether the trial word was later remembered or not-remembered, and Welch's t-test was performed to compare the means of the two distributions. Next, we shuffled the trial labels 500 times and recomputed the t-statistic, reflecting power effects that could be observed by chance. The true t-statistics were averaged across all electrodes that occur in a given ROI, as are the null distributions, and those statistics are next averaged across all subjects with electrodes in that ROI. Finally, the averaged true t-statistic was compared to the averaged null

distributions to get a z-score at each time-frequency point for a given ROI. These z-scores are reported as a heatmap in Figure 3.5b, and we find the Pearson correlation against node strength Z-scores as described in "Hub analysis" (i.e. a correlation across time-frequency pixels). Correlation P-values are then FDR corrected for multiple comparisons (corrected $P < 0.05$).

To assess correlations across all time and all ROIs (Figures 3.5c, 3.7d) or ROI subsets (Figure 3.6), we first averaged Z-scored node strength and Z-scored power within each frequency band. Then, we correlated the strength and power values across all item-presentation timepoints and all ROIs (i.e. each vector contains time windows by # ROIs total elements). To assess significance of these correlations, we adopted a permutation procedure that maintains the spatial and temporal dependency between data points: We assessed the power-synchrony correlation for each possible 1-shift of one vector against the other, and again for the mirror image of that vector. This procedure resulted in a distribution of chance correlations, against which we compared the true correlation to obtain a p-value.

Retrieval analysis

To find out whether principles of brain function uncovered in the memory encoding contrast generalize to different cognitive operations, we further analyzed connectivity in a retrieval contrast. This was done in a manner similar to Burke, et al. 2014[26], as follows. For each subject, we identified any 500 ms interval during the recall period after which no response vocalization occurred for at least 2 seconds, and compared the neural activity in these "unsuccessful memory search" intervals to the 500 ms of activity immediately prior to successful item recollection. Phase difference values were averaged across two 250 ms time windows spanning these trials, as opposed to 200 ms windows in the encoding analysis. All other data analysis and spectral methods were matched exactly. This analysis was performed on a subset of 197 subjects with detailed retrieval-period information.

Oscillations analysis

We adopted a widely-used method for oscillation detection, called $P_{episode}$ or BOSC[81,98,99] ("Better OSCillation detection"). Briefly, this method applies two criteria for the identification of a true oscillation: a minimum time (at least 3 cycles), and a significant deviation of spectral power from a robust linear fit to the log-frequency vs. log-power curve (a spectral "peak", see Fig. 8a for an example). For each timepoint and frequency assessed, BOSC indicates whether an oscillation is present under these criteria. For further details on BOSC implementation, see Hughes et al. (2012).

For each electrode in our dataset, we used BOSC to find out whether the presence of low gamma (30-58 Hz, to minimize line noise artifact) oscillations was correlated with whether a word would later be remembered or forgotten ("oscillatory SME"). We used this range because at higher frequencies, the BOSC measure becomes less reliable as the log-frequency vs. log-power becomes nonlinear. For every trial, we computed the fraction of time occupied by an oscillation in each of eight 200ms window spanning the 1600ms item presentation interval, doing so for 18 log-spaced frequencies between 30 and 58 Hz. The result was a measure of oscillatory activity in each time/frequency pixel for each trial. We then grouped the trials by whether the word presented was later remembered or forgotten, and computed Welch's t-test between the remembered and forgotten distributions. P-values were FDR corrected for multiple comparisons across time/frequency pixels ($\alpha = 0.1$, a deliberately liberal threshold to allow for enough electrodes to analyze pairwise synchronization). The count of electrodes with significant memory-correlated oscillatory power is depicted in Figure 3.8c.

To determine whether an electrode exhibited an SME without directly assessing for oscillations (and thus capturing elevations in spectral power due to non-oscillatory activity), we computed an electrode's spectral power SME (described in "Power-synchrony analysis" above) averaged across 5-Hz spaced frequencies within the 30-60 Hz and 65-100 Hz bands at each of the eight 200ms windows. P-values were FDR-corrected and declared significant at $\alpha = 0.1$, as above. The count of electrodes with significant SMEs at the 400-600ms window is depicted in Fig. 3.8d.

Since the number of electrodes exhibiting gamma oscillatory SMEs is small (approx. 260), the networks that can be constructed from that dataset are sparse. Accordingly, the same procedure as described in "Data analyses and spectral decomposition" and "Network construction and analysis" is used on this small subset of electrodes (found in 44 subjects) to generate a map of some pairwise ROI synchronizations – a subnetwork – but not a whole-brain network. No threshold was applied on the number of subjects needed to contribute to an ROI pair. In Fig. 3.8e, subnetwork connection z-scores during the 400-600 ms window were tested for significance at the $P<0.05$ level (uncorrected), and compared against the number of significant connections expected at that level by chance (i.e. shuffled trial labels). 50-55 Hz were chosen as the closest frequencies to the frequency of maximal oscillatory SME (approx. 52 Hz). In Fig. 3.8f, the z-scored mean subnetwork connection weight at 400-600 ms was plotted as a function of frequency.

Supplemental Figures

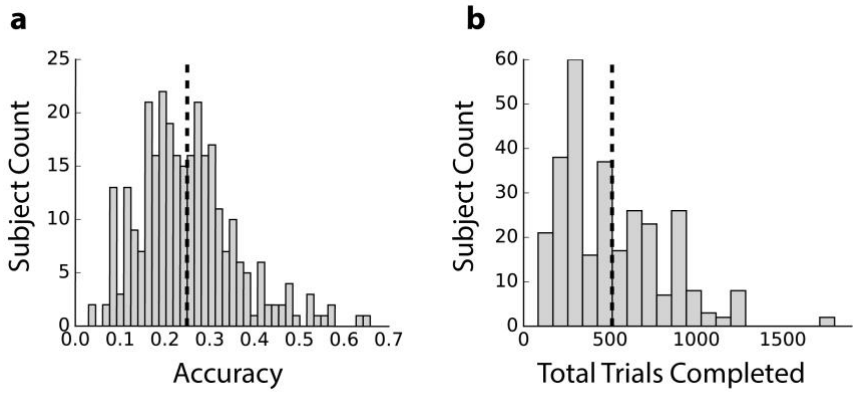

Figure 3.S1. Free-recall behavioral results. (a) Distribution of subject accuracy on the verbal delayed free-recall task, mean indicated by vertical line (n=294). (b) Distribution of number of total trials (i.e. word presentations) completed by each subject.

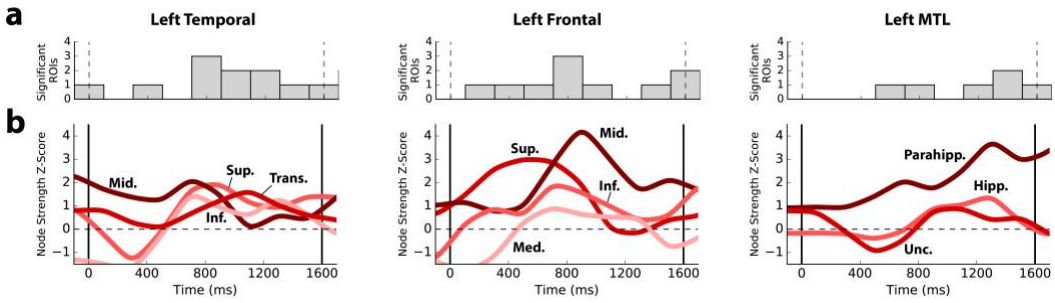

Figure 3.S2. Left-hemispheric theta (3-8 Hz) hub timecourses. (Figures organized according to caption of Figure 3.3 in the main text.) (a) Count of significant (P<0.05) node strength for ROIs within three broad regions: left temporal, frontal, and medial temporal lobes. (b) Smoothed timecourses of node strength for each ROI.

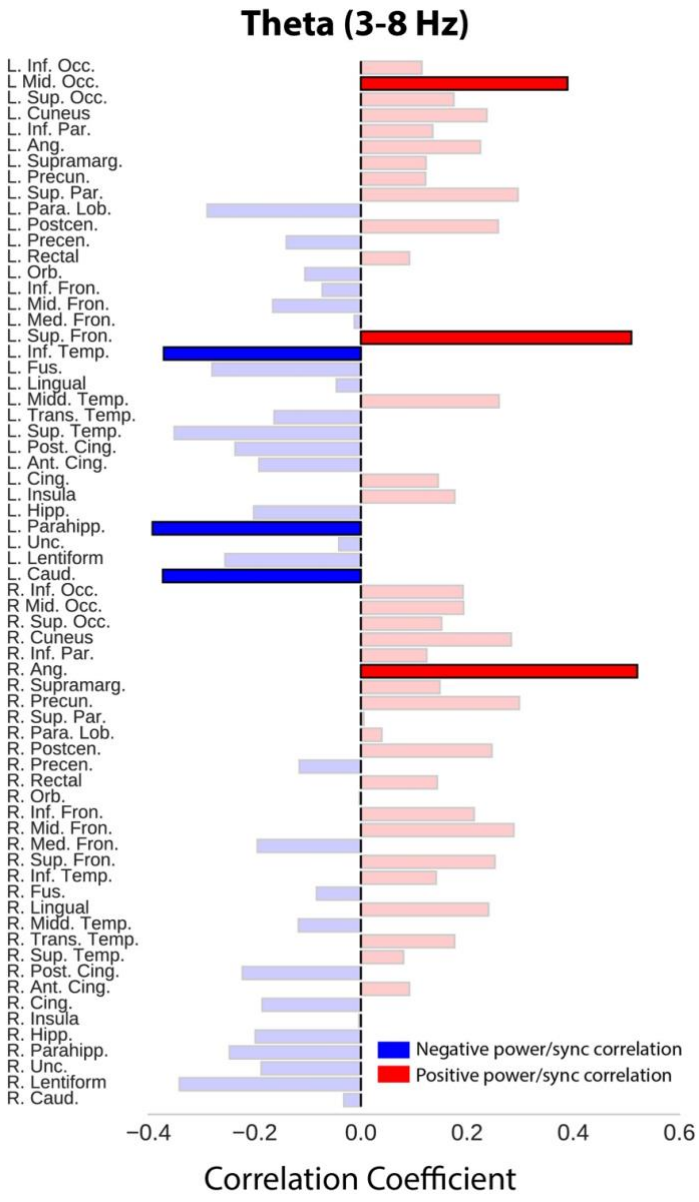

Figure 3.S3. Power-synchrony correlation in the theta band. Correlation of the modulation of theta (3-8 Hz) node strength and power across time and frequency for each ROI, during the word encoding interval (0-1600ms). Bar plots show the power-synchrony correlation for each ROI, with blue indicating negative and red indicating positive correlations. Faded bars are not significant after FDR correction for multiple comparisons (α = 0.05).

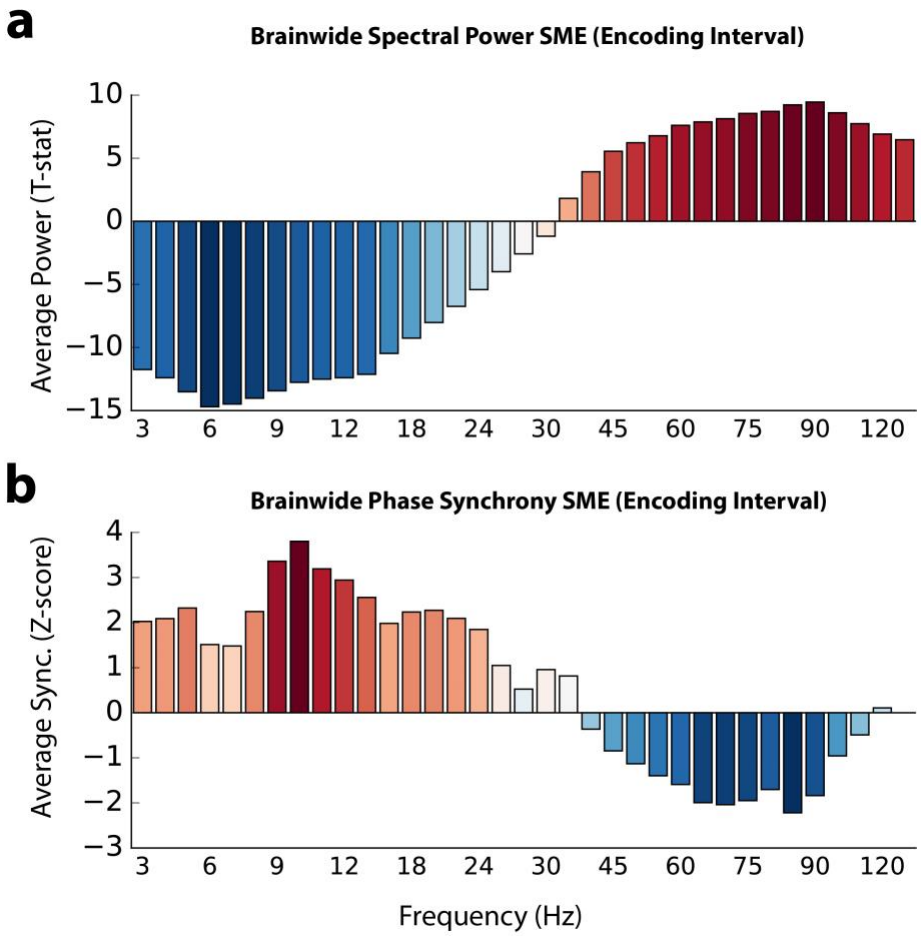

Figure 3.S4. Memory-associated brainwide spectral power and phase synchrony in the encoding interval (0-1600 ms). (a) Average brainwide t-statistic reflecting the relative change in spectral power across all electrodes and all subjects in remembered vs. not-remembered conditions (see Fig. 3.S2 and methods for details). (b) Average brainwide z-score reflecting the relative change in phase synchrony across all electrode pairs and all subjects in remembered vs. not-remembered conditions.

Region Name	Abbreviation	Z-score
Core Memory Network (in-network), corrected *P* < 0.01		
R. Extra-Nuclear	R. Extra-Nuc	N/A
R. Parahippocampal Gyrus	R. Parahipp.	4.11
R. Subgyral	R. Subgyral	N/A
R. Lingual Gyrus	R. Lingual	6.71
R. Fusiform Gyrus	R. Fus.	6.77
R. Middle Frontal Gyrus	R. Mid. Fron.	4.86
R. Inferior Frontal Gyrus	R. Inf. Fron.	5.66
R. Precentral Gyrus	R. Precen.	5.32
R. Superior Parietal Lobule	R. Sup. Par.	3.65
R. Cuneus	R. Cuneus	6.15
R. Superior Occipital Gyrus	R. Sup. Occ.	4.25
R. Middle Occipital Gyrus	R. Mid. Occ.	11.86
R. Inferior Occipital Gyrus	R. Inf. Occ.	11.05
L. Extra-Nuclear	L. Extra-Nuc.	N/A
L. Uncus	L. Unc.	5.07
L. Parahippocampal Gyrus	L. Parahipp.	8.53
L. Hippocampus	L. Hipp.	5.30
L. Cingulate	L. Cing.	4.99
L. Subgyral	L. Subgyral	N/A
L. Superior Temporal Gyrus	L. Sup. Temp.	3.97
L. Middle Temporal Gyrus	L. Mid. Temp.	9.18
L. Lingual Gyrus	L. Lingual	5.46
L. Fusiform Gyrus	L. Fus.	12.21
L. Inferior Temporal Gyrus	L. Inf. Temp.	9.21
L. Superior Temporal Gyrus	L. Sup. Temp.	7.75
L. Medial Frontal Gyrus	L. Med. Fron.	4.40
L. Middle Frontal Gyrus	L. Mid. Fron.	14.31
L. Inferior Frontal Gyrus	L. Inf. Fron.	14.12
L. Orbital Gyrus	L. Orb.	5.04
L. Precentral Gyrus	L. Precen.	4.72
L. Postcentral Gyrus	L. Postcen.	6.13
L. Superior Parietal Lobule	L. Sup. Par.	6.02
L. Supramarginal Gyrus	L. Supramarg.	5.48
L. Inferior Parietal Lobule	L. Inf. Par.	7.69
L. Cuneus	L. Cuneus	6.77
L. Middle Occipital Gyrus	L. Mid. Occ.	12.20
L. Inferior Occipital Gyrus	L. Inf. Occ.	5.67
Non-Memory Network (out-of-network), corrected *P* > 0.01		
R. Thalamus	R. Thal.	2.29
R. Caudate	R. Caud.	1.81
R. Lentiform Nucleus	R. Lentiform	0.46
R. Uncus	R. Unc.	-0.37
R. Subcallosal Gyrus	R. Subcall.	0.49

R. Hippocampus	R. Hipp.	1.01
R. Insula	R. Insula	-0.29
R. Cingulate	R. Cing.	1.65
R. Anterior Cingulate	R. Ant. Cing.	0.12
R. Posterior Cingulate	R. Post. Cing.	0.13
R. Superior Temporal Gyrus	R. Sup. Temp.	-2.26
R. Transverse Temporal Gyrus	R. Trans. Temp.	-0.09
R. Middle Temporal Gyrus	R. Mid. Temp.	1.78
R. Inferior Temporal Gyrus	R. Inf. Temp.	0.80
R. Superior Frontal Gyrus	R. Sup. Fron.	0.80
R. Medial Frontal Gyrus	R. Med. Fron.	-1.39
R. Orbital Gyrus	R. Orb.	0.93
R. Rectal Gyrus	R. Rectal	0.94
R. Postcentral Gyrus	R. Postcen.	1.67
R. Paracentral Lobule	R. Para. Lob.	-0.46
R. Precuneus	R. Precun.	0.86
R. Supramarginal Gyrus	R. Supramarg.	-2.30
R. Angular Gyrus	R. Ang.	-1.52
R. Inferior Parietal Lobule	R. Inf. Par.	-0.69
L. Thalamus	L. Thal.	1.64
L. Caudate	L. Caud.	1.35
L. Lentiform Nucleus	L. Lentiform	-0.19
L. Subcallosal Gyrus	L. Subcall.	0.96
L. Insula	L. Insula	1.78
L. Anterior Cingulate	L. Ant. Cing.	-1.29
L. Posterior Cingulate	L. Post. Cing.	2.50
L. Transverse Temporal Gyrus	L. Trans. Temp.	2.23
L. Rectal Gyrus	L. Rectal	2.01
L. Paracentral Lobule	L. Para. Lob.	-1.07
L. Precuneus	L. Precun.	0.17
L. Angular Gyrus	L. Ang.	-1.15
L. Superior Occipital Gyrus	L. Sup. Occ.	2.07

Table 3.T1. List of ROIs included in the core memory network. List of the 74 ROIs (37 per hemisphere) used in this study, with abbreviations. Z-scores reflect a comparison of the spectral power between remembered and not-remembered trials, averaged across subjects and electrodes. ROIs in the core memory network had significant power differences between the two conditions ($P < 0.01$, Benjamini-Hochberg corrected for multiple comparisons; see Methods for details). Four subcortical ROIs indicated with N/A were excluded from this analysis due to limited data (less than 5 subjects with electrodes placed in the ROI).

CHAPTER 4:

Mesoscale Networks in the MTL

Solomon, Ethan A., et al. "Functional wiring of the human medial temporal lobe." *bioRxiv* (2018): 257899. (*in revision*)

Abstract

The medial temporal lobe (MTL) is a locus of episodic memory in the human brain. It is comprised of cytologically distinct subregions that, in concert, give rise to successful encoding and retrieval of context-dependent memories. However, the functional connections between these subregions are poorly understood. To determine functional connectivity among MTL subregions, we had 126 subjects fitted with indwelling electrodes perform a verbal memory task, and asked how encoding or retrieval correlated with interregional synchronization. Using phase-based measures of connectivity, we found that synchronous theta (4-8 Hz) activity underlies successful episodic memory, whereas high-frequencies exhibit desynchronization. Moreover, theta functional connectivity during encoding aligned with key anatomic connections, including critical links between the entorhinal cortex, dentate gyrus, and CA1 of the hippocampus. Retrieval-associated networks demonstrated enhanced involvement of the subiculum, reflecting a substantial reorganization of the encoding-associated network. We posit that coherent theta activity within the MTL marks periods of successful memory, but distinct patterns of connectivity dissociate key stages of memory processing.

Introduction

Storing episodic memory is an inherently integrative process, long conceptualized as a process that links information about new items to an observer's current thoughts, emotions, and environment[5]. Decades of behavioral observations, clinical case studies, and scalp electroencephalography (EEG) in humans have shed light on the key principles and diverse set of brain structures underlying this integration, including frontal, lateral temporal, and medial temporal cortex (MTL)[80]. Recent hypotheses invoke the idea that communication among these regions supports memory formation, spurred by a growing number of functional imaging and intracranial EEG (iEEG) experiments that show synchronized activity among the MTL and cortical structures during memory tasks[6,70,100,101].

However, the MTL has a unique role in supporting episodic memory. Damage to the MTL results in profound deficits of memory[102], and it has been shown to exhibit enhanced neural activity during memory processing in a range of tasks and experimental models[82,103], identifying this area as a key anatomic hub of episodic encoding and retrieval. The MTL is structurally complex; it is subdivided into hippocampus, rhinal cortex, and parahippocampal cortex. The cornu ammonis (CA), dentate gyrus, and subiculum comprise the hippocampus, while the entrorhinal and perirhinal cortices form rhinal cortex. Microscale recordings in animals have revealed that these substructures exhibit distinct patterns of activity during memory and navigation tasks, including the generation of oscillations, inter-regional synchronization, and neuronal selectivity for time and space[57,104–109]. Computational models of MTL function have assigned unique roles to MTL substructures, pertaining to episodic encoding, retrieval, or recognition[104,110–113] – typically, these models suggest extrahippocampal regions are responsible for placing sensory inputs in a useful representational space, while the hippocampus itself forms associative links between these representations and their prevailing context.

Notably, virtually all of the aforementioned animal and modeling literature suggests that MTL substructures communicate with one another as they engage in memory processing. However, the volume of aforementioned work on intra-MTL connectivity has not been

matched by validation studies in humans. Though a handful of investigations have begun to address this question in neurosurgical patients[59,66,114], limited electrode coverage and imprecise localizations have made it difficult to study the fine spatial scale and complete extent of neural synchronization within the MTL. But doing so is a crucial component of (1) confirming that intra-MTL synchronization observed in animal models also correlates with memory processing in humans, and (2) validating models of MTL function that suggest communication among specific regions – such as rhinal cortex versus hippocampus – supports computations necessary for associative memory formation and retrieval.

The use of intracranial depth electrodes to study neural activity in the MTL also allows neural activity to be studied at different timescales. Slow theta (4-8 Hz) oscillations in the hippocampus have been observed during memory processing in humans[115–118], as have fluctuations at higher frequencies, including the gamma (30-60 Hz) band[119,120]. These oscillations have been theorized to support synchronization between neural assemblies in the MTL[108,110,121–123], but MTL connectivity has not been fully mapped across frequency bands. The extent to which different frequencies underlie neural synchronization in memory therefore remains an open question, though converging lines of evidence strongly suggest the most prominent connectivity effects occur at low frequencies[71,73,124–126]. Moreover, no studies have deeply considered how observations of within-MTL synchronization reflect an experimenter's choice of connectivity metric, including those that are designed to limit the effects of volume-conducted signals that may affect connectivities measured across relatively short distances[127].

In this study, we aimed to define the patterns of functional connectivity that emerge in the human MTL and to specifically characterize how MTL-subregional connectivity differs when memories are being stored versus when they are being subsequently retrieved. Additionally, we asked whether functional networks were sensitive to the choice of connectivity metric, utilizing the phase-locking value (PLV) and weighted phase-lag index (wPLI; insensitive to volume conduction). We leveraged a large dataset of 126 subjects with depth electrodes placed in the MTL, localized with hippocampal subfield resolution, and

focused on two key contrasts: (1) the encoding subsequent memory effect (SME), differentiating remembered from forgotten items, and (2) successful retrieval versus periods of unsuccessful memory search. We found that successful encoding was characterized by low-frequency connections which converged on left entorhinal cortex, while retrieval was associated with enhanced theta connectivity to the subiculum and CA1. However, these differing connectivity patterns were not correlated with markedly different patterns of local spectral power between encoding and retrieval, suggesting functional connections are a key mechanism by which the MTL may switch between distinct memory operations. Furthermore, we noted that theta-band connectivity was present regardless of choice of connectivity metric or referencing scheme, though connectivity was generally blunted when using the wPLI. Taken together, our findings show that low-frequency functional coupling in the MTL supports the formation of new memories, with the specific pattern of connections acting as the key determinant of successful encoding and retrieval, respectively.

Results

Our general approach to characterizing intra-MTL connectivity was to (1) examine the structure of functional connectivity networks using graph-theoretic analysis, (2) examine the timecourse of connectivity in key connections, and (3) relate changes in connectivity to changes in local activity, as reflected by spectral power. To do this, we correlated intra-MTL synchronization with memory state using two contrasts in a verbal free-recall paradigm. First, we examined the subsequent memory effect (SME), which has been widely employed to characterize whole-brain modulations of spectral power (e.g. Burke et al., 2014a, 2014b) that correlate with successful memory encoding. Second, we examined a memory retrieval contrast, wherein epochs of time leading up to verbalization of a recalled item are compared to matched epochs of time, from other word lists, where no recall occurs (e.g. 29, 40, 41; see Methods for details). We refer to these matched periods as “deliberation” intervals.

For each contrast, we constructed intra-MTL functional connectivity maps at each frequency band, using the phase-locking value (PLV) and weighted phase-lag index (wPLI). The PLV[76] has long been used to assess whether, across trials, there is a consistent phase difference between two electrodes. The wPLI is a more recent modification of the PLV[127], which downweights phase differences near zero under the assumption that two such electrodes are detecting a volume-conducted signal through brain tissue, and not true physiologic coupling (Figure 4.1D). We had 126 subjects perform a verbal free-recall task during which iEEG was collected from depth electrodes placed in the MTL. Subjects were serially presented with 12-item word lists and asked to recall as many words as possible after a brief distractor task (Figure 4.1A-C; see Methods for details). For each electrode pair, phase differences were computed for each trial, i.e. an encoding or retrieval event. Trials were sorted by whether a word was later recalled or forgotten (or, in the retrieval contrast, a successful retrieval event or matched deliberation; Figure 4.1E). PLV/wPLI were computed for successful/unsuccessful groups separately, and tested for significant differences via a nonparametric permutation procedure (see Methods for details). Effects were averaged across electrode pairs, subjects, and time, yielding a z-score that indicates the relative synchronization in successful vs. unsuccessful memory encoding/retrieval for each pair of MTL regions (see Figure 4.2A for an example pair; see Figure 4.S1 for subject count per region-pair). Unless indicated otherwise, we use a common average reference for all analyses; the bipolar reference is used in some cases to demonstrate generality of key results regardless of referencing scheme.

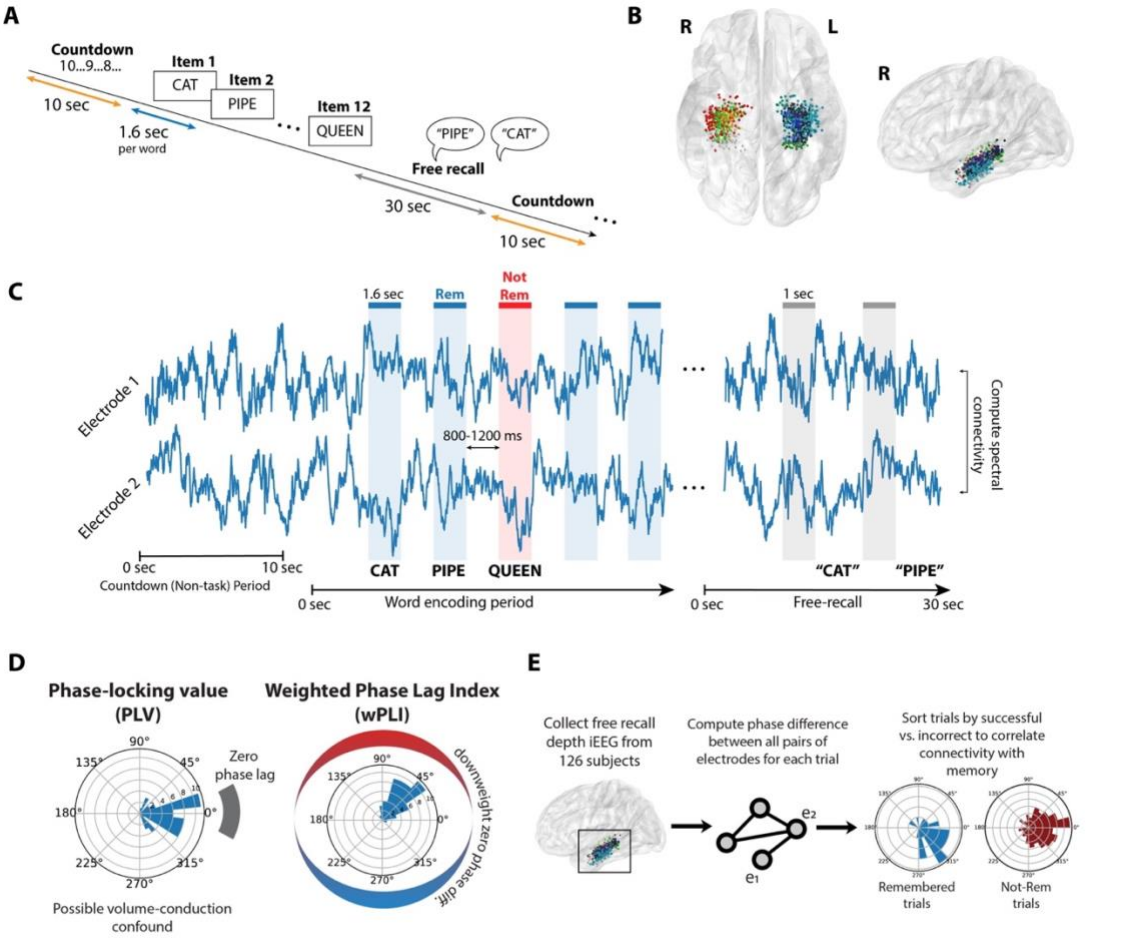

Figure 4.1. Task structure and analysis methods. A. Subjects performed a verbal free-recall task, consisting of alternating periods of pre-list countdowns (orange), word encoding (blue), and free-recall (gray). See Methods for details. **B.** 126 subjects with indwelling electrodes in the medial temporal lobe (MTL) participated. Electrodes were localized to CA1, CA3, dentate gyrus (DG), subiculum (Sub), perirhinal cortex (PRC), entorhinal cortex (EC), or parahippocampal cortex (PHC). Each dot shows an electrode in this dataset, colored by MTL subregion. **C.** To construct networks of intra-MTL activity, we used PLV and wPLI to analyze phase differences between electrode pairs. Time windows in two conditions were analyzed: 1.6-second epochs during word encoding (blue/red), and 1-second periods leading up to recall vocalizations (gray). **D.** PLV reflects the consistency of phase differences across trials, indicated in example data as clustered phase lags around zero (left). The wPLI works similarly, but downweights the contribution of phase lags near the zero axis, which may reflect volume conduction (right). Accordingly, stronger connectivity is observed if phase lags are clustered around a direction far from zero (or 180 degrees). **E.** To assess intra-MTL connectivity, phase differences are computed for each electrode pair in all trials, and trials are then sorted by successful vs. unsuccessful memory. PLV or wPLI is computed for each distribution, and a nonparametric permutation procedure is used to determine whether connectivity is significantly different between distributions. Connectivity values are averaged across electrode

pairs and subjects to yield the final MTL network maps depicted in Figure 3.2 (see Methods for details).

Theta networks of memory encoding and retrieval

Given strong evidence in the literature for synchronous memory effects in the theta band[71,73,124–126], we first sought to characterize the detailed structure of theta networks in the MTL. To do this, we asked whether any regions acted as "hubs" of the MTL by computing the node strength for each region, using theta PLV connection weights. Node strength reflects the overall connectivity to a given node of the network by summing all of its connection weights. In the SME contrast, left entorhinal cortex emerged as a significant hub (corrected permuted $P < 0.05$; Figure 4.2D). In the retrieval contrast, left CA1 was numerically greatest and significant if not corrected for multiple comparisons (permuted $P = 0.013$; Figure 4.2F). The single strongest connection for the encoding/retrieval contrasts were EC-PRC ($Z = 2.65$) and CA1-Sub ($Z = 2.00$), respectively (see Figure 4.1 legend for region abbreviations). For each contrast, the strongest synchronous connections are depicted schematically in Figures 4.2C and 4.2E. In both retrieval and encoding, entorhinal cortex exhibits enhanced connectivity to CA1 and subiculum, with additional perirhinal-hippocampal connections present exclusively in encoding. Additionally, in both contrasts, connections within the left MTL are significantly greater than zero (encoding, $P = 0.005$; retrieval, $P = 0.04$), and stronger than connections within the right MTL, though not significantly so for encoding (encoding, $P = 0.15$; retrieval, $P = 0.03$).

These findings align with known anatomical connections and functional roles of MTL subregions. The entorhinal cortex acts as a key input structure to the hippocampus and represents the convergence of information from the perirhinal and parahippocampal cortices[1,130] – it is fitting that this structure exhibits enhanced theta connectivity to other MTL structures during with successful memory encoding. Furthermore, a reorganization of theta networks featuring enhanced connectivity between the subiculum and CA1 comports with anatomical connectivity and notion of subiculum's role as a major output structure of the hippocampus[131,132]. However, this network-based analysis (1) averages synchrony effects over the entire word presentation or retrieval intervals, obscuring time-varying

dynamics, and (2) considered only PLV connectivity, which may reflect nonphysiologic volume conduction.

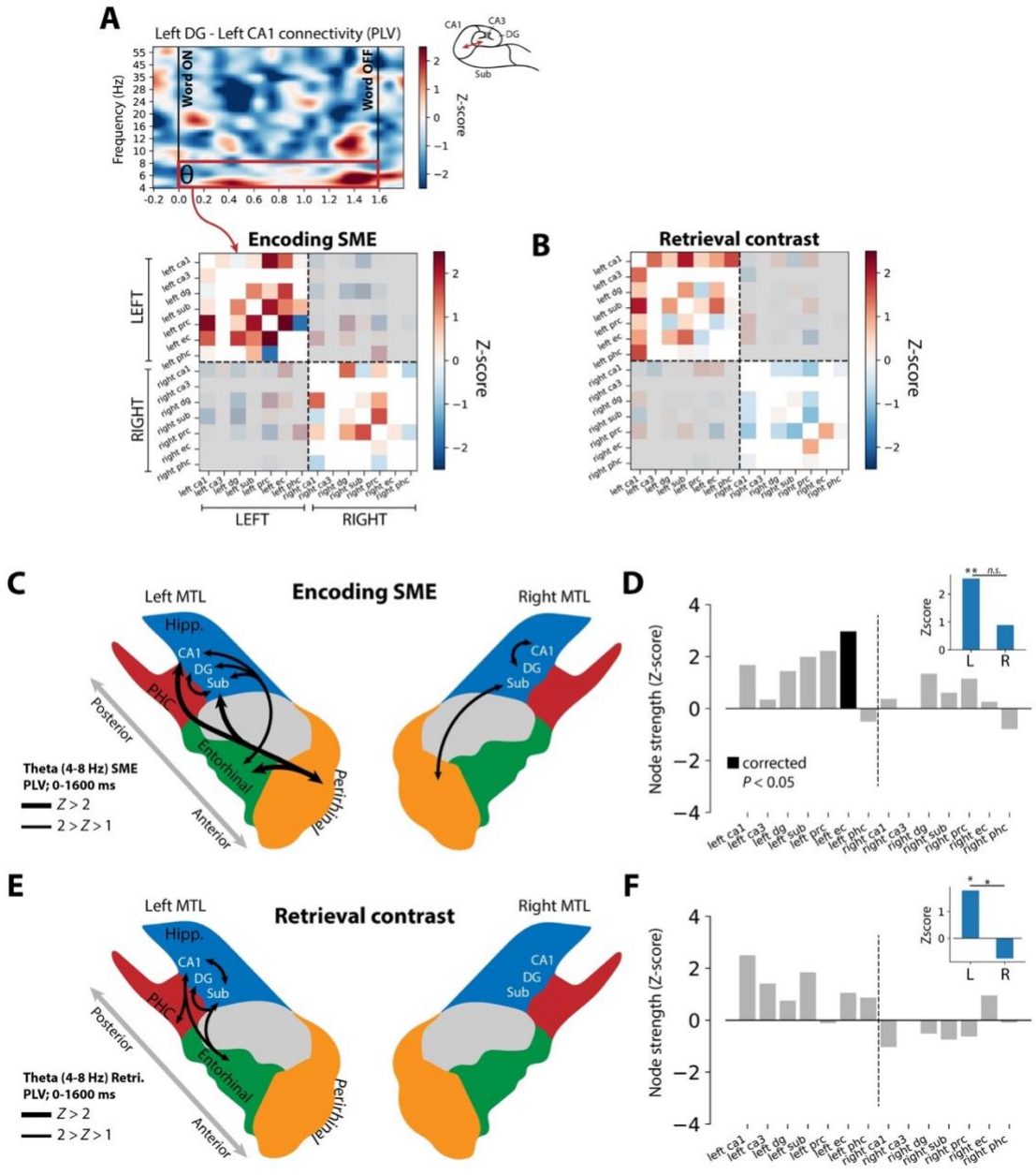

Figure 4.2. Structure of theta networks supporting episodic memory. A. To determine overall connectivity for each pair of MTL subregions, PLV or wPLI is averaged over the encoding (word presentation, 0-1.6 seconds) or retrieval (-1.0 to 0 seconds prior to retrieval onset) intervals, yielding

a single z-scored connection weight. (see Methods for details). The matrix representation of all these weights is called an adjacency matrix, shown here for the encoding contrast in the theta band (PLV). Any inter-regional connection with fewer than 5 subjects' worth of data is excluded from analysis (white cells). Because interhemispheric connections are less well sampled than intra-hemispheric connections, and because interhemispheric connectivity is largely asynchronous, they are excluded from this analysis of network structure (gray shading). **B.** Retrieval contrast theta adjacency matrix (PLV), organized as in (A). **C.** Depiction of strongest ($Z > 1$) synchronous PLV connectivity in the SME contrast, derived from the theta adjacency matrix in (A). These connections reflect the averaged connection strength over the word presentation interval (0.0-1.6 seconds; see Methods for details). Thicker lines reflect Z-scores above 2. **D.** Z-scored node strength for each MTL region, computed only for connections to ipsilateral MTL regions (see Methods for details). Node strength indicates the sum of all connections to a given region, with positive Z-scores indicating enhanced overall connectivity to a given region during successful encoding epochs (a "hub" of connectivity). Left EC exhibited significant positive node strength (FDR-corrected permuted $P < 0.05$) correlated with words that were successfully remembered. **Inset:** Z-scored total network strength for all intra-hemispheric MTL connections, computed by summing the connection weights for each hemisphere's MTL subregions separately. Intra-MTL connections on the left are significantly greater than chance ($P = 0.005$), and trend greater than right-sided connections ($P = 0.15$). **E.** Schematic of strongest theta retrieval connections, reflecting increased PLV between two MTL subregions in the 1-second immediately prior to successful retrieval of a word item. **F.** Same as (D), but reflecting synchronous activity from the 1-second period prior to successful retrieval of a word item. No region exhibits a significant node strength after correction for multiple comparisons, but left CA1 is significant if uncorrected ($P = 0.013$). **Inset:** Z-scored total network strength for all intra-hemispheric MTL connections. Left-sided connections are significantly greater than chance ($P = 0.04$) and significantly greater than right-sided connections ($P = 0.03$).

Temporal dynamics of memory-related connectivity

Having shown that encoding- and retrieval-associated theta networks differ in their structure but align with known anatomical connectivity of the MTL, we next asked whether our previously-identified synchronous connections exhibited time-varying dynamics. Additionally, we aimed to determine whether these connectivity effects were robust to use of the PLV or wPLI, which discounts phase differences near zero. In particular, we hypothesized that two possibilities could underlie changes in PLV and wPLI between conditions. First, tightly-clustered phase lags in a nonzero direction could rotate towards zero, resulting in a reduced wPLI since phase lags are downweighted closer to zero (Figure 4.3A, top row). In this case, PLV would remain unchanged. However, the correction for volume-conduction comes at a cost: tightly-clustered phase lags could still be well within a believable, nonzero range, yet wPLI would indicate a relative decrease in synchronization between conditions. The second possibility is that tightly clustered nonzero phase lags

could increase in variance between conditions, resulting in decreased PLV and wPLI (Figure 4.3A, bottom row). In experimental reality, both between-condition changes could occur simultaneously.

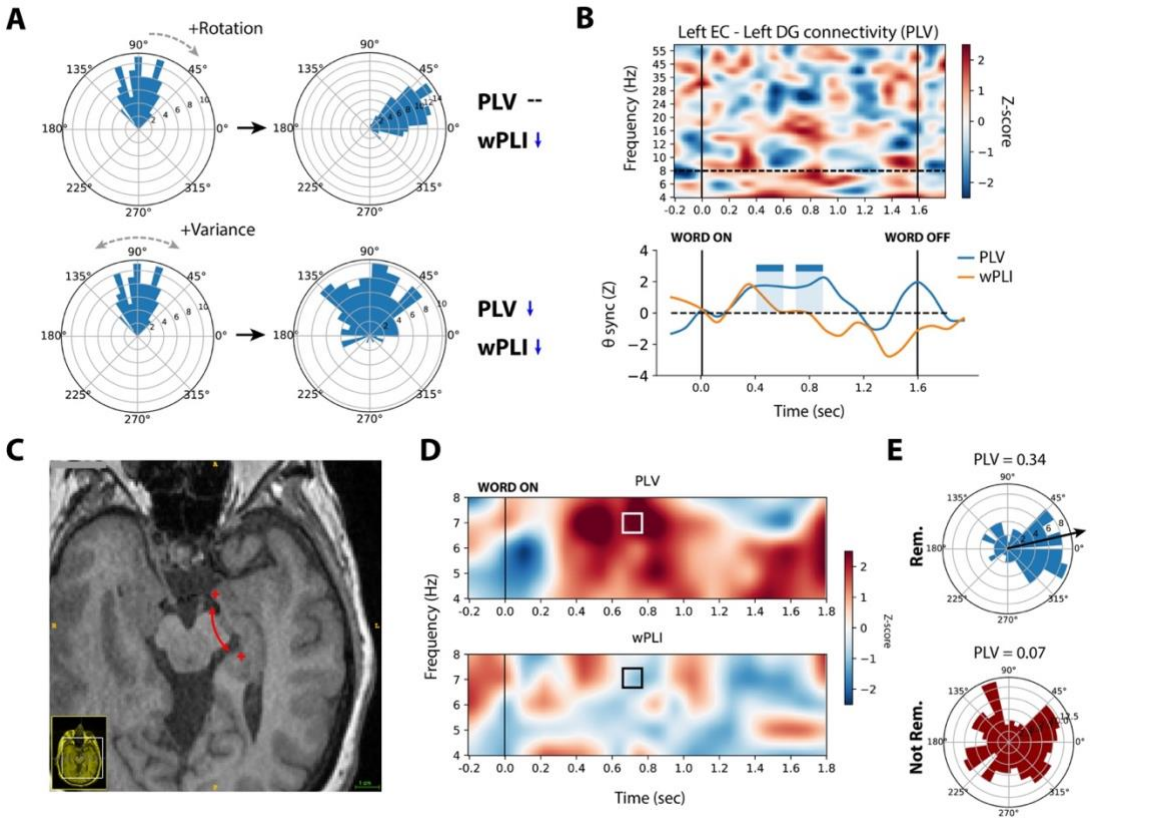

Figure 4.3. Time-varying dynamics of left EC to left DG coupling. A. As demonstrated using simulated data, the wPLI can differ between conditions for two reasons. First, depicted in the top row, well-clustered phase lags can rotate toward zero – decreasing wPLI which downweights phase lags closer to zero to account for volume conduction. In this case, the PLV will remain unchanged. Second, depicted in the bottom row, the variance of a nonzero phase lag distribution can increase between conditions, causing decreases in PLV and wPLI. **B.** *Top*: Time-frequency plot of PLV synchronization between left EC and left DG in the encoding contrast, averaged across subjects. Red colors indicate relative synchronization in remembered versus not-remembered trials, blue colors indicate relative desynchronization. Vertical black lines indicate word onset and offset, dotted horizontal line indicates the max theta frequency considered for connectivity analyses. *Bottom*: In non-overlapping 100 ms windows, PLV (blue) and wPLI (orange) values are averaged across all theta frequencies, yielding a synchronization timeseries. Any two consecutive 100 ms windows with synchronization significantly greater than chance ($P < 0.05$) are marked as significant with blue or

orange colored rectangles (see Methods for details). In this region-pair, PLV is significant from 400-600 ms and 700-900 ms after word onset. **C.** Axial T1-weighted MRI slice depicting electrode locations for a representative pair spanning the left DG and EC. **D.** Time-frequency plots for the indicated electrode pair, theta frequencies only. Top row shows PLV synchronization during successful encoding, bottom row shows wPLI synchronization. The considered interval and frequency for phase lags in (E) is marked with a square. **E.** For the highlighted frequency and interval, phase lags were binned according to whether the trial was later remembered (blue) or not-remembered (red). The mean direction of the clustered remembered trials is 9.7 degrees (PLV = 0.34), indicated with the black arrow. Not-remembered trials are unclustered, as reflected by a low PLV of 0.07.

To illustrate this, we examined phase lag distributions for a key connection in the encoding contrast – left EC versus left DG. Across all subjects, we observed significantly enhanced theta PLV (permuted $P < 0.05$ from 400-600 ms and 700-900 ms) with successful encoding, though no significant wPLI during those same intervals (Figure 4.3B). In a representative subject who exhibited enhanced PLV and minimal wPLI modulation in similar intervals, we examined phase lags between remembered and not-remembered trials for a pair of electrodes in the left EC and DG (Figure 4.3C-D). Phase lags for remembered trials were clustered near zero (PLV = 0.34, mean direction = 9.7 degrees), and uniformly distributed in the not-remembered condition (PLV = 0.07; Figure 4.3E). One interpretation of these results is that wPLI is operating as intended; small phase lags could be reflecting volume-conducted signal from a common source that should be discounted. Therefore, even the tightly-clustered phase distribution in the remembered condition does not yield a relative increase in wPLI. Conversely, it is not clear whether a mean phase lag of 9.7 degrees is close enough to zero to justify substantially discounting those signals; prior studies have excluded phase differences less than 5 degrees from zero[73]. Finally, in this example, the DG and EC recording contacts are separated by more than 2 cm, a spacing which is greater than putative distances in which common signal is conducted in brain tissue[133]. It is therefore possible that use of wPLI is inappropriately rejecting true, near-zero phase coupling.

Temporal dynamics of theta connectivity differed between MTL subregion pairs. Left EC and left PRC showed significantly enhanced PLV connectivity (permuted $P < 0.05$) in the -100-300 ms interval relative to word onset (Figure 4.4A). Left EC and left CA1, linked by the perforant pathway, exhibited enhanced PLV synchrony from 500 ms to 800 ms after word

onset, similar to the EC-DG connection (Figure 4.4B). In both cases we observed subthreshold increases in wPLI during the word encoding interval.

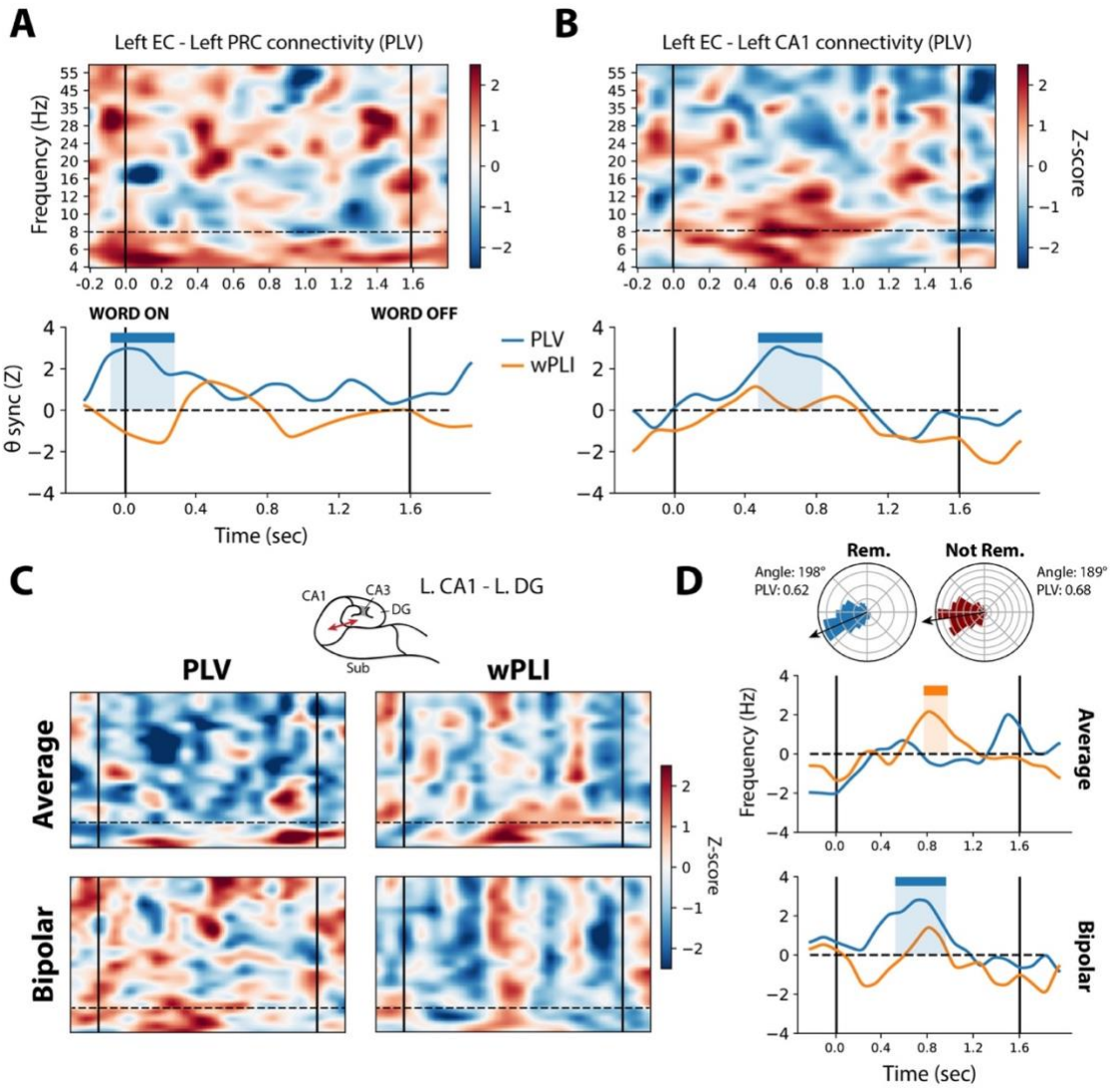

Figure 4.4. Timing analysis of key encoding connections. A. *Top:* Time-frequency plot of left EC-PRC synchronization (PLV) in the encoding contrast, averaged across subjects. *Bottom:* Timecourse of PLV/wPLI theta synchronization, averaged across subjects. Significant ($P < 0.05$) PLV synchronization is marked from -100 to 300 ms after word onset. **B.** Same as (A), but for the EC vs. CA1 connection. Significant PLV synchronization is marked from 500 to 800 ms after word onset. **C.** *Top row:* PLV and wPLI time-frequency plots for left CA1 vs. left DG, under the common average

reference. *Bottom row:* PLV/wPLI time-frequency plots under the bipolar reference. See Methods for details. **D.** For the left CA1 vs. left DG connection, timecourses of theta PLV/wPLI connections, organized as in (A). Significant wPLI was observed under the average reference from 800-1000 ms, while significant PLV was observed under the bipolar reference from 500-900 ms. Phase lag distributions from a representative electrode pair (average reference) are depicted above the timeseries, indicating a relative rotation away from zero for remembered trials.

Connectivity between left CA1 and left DG illustrates convergent results regardless of connectivity metric or referencing scheme. We observed general increases in theta connectivity in all measured conditions (Figure 4.4C), though PLV increases were subthreshold under the average reference, while wPLI increases were significant (permuted $P < 0.05$, 800-1000 ms; Figure 4.4D). To understand this unique case, we examined the phase lag distributions for a representative electrode pair (Figure 4.4D, top row). In both remembered and not-remembered distributions, phase lags were tightly clustered (PLV = 0.62, 0.68 respectively), though the not-remembered distribution was rotated towards the zero axis (-9 degrees versus -18 degrees). This rotation yielded a relative increase in wPLI even as overall phase lag clustering fell slightly. Notably, we also found enhanced PLV in this region-pair under the bipolar reference (500-900 ms) and a concomitant subthreshold wPLI increase (Figure 4.4D, bottom panel).

Finally, synchronization during memory retrieval intervals also exhibited time-varying structure. In two key connections, left CA1 vs. subiculum and left CA1 vs. left EC, we observed increases in theta connectivity in the period leading up to vocalization of a recalled word (CA1-Sub, $P < 0.05$ -200-0 ms prior to retrieval; CA1-EC, -300-100 ms; Figure 4.5A-B). In a representative electrode pair, we noted CA1-Sub synchronization was associated with clustered near-zero phase lags (PLV = 0.47, 8.6 degrees; Figure 4.5C left), explaining no observed increase in relative wPLI. In the CA1-EC pair, phase lags were well-clustered in both conditions but rotated near zero for successfully retrieved events (PLV = 0.70, 1.9 degrees; Figure 4.5C right).

Taken together, we found that the general increase in left-MTL synchronization is driven by time-varying increases in connectivity between key regions, including left EC, CA1, DG, and

subiculum. Connections to or within the hippocampus typically occurred more than 500 ms after word onset in the encoding interval, while EC and PRC exhibited an early synchronization approximately coincident with word onset. Differences between observed PLV and wPLI derive from complex differences in underlying phase lags, though we note that clustered phase lags near – but not at – zero tend to blunt wPLI's sensitivity to memory-related effects.

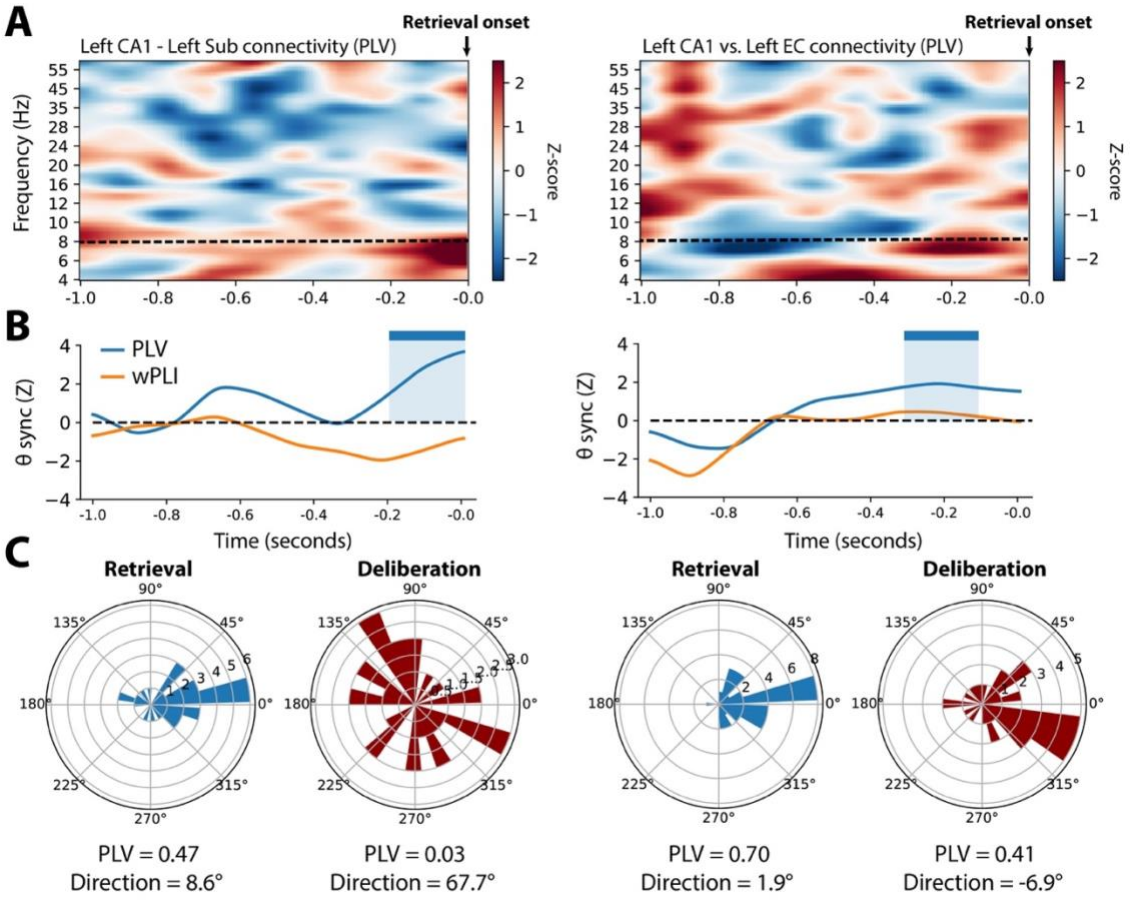

Figure 4.5. Timing analysis of key retrieval connections. A. *Left:* Time-frequency plot of left CA1-subiculum PLV synchronization in the retrieval contrast, averaged across subjects. *Right*: Time-frequency plot of left CA1-EC PLV synchronization in the retrieval contrast. **B.** *Left:* Timecourse of left CA1-subiculum PLV/wPLI synchronization, organized as in Figure 4.4B. Significant ($P < 0.05$) PLV synchronization is marked from -200 to 0 ms prior to recall onset. *Right:* Timecourse of left CA1-EC

synchronization. Significant PLV synchronization is marked from -300 to -100 prior to recall onset. **C.** *Left:* In a representative CA1-sub electrode pair demonstrating enhanced PLV in the significant interval, successfully-retrieved trials demonstrated phase lag clustering around a mean direction of 8.6 degrees (PLV = 0.47). No clustering was evident for epochs where no recall occurred, called "deliberation" trials. *Right:* In a representative CA1-EC electrode pair, successful retrieval events showed greater phase clustering than deliberation events, but retrieval events were aligned with the zero axis (mean direction, 1.9 degrees). Therefore, PLV reflected a memory-related increase, but wPLI did not.

Relationship between connectivity and spectral power

Our primary focus was to characterize patterns of intra-MTL connectivity, but it is known that MTL subregions exhibit distinct patterns of local activation associated with episodic memory (e.g. 50, 51). We therefore asked whether changes in local spectral activity within the MTL correlate with encoding and retrieval states, and whether such changes relate to inter-regional theta connectivity. To do this, we analyzed the relative spectral power between successful and unsuccessful encoding/retrieval trials, in the theta band (4-8 Hz) and frequencies that correspond to high-frequency activity (HFA, 30-90 Hz). HFA is established as a general marker of neural activation that likely includes gamma oscillatory components and spectral leakage from aggregate unit spiking activity[29]. For each MTL subregion, we computed the power SME and retrieval contrast for each electrode at each frequency, and averaged these effects across electrodes and subjects (see Methods for details). This procedure results in a t-statistic that reflects the relative power in a given region between successful and unsuccessful encoding/retrieval events.

Though we broadly observed positive theta connectivity associated with successful episodic memory, spectral power contrasts at the same frequencies went in the opposite direction. Bilateral CA1 and PRC exhibited significant decreases in theta power associated with successful encoding, as did left DG, left PHC, and right subiculum (FDR-corrected $P < 0.05$; Figure 4.6A). Bilateral CA1 also exhibited significantly enhanced HFA, and HFA was otherwise nonsignificantly increased in all MTL regions. Power dynamics associated with successful retrieval were similar to those observed in the encoding contrast. Theta was generally decreased in the left MTL, significantly so in left PRC and CA1 (FDR-corrected $P < 0.05$). Furthermore, HFA was elevated in bilateral CA1 and DG. The general trend of

decreased theta power and increased HFA aligns with a robust literature demonstrating this same effect across a diverse array of cortical regions and the MTL[84,100,119,120].

Between left EC and CA1 – both exhibiting memory-related increases in theta connectivity – we further asked whether there was a relationship between modulations of spectral power and connectivity. During successful encoding, left CA1 showed a significant ($P < 0.05$) increase in HFA from 700-900 ms after word onset, coincident with the 500-800 ms theta connectivity to EC shown in Figure 5B (Figure 4.6B, top row). Additionally, CA1 exhibited a sustained and significant decrease in theta power beginning at 500 ms, while EC showed a transient decrease from 200 to 600 ms (no significantly increased HFA was observed in EC). In the retrieval contrast, HFA increased and theta power decreased in CA1 prior to onset of a successfully retrieved word (HFA, -600-0 ms prior to onset; theta, -300-0 ms). Both of these intervals overlapped with the period of enhanced CA1-EC theta synchrony from -300 to -100 ms (Figure 4.6C). We observed no significant modulations of power in either band in EC during retrieval, but note subthreshold increases in HFA and decreases in theta power in the pre-retrieval interval (Figure 4.6C, right panel). Time-frequency analyses for all MTL regions are reported in Figures 4.S2. Collectively, these results recapitulate a theme noted in an earlier study of whole-brain connectivity[100]: Increases in low-frequency connectivity are associated with increases in high-frequency power and decreases in low-frequency power.

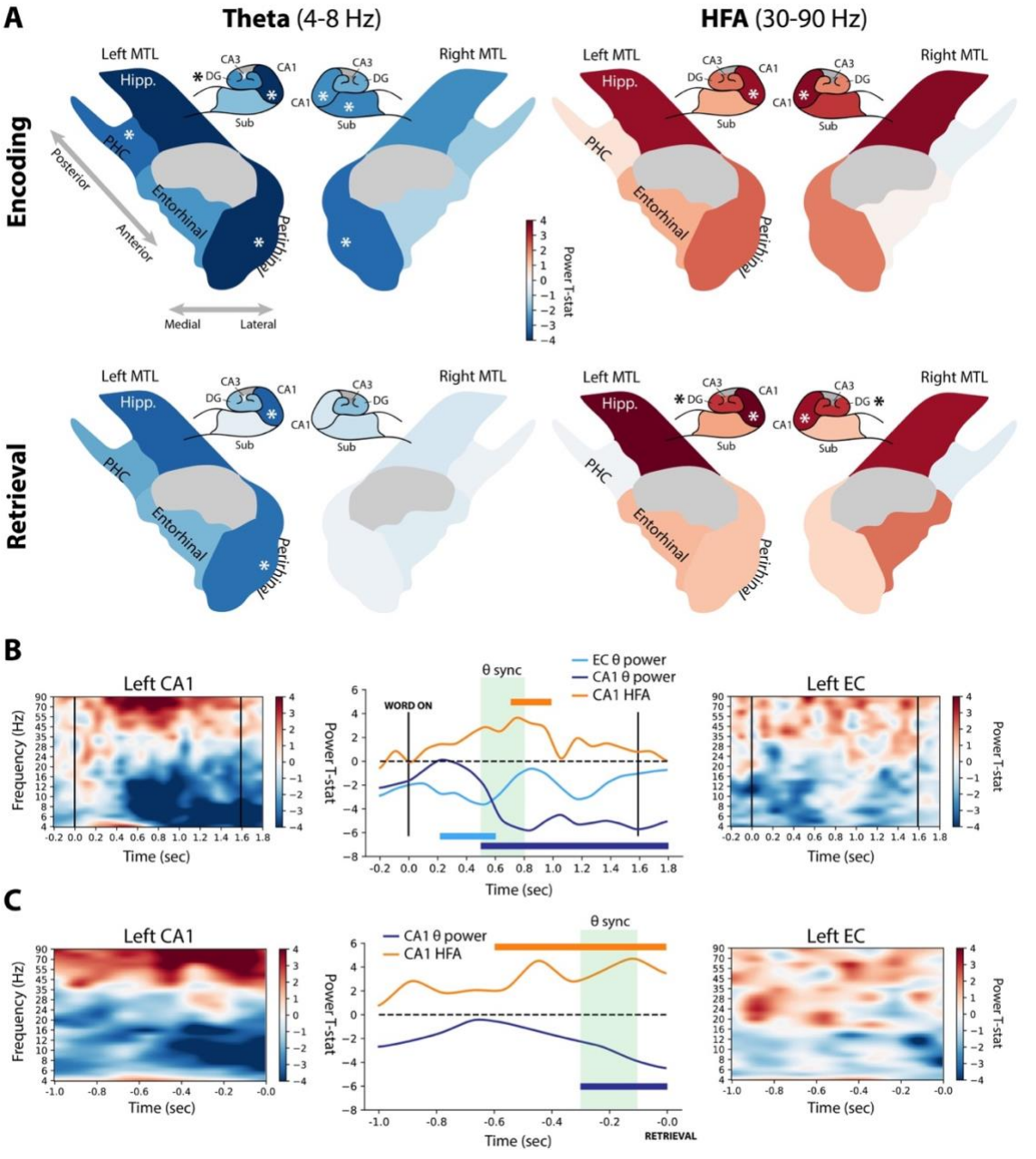

Figure 4.6. Dynamics of spectral power associated with memory encoding and retrieval. A. For each MTL subregion and hippocampal subfield, the spectral power during successful vs. unsuccessful encoding or retrieval epochs was computed in the theta (4-8 Hz) and high-frequency activity (30-90 Hz) bands. For encoding periods, powers were averaged in the 400-1100 ms interval, and between -500-0 ms for retrieval periods, which were the times featuring the most prominent network-wide power change (see Methods for details). The t-statistic indicating the relative power during successful versus unsuccessful encoding or retrieval is mapped to a color, with reds indicating

increased power and blues indicating decreased power. These colors are displayed on schematics of MTL and hippocampal anatomy for encoding and retrieval conditions (rows), and theta or HFA bands (columns). Asterisks indicate significant ($P < 0.05$) memory-related power modulation, FDR corrected across tested regions. "Hipp" was not tested collectively but is colored according to CA1. **B.** Left CA1 and left EC showed changes in spectral power that were temporally associated with enhanced connectivity between the regions (see Figure 4.5B). Significant ($P < 0.05$) increases in CA1 HFA occurred from 700-1000 ms after word onset, while CA1 theta power decreased from 500 ms to the end of the word encoding interval. Left EC theta power decreased from 200-600 ms. The period of significantly enhanced theta PLV is marked in green. **C.** Organized as (B), but for the EC-CA1 interactions in the retrieval contrast. No significant modulations of left EC power were observed in the pre-recall interval.

Memory effects by frequency band

As several frequency bands have been implicated in intra-MTL synchronization[87,104,114,124,135] – notably theta (4-8 Hz) and low gamma (30-60 Hz) – we finally asked whether memory-related connectivity in the MTL was also present at higher frequency bands. For the theta, alpha (9-13 Hz), beta (16-28 Hz), and low gamma bands, network-wide synchronization was only positive for both encoding/retrieval using PLV in the theta band, though not significantly greater than synchronicity expected by chance (permuted $P = 0.22, 0.53$; Figure 4.7A; see Methods for details). Specific connection weights for each contrast and connectivity metric are depicted in Figure 4.7B. Network-wide wPLI was not positive in any band for either contrast. Significant desynchronization was observed for PLV in the beta band and wPLI in the gamma band (permuted $P < 0.05$). In general, synchronization tended to decrease with increasing frequency – considering both PLV and wPLI, and under the bipolar or common average reference, the greatest desynchronization was observed in either the beta or low gamma bands. We note that the bipolar PLV was net positive – though not significant – in the low gamma band, though the effect reversed when considering the bipolar wPLI.

Taken together, MTL-wide networks exhibited net increases in connectivity for both encoding and retrieval only in the theta band. These increases were not significantly greater than chance, likely reflecting an underlying mix of synchronous and asynchronous connection weights (Figure 4.7B). This trend is consistent across referencing scheme and choice of connectivity metric, though strong increases in connectivity using wPLI are not

apparent at any band, perhaps due to the reduced sensitivity of this metric if phase differences are near zero. We note that, as shown in earlier analyses, this finding does not preclude the possibility that significantly positive wPLI interactions correlate with successful memory, just that network-wide effects averaged over time could obscure such effects.

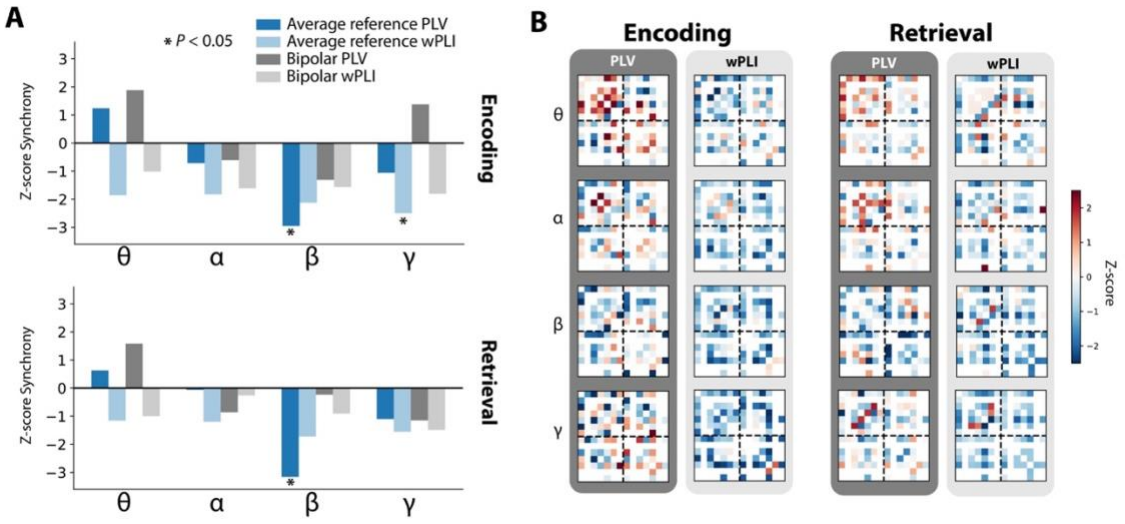

Figure 4.7. Network-wide synchrony by frequency band. A. Network-wide synchronization is computed by averaging all inter-regional connection weights for each frequency, connectivity metric, and referencing scheme. Positive network-wide synchrony was noted for both retrieval and encoding contrasts in the theta band. Significant PLV desynchronization (*$P < 0.05$) was noted in the beta band for encoding and retrieval, and in the gamma band for encoding. **B.** Adjacency matrices for both contrasts (left vs. right) using PLV and wPLI, organized as shown in Fig. 4.2A.

Discussion

We set out to understand neural interactions between substructures of the MTL during episodic encoding and retrieval. As 126 subjects performed a verbal free-recall task, we recorded intracranial EEG from the MTL and compared inter-regional connectivity between periods of successful and unsuccessful memory operations. Using these methods, we discovered that low-frequency phase locking correlates with successful memory encoding

and retrieval, with left entorhinal cortex acting as a key hub for theta connectivity during encoding, and a reorganized left-MTL network supporting retrieval. We additionally used the weighted phase-lag index to account for volume conduction, and noted periods of theta synchronization between key regions but generally blunted effects across all frequency bands. Concurrent with these dynamics was a general decrease in theta power and increase in high-frequency activity in both retrieval and encoding, though the degree of power modulation was not predictive of network hubs.

Low-frequency synchronization in the MTL has been conjectured to underlie diverse cognitive operations, including spatial navigation and working memory[104,110]. Under these hypotheses, theta oscillations result in long-term potentiation of synapses in the hippocampus by linking the time of stimulus onset with a cell's state of maximum depolarization. Relatedly, it is well-established that activity in the gamma-band can be modulated by the phase of an ongoing theta oscillation, representing another mechanism that supports inter-regional plasticity[24,74,123]. Our data align with this hypothesis – increases in theta connectivity occurred alongside enhanced HFA in connected areas. We show this theta/gamma dynamic in the context of successful encoding of individual words, suggesting that the cognitive operations which support working memory, navigational memory, and episodic memory are not so different; indeed, episodic encoding of list items is known to involve the contextual binding of one item to another[13], not dissimilar to holding a list in working memory or building a map of a spatial environment[113,136].

Our identification of encoding and retrieval-associated networks enriches computational models of memory in the MTL. An influential theory of MTL function postulates that theta oscillations within the hippocampal-entorhinal system constitute a common substrate of navigation and episodic memory, by synchronizing EC representations of physical or mental space with hippocampal mechanisms that serve to neurally associate these representations with context (and later serve to retrieve information)[111,112,121]. In support of this theory, we found theta connectivity between the EC and CA1/DG in the hippocampus (in addition to a less robust increase in connectivity between CA1 and DG directly). Enhanced theta connectivity between EC and PRC has not been reported before in humans but supports the

notion that EC's representations are built on sensory input from the neocortex, routed through extrahippocampal MTL regions.

Our findings also indicate a role for theta synchronization during memory retrieval. Indeed, as suggested by anatomical evidence[131] and models of hippocampal function[137], successful retrieval was associated with enhanced connectivity between CA1-EC and CA1-subiculum. Both of these functional connections may support the reinstatement of neocortical activity associated with contextually-retrieved information, driven by pattern completion in CA3.

In this study, we rigorously assessed the utility of two common metrics of phase-based connectivity: the phase-locking value and the weighted phase-lag index. In general, neither metric showed strong evidence for high-frequency synchronization (beta or above), and only the PLV showed truly robust evidence for synchronization in the theta band. Indeed, a total reliance on the wPLI – even in this large dataset – would suggest a general absence of any connectivity-related phenomena during episodic memory processing in the MTL. For several key connections, we demonstrated why there are interpretive difficulties in using the wPLI: it is sensitive to changes in the variance of clustered phase lags *and* the mean direction of clustered phase lags. As such, differences in wPLI between conditions could reflect either (or both) of these underlying dynamics. In regards to the mean direction of phase lags, it is especially difficult to determine whether a change in wPLI is meaningful, because wPLI will statistically discount phase lags as they rotate towards the zero axis, even if they are still well within believable ranges[138]. Furthermore, it is not clear that exactly-zero phase lags are biologically implausible and should be ignored outright[70], especially at low frequencies. We observed that, in this dataset, significant increases in PLV were often accompanied by subthreshold increases in wPLI – suggesting that this conservative statistic was, averaged across subjects, reducing physiologic signal to the point that it was no longer significant. At the risk of doubling the number of statistical comparisons, we advise that researchers consider PLV and wPLI simultaneously, and further examine the underlying distribution of phase differences to gain insight into the biological processes that might drive their effects.

Our use of a verbal free-recall task – though a powerful paradigm for studying episodic memory – necessitated the construction of a retrieval contrast that merits further discussion. In this manuscript, we compared neural activity in 1-second intervals leading up to vocalization of a word against 1-second intervals at matched periods of time with no recalls, in free-recall periods from other lists. In this way, we aimed to contrast activity related to successful retrieval against activity during which subjects were liable to try, but fail, to recall a word. This paradigm has been employed in several prior studies examining the neural correlates of free recall[100,120,128,129]. However, free-recall tasks inherently confound neural process responsible for episodic retrieval with processes responsible for vocalization and motor preparatory behavior. To account for this, our analyses exclusively consider the MTL – not canonically associated with speech preparation – and only examine activity in the time period preceding onset of vocalization. It is still possible that speech-related activity contaminates the retrieval contrast reported here -- other possible contrasts could leverage nonword vocalizations or intrusion events, though these are typically too rare to serve as a statistically valid basis for connectivity computations. Replicating the finding of recalled-associated theta synchrony in a cued-recall paradigm would therefore be a valuable complement to this work.

In this study, we failed to find strong evidence for memory-related gamma synchronization within the MTL – rather, we noted substantial time-averaged decreases in synchronization in the 30-60 Hz range, especially when using the wPLI. However, earlier reports of hippocampal-rhinal connectivity have reported effects in the gamma band[59,114]. To constrain our hypothesis space, we did not statistically assess possible gamma-band synchronization in detail, though our time-frequency analyses of key hippocampal-rhinal connections such as EC-CA1 and EC-DG do not indicate robust increases in gamma synchronization associated with successful encoding (see Figures 4B and 5B). These data recapitulate an earlier study that utilized a superset of the data here, wherein gamma connectivity was found to decrease during good memory encoding, across a diverse array of cortical regions and hippocampus[100].

In summary, we found that theta band connectivity characterizes intra-MTL interactions that are related to memory encoding and retrieval processes, but distinct networks correlate with successful encoding and retrieval. During encoding, we found EC to be a hub of theta connectivity, with connections to CA1 and DG. During retrieval, we observed a reorganized theta network, with no clear hubs but enhanced connectivity between EC-CA1 and CA1-subiculum. However, both retrieval and encoding were broadly characterized by enhanced HFA and decreased theta power. These findings point to low-frequency interactions as the key to unlocking the way in which medial temporal structures give rise to episodic memories.

Methods

Participants

For connectivity analyses, 126 patients with medication-resistant epilepsy underwent a surgical procedure to implant subdural platinum recording contacts on the cortical surface and within brain parenchyma. Contacts were placed so as to best localize epileptic regions. Data reported were collected at 8 hospitals over 3 years (2015-2017): Thomas Jefferson University Hospital (Philadelphia, PA), University of Texas Southwestern Medical Center (Dallas, TX), Emory University Hospital (Atlanta, GA), Dartmouth-Hitchcock Medical Center (Lebanon, NH), Hospital of the University of Pennsylvania (Philadelphia, PA), Mayo Clinic (Rochester, MN), National Institutes of Health (Bethesda, MD), and Columbia University Hospital (New York, NY). Prior to data collection, our research protocol was approved by the Institutional Review Board at participating hospitals, and informed consent was obtained from each participant.

Free-recall task

Each subject participated in a delayed free-recall task in which they studied a list of words with the intention to commit the items to memory. The task was performed at bedside on a

laptop. Analog pulses were sent to available recording channels to enable alignment of experimental events with the recorded iEEG signal.

The recall task consisted of three distinct phases: encoding, delay, and retrieval. During encoding, lists of 12 words were visually presented. Words were selected at random, without replacement, from a pool of high frequency English nouns (http://memory.psych.upenn.edu/WordPools). Word presentation lasted for a duration of 1600 ms, followed by a blank inter-sitmulus interval of 800 to 1200 ms. Before each list, subjects were given a 10-second countdown period during which they passively watch the screen as centrally-placed numbers count down from 10. Presentation of word lists was followed by a 20 second post-encoding delay, during which time subjects performed an arithmetic task during the delay in order to disrupt memory for end-of-list items. Math problems of the form A+B+C=?? were presented to the participant, with values of A, B, and C set to random single digit integers. After the delay, a row of asterisks, accompanied by a 60 Hz auditory tone, was presented for a duration of 300 ms to signal the start of the recall period. Subjects were instructed to recall as many words as possible from the most recent list, in any order, during the 30 second recall period. Vocal responses were digitally recorded and parsed offline using Penn TotalRecall (http://memory.psych.upenn.edu/TotalRecall). Subjects performed up to 25 recall lists in a single session (300 individual words).

Electrocorticographic recordings

iEEG signal was recorded using depth electrodes (contacts spaced 5-10 mm apart) using recording systems at each clinical site. iEEG systems included DeltaMed XlTek (Natus), Grass Telefactor, and Nihon-Kohden EEG systems. Signals were sampled at 500, 1000, or 1600 Hz, depending on hardware restrictions and considerations of clinical application. Signals recorded at individual electrodes were first referenced to a common contact placed intracranially, on the scalp, or mastoid process. To eliminate potentially confounding large-scale artifacts and noise on the reference channel, we next re-referenced the data using the common average of all depth electrodes in the MTL that were used for later analysis. For

some analyses (Figure 4.2 and Figure 4.5) raw signals recorded at individual recording contacts were converted to a bipolar montage by computing the difference in signal between adjacent electrode pairs on each depth electrode. Signals were notch filtered at 60 Hz with a fourth-order 2 Hz stop-band butterworth notch filter in order to remove the effects of line noise on the iEEG signal, and downsampled to 256 Hz.

As determined by a clinician, any contacts placed in epileptogenic tissue or exhibiting frequent inter-ictal spiking were excluded from all subsequent analyses. Any subject with fewer than 3 remaining recording contacts in the MTL were not included in the analysis. Any subject with fewer than 15 trials of successful encoding or successful retrieval (see "Retrieval analyses") were excluded from analysis (encoding, 3 subjects excluded; retrieval, 21 subjects excluded).

Limitations of the bipolar reference: In this manuscript, we considered use of the common average and bipolar reference, to account for the possibility that the filtering properties of a given reference scheme could affect connectivity measures. However, the use of the bipolar reference for studies of intra-MTL connectivity is limited by the geometry of linear depth electrodes relative to MTL structures; it is often the case that a bipolar midpoint "virtual" electrode will fall in a subregion/subfield where neither physical contact was placed, raising interpretive difficulties. Additionally, connectivities between bipolar electrodes that share a common monopolar contact are contaminated by shared signal between the two – ideally, such pairs should be excluded from analysis. However, doing so drastically reduces the number of possible region-to-region pairs within the MTL. In the bipolar analyses considered here, all possible pairs were retained even if they shared a common contact, but the bulk of our analyses therefore focus on the average reference. (The use of behavioral contrasts and wPLI may mitigate the effect of shared signal between bipolar virtual contacts.)

Anatomical localization

To precisely localize MTL depth electrodes, hippocampal subfields and MTL cortices were automatically labeled in a pre-implant, T2-weighted MRI using the automatic segmentation

of hippocampal subfields (ASHS) multi-atlas segmentation method[94]. Post-implant CT images were coregistered with presurgical T1 and T2 weighted structural scans with Advanced Normalization Tools [93]. MTL depth electrodes that were visible on CT scans were then localized within MTL subregions by neuroradiologists with expertise in MTL anatomy. MTL diagrams were adapted with permission from Moore, et al.[139].

Data analyses and spectral methods

To obtain phase-locking values (PLV) and weighted phase lag index (wPLI) between electrode pairs, we used the MNE Python software package[140], a collection of tools and processing pipelines for analyzing EEG data. PLV reflects the consistency of phase differences between two electrodes across trials[76]. wPLI operates similarly to PLV, but weights phase differences according to their rotation away from the zero axis, to account for volume conduction[127]. Stated differently, the wPLI weights cross-spectra by the magnitude of the imaginary component of the cross spectrum. Therefore, maximum wPLI is achieved if phase differences are tightly clustered around 90 (or 270) degrees. Both metrics range from 0 (no synchronization) to 1 (maximal synchronization).

To obtain phase information, we convolved signals from each MTL recording contact with compelx-valued Morlet wavelets (6 cycles). We used 24 wavelets from 3-60 Hz as follows: theta (4-8 Hz, spaced 1 Hz), alpha (9-13 Hz, spaced 1 Hz), beta (16-28 Hz, spaced 2 Hz), low gamma (30-60 Hz, spaced 5 Hz). For encoding analyses, each wavelet was convolved with 4000 ms of data surrounding each word presentation (referred to as a "trial"), from 200 ms prior to word onset to 1800 ms afterwards, buffered with 1000 ms on either end (clipped after convolution). Retrieval analyses considered 1000 ms of data prior to each retrieval event, also buffered with 1000 ms on either end.

For each subject, for all possible pairwise combinations of MTL electrodes, we compared the distributions of phase differences in all remembered trials against all not-remembered trials, asking whether there is a significantly higher PLV/wPLI in one or the other. In the encoding contrast, values were compared between all epochs where words were later remembered versus forgotten. In the retrieval contrast, values were compared between

epochs leading up to onset of a verbal recall versus matched periods of time when no recall occurred ("deliberation" events, see "Retrieval analysis"). To do this, we found the difference of PLV/wPLI across conditions, e.g.:

$$D_{pq}(f,t) = PLV_{rem} - PLV_{nrem} \quad (1)$$

Where *pq* is an electrode pair, *f* is a frequency of interest, and *t* is a window in time. Higher positive differences (*D*) indicate greater connectivity for remembered trials, whereas lower negative differences reflect greater connectivity for not-remembered trials. *D* was computed for each frequency spanning a range from 3 to 60 Hz, averaged into 100 ms non-overlapping windows spanning each trial (i.e. word encoding or pre-retrieval event). 20 windows covered encoding events, from 200 ms prior to word onset to 200 ms after offset. 10 windows covered retrieval/deliberation events, starting 1 second prior to word onset (or 1-second of time during matched deliberation period).

PLV and wPLI values are biased by the number of vectors in a sample. Since our subjects generally forget more words than they remember, we adopt a nonparametric permutation test of significance. For each subject, and each electrode pair, the synchrony computation described above was repeated 250 times with the trial labels shuffled, generating a distribution of *D* statistics that could be expected by chance for every electrode pair, at each frequency and time window. Since only the trial labels are shuffled, the relative size of the surrogate remembered and not-remembered samples also reflect the same sample size bias. Consequently, the true *D* (D_{true}) can be compared to the distribution of null *D*s to derive a z-score or p-value. Higher z-scores indicate greater synchronization between a pair of electrodes for items that are successfully recalled.

To construct a network of synchrony effects between all MTL subregions, we pooled synchrony effects across electrode pairs that span a pair of subregions, and then pooled these subregion-level synchronizations across subjects with that pair of subregions sampled. To do this, we first averaged the D_{true} values across all electrode pairs that spanned a given pair of subregions within a subject. Next, we averaged the corresponding null distributions of these electrode pairs, resulting in a single D_{true} and a single null distribution

for each subregion-pair in a subject. We then averaged the D_{true} values and null distributions across all subjects with electrodes in a given ROI pair. By comparing the averaged D_{true} to the averaged null distribution, we computed a z-score (and corresponding p-value) at each frequency and temporal epoch that indicates significant synchrony or asynchrony, depending on which tail of the null distribution the true statistic falls.

Statistical considerations: Our procedure for averaging the true and null statistics across subjects enables us to construct whole-MTL networks across datasets in which no single subject has electrodes in every region of interest. We compute statistics on these networks that leverage their completeness, including overall connection strength (Figure 4.2B) and node strengths (Figure 4.3). Such statistics cannot be assessed at the level of individual subjects who may only have electrode pairs that span a small subset of MTL regions. However, the connection strengths for individual region-pairs can be statistically evaluated across subjects using a 1-sample T-test, so long as a sufficient number of subjects have been sampled for that pair. To demonstrate the correspondence between these two approaches, we correlated the connection weight of population-level z-scores (derived from the permutation procedure above) to t-statistics computed derived from a 1-sample T-test on z-scores from individual subjects. Across all possible region-pairs, connection weights are highly correlated between the two methods (Pearson'r r = 0.88, Figure 4.S3).

Network analyses

Using the population-level statistics described above, a 14-by-14 adjacency matrix was constructed for each of the temporal epochs in encoding/retrieval conditions, for each frequency. This matrix represented every possible interaction between all MTL subregions. The z-score of the true D relative to the null distribution was used as the connection weight of each edge in the adjacency matrix. Negative weights indicate ROI pairs that, on average, desynchronized when a word was recalled successfully, and positive weights indicate ROI pairs that synchronized when a word was recalled successfully. We zeroed-out any ROI pairs in the matrix represented by less than 5 subjects' worth of data, to limit the likelihood

that our population-level matrix is driven by strong effects in a single or very small number of individuals (see Figure 4.S1 for subject counts at each pair).

Since it is possible that collections of weaker connection weights may still account for significant structure in our network, we did not apply a *z*-score threshold before further analyses. To assess for the significance of phenomena at the network level, we instead used 250 null networks that can be constructed on the basis of *D*s derived from the shuffled trial labels to generate a distribution of chance network-level statistics. True statistics were compared to these null distributions to obtain a *P*-value or *z*-score (e.g. network-wide summed connections weights were computed for true and null networks and reported in Fig. 4.2B).

Adjacency matrices reflect the average connectivity strength during the item presentation interval (0–1600 ms) or retrieval period (-1000-0 ms) for each frequency band. To create them, we averaged true connection strengths within frequency bands, then averaged across all the 100 ms time windows in the encoding/retrieval intervals, and compared the result to the time/frequency average from each of the 250 null networks, resulting in a new *Z*-score for the time/frequency-averaged network (e.g. Figure 4.2A).

In analyses of connectivity timecourses (Figures 4.4-4.6), intervals are marked as significant so long as the p-value of PLV/wPLI connectivity exceeds a threshold of $P < 0.05$ (relative to the null distribution for that epoch) for at least 2 consecutive 100 ms epochs.

Hub analysis

To determine which MTL regions act as significant "hubs," or regions that have enhanced connectivity to many other nodes in the network, we use the node strength statistic from graph theory (Equation 2)[39]:

$$k_i^w = \sum_{j \epsilon N} w_{ij} \quad (2)$$

Where k is the node strength of node i, and w_{ij} refers to the edge weight between nodes i and j. N is the set of all nodes in the network. In this paper, we only use ipsilateral MTL

regions to compute the node strength of each region, so as to (1) better reflect the engagement of a region with its immediate neighbors and (2) acknowledge the sparser sampling of interhemispheric connections. The z-scored connectivity between MTL regions is used as the edge weight. To assess the significance of a hub, we used edge weights derived from each of the 250 null networks, generated by shuffling the original trial labels (see "Network analyses"). For each region, the true node strength is compared to the distribution of null node strengths to derive a z-score or p-value. In Figure 4.3, p-values were Benjamini-Hochberg corrected for multiple comparisons and thresholded at $P < 0.05$.

Analysis of spectral power

To determine the change in spectral power associated with successful memory encoding or retrieval, we convolve each electrode's signal with complex-valued Morlet wavelets (6 cycles) to obtain power information. For high-frequency activity (HFA) we used 13 wavelets spaced 5 Hz (30-90 Hz). Frequencies, time windows, buffers, and spectral methods are otherwise identical to those used in the earlier phase-based analysis (see "Data analyses and spectral methods").

For each electrode in each subject, we log transformed and z-scored power within each session of the free-recall task, which comprises approximately 300 trials. Power values were next averaged into non-overlapping 100 ms time bins spanning the trial. To assess the statistical relationship between power and later recollection of a word (the power SME), power values for each electrode, trial, time, and frequency were separated into two distributions according to whether the word was later or not remembered, a Welch's t-test was performed to compare the means of the two distributions. The resulting t-statistics were averaged across electrodes that fell in a common MTL region (either hippocampal subfields or MTL cortices), generating an average t-statistic per subject. Finally, for all MTL regions with more than 5 subjects' worth of data (all regions except right CA3 met this criteria), we performed a 1-sample t-test on the distribution of t-statistics against zero. The result is a t-statistic that reflects the successful encoding-related change in power across

subjects. We report these t-statistics in time-frequency plots in Figure 4.7B, along with time-averaged t-statistics in Figure 4.7A (encoding, 400-1100 ms; retrieval, -500-0 ms).

Retrieval analysis

To find out whether functional connectivity networks uncovered in the memory encoding contrast generalized to different cognitive operations, we further analyzed connectivity in a retrieval contrast. This was done in a manner similar to Burke, et al. 2014 as follows:

For each subject, we identified any 1000 ms period preceding vocal onset of a successfully recalled word, so long as that word was not preceded or followed by any other vocalization for at least 2 seconds. For each retrieval event, we then searched for a 1000 ms interval from a different list during which no successful retrieval (or vocalization) took place, occurring at the same time as the original recall relative to the beginning of the recall period (30-second recall periods followed each of 25 lists per session). These 1000 ms intervals are called "deliberation" intervals, reflecting a time during which a subject was liable to be attempting recall. If no match could be found for the exact time of a given recall, we searched for, still from a different list, a matched deliberation interval within 2 seconds surrounding the onset time of the retrieval event. If no match was available within 2 seconds, the original recall event was discarded from analysis. In this way, each successful retrieval is matched with exactly one deliberation interval, of equal length, from a different recall list.

Analyses of the retrieval contrast were otherwise treated identically to analyses of the encoding contrast, described in "Data analyses and spectral methods."

Supplemental Figures

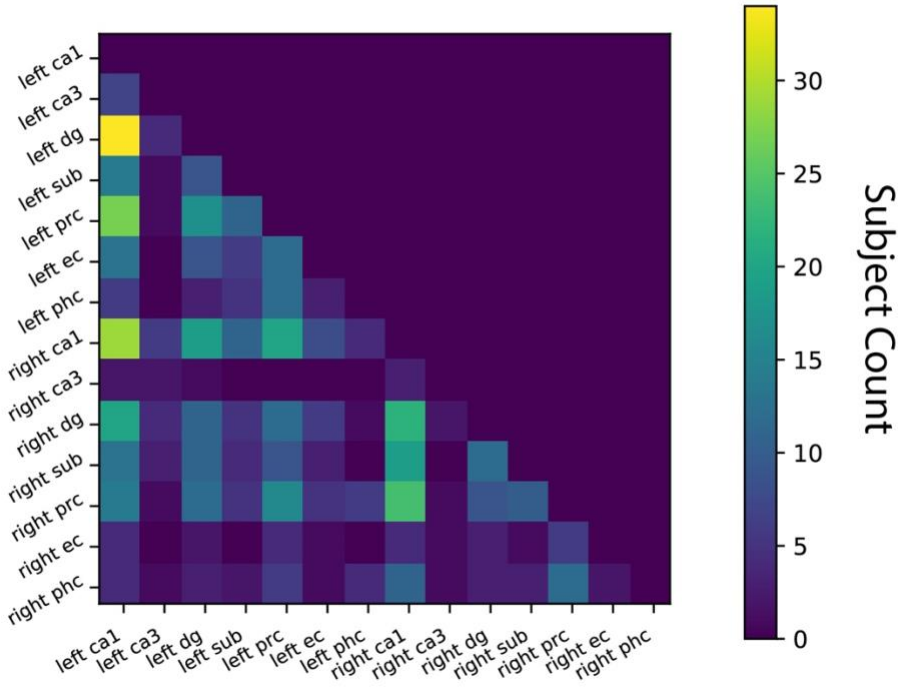

Figure 4.S1. Related to Figure 4.1. Number of subjects contributing to each region pair. To construct networks of intra-MTL connectivity, we pooled connectivity effects across subjects with electrode pairs that span at least one pair among 14 possible MTL subregions. Here we depict the number of subjects who contribute to each pairwise estimate in adjacency matrix format, with a minimum of 5 subjects needed to include a region-pair in this manuscript's analysis.

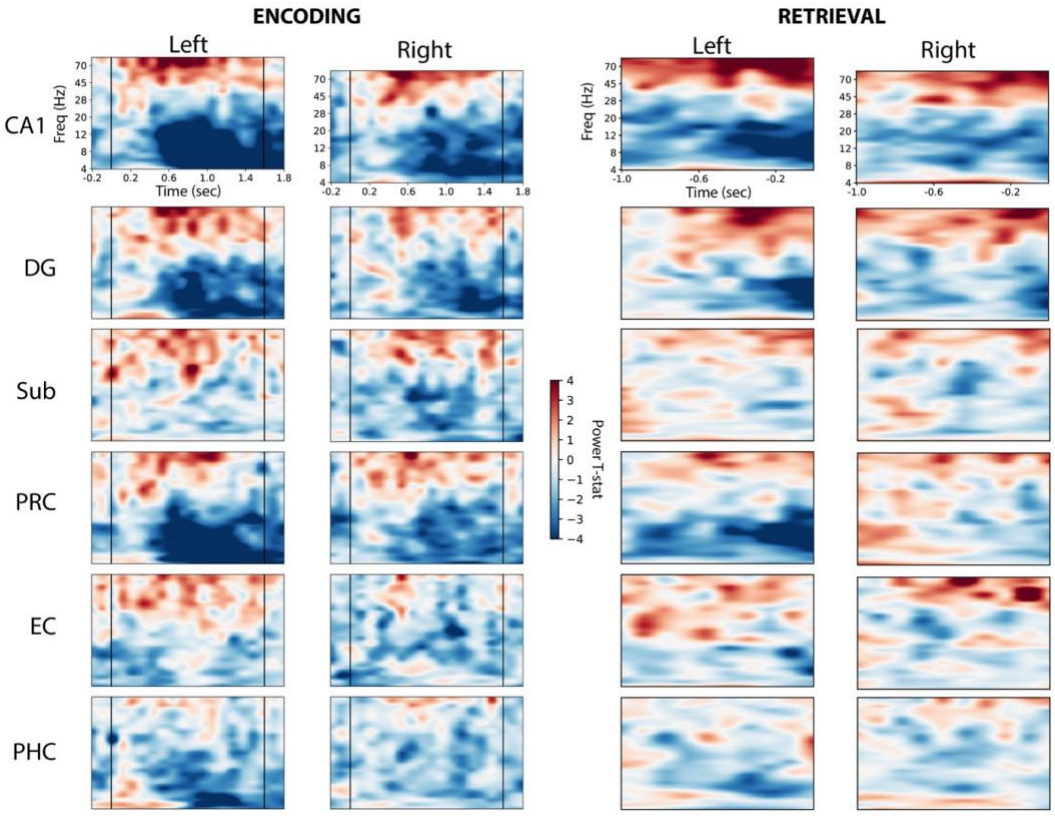

Figure 4.S2. Memory-related spectral power at all MTL subregions. Related to Figure 4.6. For each MTL subregion, the spectral power during successful vs. unsuccessful encoding or retrieval epochs was measured for frequencies spanning 4-90 Hz. *Left*: Time-frequency plots of the successful vs. unsuccessful encoding contrast. Vertical bars indicate word onset and offset. *Right:* Contrast of successful retrieval vs. deliberation epochs. Retrieval occurs at 0.0 seconds, or the rightmost edge of each plot. Subregion acronyms are defined in Figure S1.

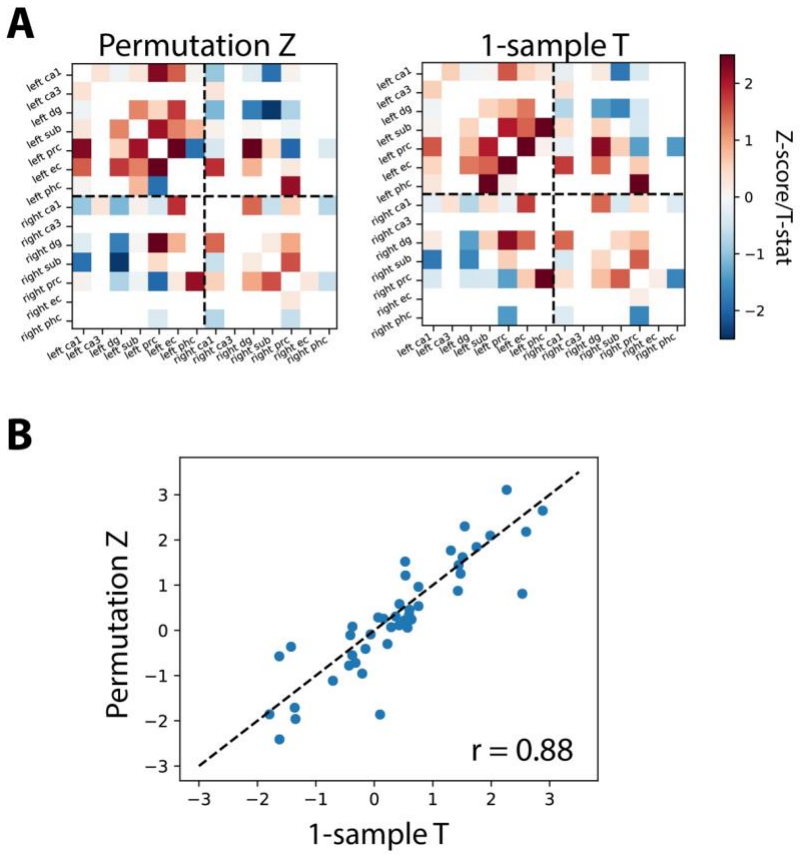

Figure 4.S3. Related to Figure 4.2. Comparison of permutation Z-scores against 1-sample T statistics. A. *Left*: Original theta encoding adjacency matrix, reflecting a Z-score derived by averaging subject's connectivity statistics and corresponding null distributions. *Right*: Theta encoding adjacency matrix reflecting T-statistics computed for every possible region-pair, via a 1-sample T-test across subject's individual connection Z-scores. **B.** T-statistics and z-scores are highly correlated (Pearson's r = 0.88) across all assessed region-pairs.

CHAPTER 5:

Perturbation of Brain Networks

Solomon, E. A., et al. "Medial temporal lobe functional connectivity predicts stimulation-induced theta power." *Nature communications* 9.1 (2018): 4437.

Abstract

Focal electrical stimulation of the brain incites a cascade of neural activity that propagates from the stimulated region to both nearby and remote areas, offering the potential to control the activity of brain networks. Understanding how exogenous electrical signals perturb such networks in humans is key to its clinical translation. To investigate this, we applied electrical stimulation to subregions of the medial temporal lobe in 26 neurosurgical patients fitted with indwelling electrodes. Networks of low-frequency (5-13 Hz) spectral coherence predicted stimulation-evoked increases in theta (5-8 Hz) power, particularly when stimulation was applied in or adjacent to white matter. Stimulation tended to decrease power in the high-frequency broadband (HFB; 50-200 Hz) range, and these modulations were correlated with HFB-based networks in a subset of subjects. Our results demonstrate that functional connectivity is predictive of causal changes in the brain, capturing evoked activity across brain regions and frequency bands.

Introduction

Intracranial brain stimulation is increasingly used to study disorders of human behavior and cognition, but very little is known about how these stimulation events affect neural activity. Though several recent studies have demonstrated the ability to modulate human memory with direct electrical stimulation (DES) of the cortex[47,49–51,53,141,142], none have described the mechanism by which stimulation yields altered cognitive states. However, understanding how the brain responds to these exogenous currents is necessary to ultimately develop therapeutic interventions that rely on DES[143,144].

Specifically, investigators have long have asked whether the brain's intrinsic functional or anatomical architecture can predict how mesoscale stimulation events propagate through the brain. Early work focused on inferred connectivity through stimulation-evoked behavior in rodents[145,146]. More recently, Logothetis and colleagues demonstrated that the effects of electrical stimulation propagated through known anatomical connections in the macaque visual system[44,147]. In humans, corticocortical evoked potentials (CCEPs), measured with intracranial EEG (iEEG), have also been shown to propagate through anatomical and functional connections[45,148], as has the fMRI BOLD response to stimulation[149]. These studies provide powerful evidence that the effects of stimulation are determined by the connectivity profile of a targeted region. More broadly, renewed interest in the idea of the brain as a controllable network[4,92,150] raises a testable hypothesis in need of empirical validation: to what extent does a brain's network architecture predict the cascade of physiologic change that accompanies a stimulation event?

In this study, we asked whether the functional connectivity of a stimulated region predicts where we observe changes in neural activity. To expand on prior work that has examined network architecture and stimulation, we adopted a paradigm that (1) focuses on stimulation's effect on low-frequency (theta) power, a cognitively-relevant electrophysiological biomarker, and (2) simultaneously considers the structural and functional connectivity of a targeted region. In 26 neurosurgical patients with indwelling electrodes, we stimulated different regions of the medial temporal lobe (MTL) and asked

whether low-frequency coherence predicted modulations of theta power in distributed cortical regions. We showed that coherence was mostly predictive of theta modulation when stimulation occurred in or near a white matter tract, but in those cases, stimulation could evoke sustained increases in theta power even in distant regions. With this initial finding in hand, we expanded our paradigm to consider additional measures of functional connectivity and evoked power at higher frequencies. We principally considered the amplitude envelope of the high-frequency broadband signal (HFB; 50-200 Hz)[151], shown to correlate with the resting-state fMRI BOLD correlations that are widely used in network neuroscience[16,151–153]. We demonstrated that while low-frequency coherence accurately predicts increases in low-frequency power, HFB-based networks can explain decreases of HFB power. Taken together, functional connectivity can predict the widespread changes in local spectral power induced by direct electrical stimulation of the MTL.

Results

Calculating network-mediated activation

To determine how direct cortical stimulation propagates through brain networks, we collected intracranial EEG (iEEG) data from 26 patients undergoing clinical monitoring for seizures. Subjects rested passively in their hospital bed while we applied bipolar macroelectrode stimulation at varying frequencies (10-200 Hz) and amplitudes (0.25 to 1.5 mA) to MTL depth electrodes (see online Methods for details). Rectangular stimulation pulses were delivered for 500 ms, followed by a 3-second inter-stimulation interval (Figure 1A-C). Each subject received at least 240 stimulation events ("trials") at 1-8 distinct sites in MTL gray or white matter (mean 2.7 sites; see Table 5.T2 for stimulation locations). During a separate recording session in which no stimulation occurred, for each subject we computed resting networks of low-frequency (5-13 Hz) coherence, motivated by prior literature that shows robust iEEG functional connectivity at low frequencies[73,100,154,155]. These networks reflect correlated low-frequency activity between all possible pairs of

electrodes in a subject, during a period when subjects are passively waiting for a task to begin (Figure 5.2A).

For each stimulation trial, we computed theta power (5-8 Hz) in 900 ms windows before and after each 500 ms stimulation event, and compared the pre- vs. post-stimulation power across all trials with a paired *t*-test (Figure 5.1D). Next, we used linear regression to correlate the strength of a stimulation site's network connectivity to a recording electrode with the power t-statistic at that electrode (Figure 5.2A-D). We included absolute distance as a factor in our regression, to only consider how connectivity relates to stimulation beyond the brain's tendency to densely connect nearby regions[156]. The result is a model coefficient that indicates, independent of distance, the degree to which functional connectivity predicts stimulation-induced change in theta power at a recording site. The regression was repeated using permuted connectivity/evoked power relationships to generate a null distribution of model coefficients against which the true coefficient is compared. We refer to the resulting z-score as the "network-mediated activation (θ)," or NMA_θ . High NMA_θ indicates functional network connectivity predicts observable stimulation-related change in theta power at distant sites.

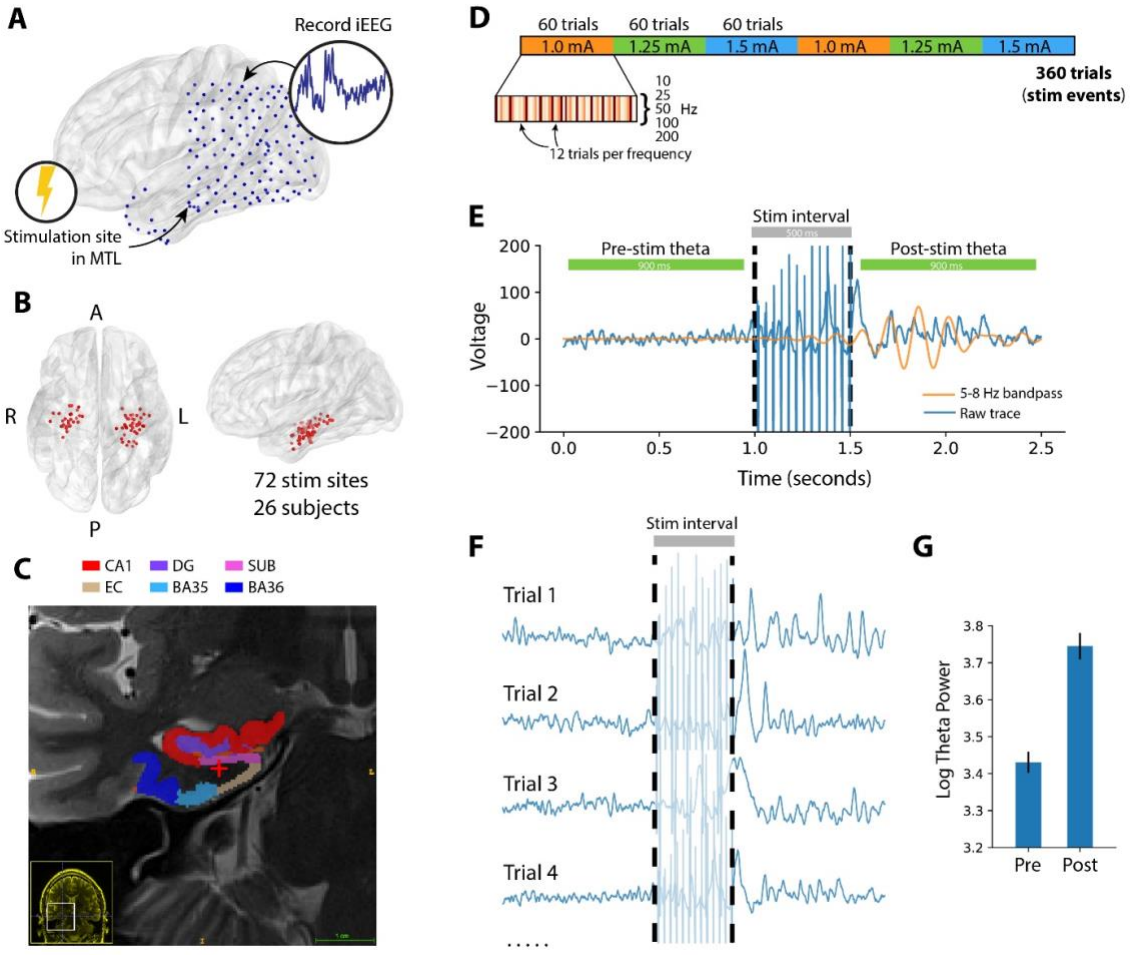

Figure 5.1. Comparison of pre- vs. post-stimulation theta (5-8 Hz) power in an example subject. (A) Each of 26 subjects received a series of 500 ms bipolar stimulation events, at 1-7 sites within the MTL; an example subject schematic is shown here. **(B)** Anatomical distribution of all MTL stimulation sites in the 26-subject dataset. **(C)** T2 MRI and MTL subregion segmentation for an example subject. Stimulation location, in white matter, is indicated at the red cross. See Figure 5.S1 for subregion labels. **(D)** Schematic of a typical stimulation session. Each stimulation site receives stimulation at three amplitudes (within the 0.25-2.00 mA range) and five pulse frequencies (50-200 Hz; see Methods for details). During each session, amplitudes are delivered in 60-trial blocks, within which 12 stimulations are delivered at each frequency. For the main results, effects are aggregated across all stimulation parameters; see Figure 5.S2 for analysis of stimulation amplitude and frequency. **(E)** Using the multitaper method, theta power (5-8 Hz) was measured in 900 ms windows preceding and following each stimulation event, with 50 ms buffers before and after stimulation. In an example stimulation event, the 5-8 Hz bandpass signal (orange) is overlayed on the raw bipolar signal (blue), to emphasize a change in pre- vs. post-stimulation theta power. **(F)** Theta power is extracted in the pre- and post-stimulation intervals for at least 240 events ("trials") per stimulation site. **(G)** The log-transformed theta power is aggregated for all pre- and post-stimulation intervals separately, for later statistical comparison (Fig. 5.2).

NMA_θ is correlated with proximity to white matter

At a group level of stimulation sites, NMA_θ was significantly greater than zero (1-sample *t*-test, $t(71) = 4.18$, $P = 8.2 \times 10^{-5}$; Figure 5.3A), indicating that stimulation in the MTL tends to evoke network-driven change in theta power in distant regions. However, we noted substantial heterogeneity between stimulation sites, with some showing little or no ability to modulate network-wide theta activity, as reflected by NMA_θ near zero. To explain this heterogeneity, we hypothesized that, as earlier work demonstrated[44,148,157], structural connections (i.e. white matter tracts) may be key to the propagation of electrical stimulation throughout the brain.

To test whether structural connections play a role in stimulation propagation, we asked whether NMA_θ was correlated with the proximity of a stimulation site to white matter. If these measures are correlated, it would indicate that functional connectivity is predictive of physiology only insofar as white matter tracts are accessible. We binned stimulation sites according to whether they were placed in gray matter (n = 32, lower 50th percentile of distances to white matter), near white matter (n = 33, upper 50th percentile of distances to white matter), or within white matter (n = 7, manually identified by a neuroradiologist; Figure 5.3A; see Figure 5.S1 for anatomical placement of each white matter target). We found that NMA_θ was significantly increasing with white matter placement, relative to a permuted distribution (permuted $P < 0.001$; Figure 5.3B). The NMA_θ for gray matter sites was not significantly different than zero (1-sample *t*-test, $t(31) = 1.4$, $P = 0.18$), while NMA_θ for sites near or in white matter was significant ($P < 0.05$). This relationship holds in a Pearson correlation agnostic to any electrode categorization ($r = 0.33$, $P = 0.005$; Figure 5.S3). This finding does not mean gray matter stimulation fails to induce theta activity, but it does suggest that stimulation far from white matter tracts may result in theta activity that is uncorrelated with connectivity to remote sites.

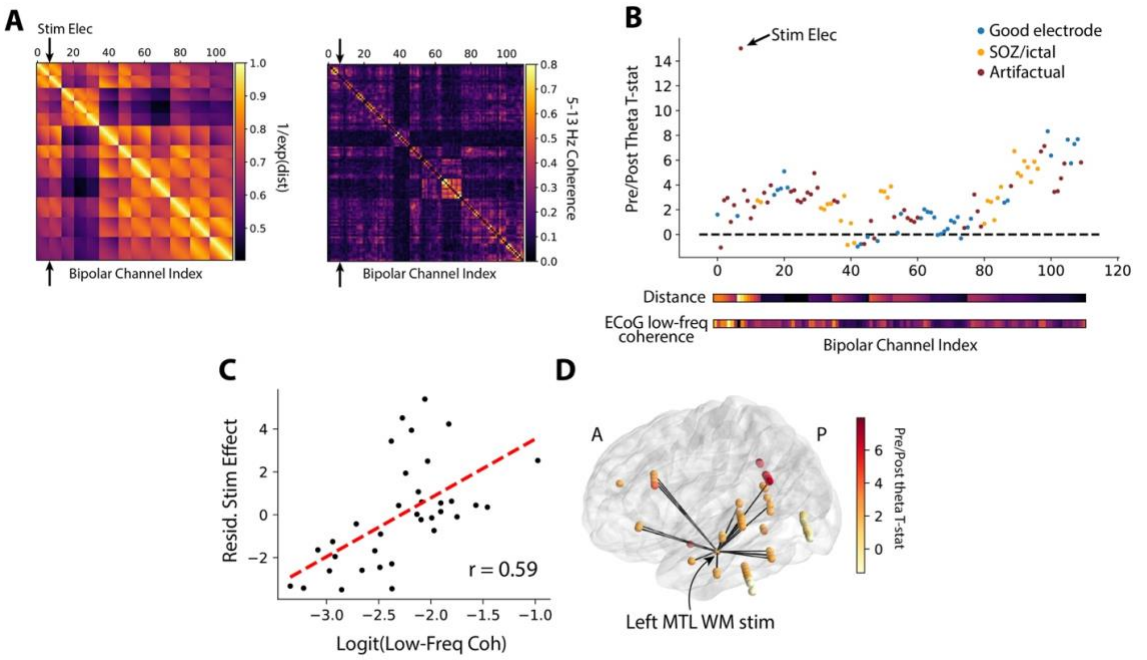

Figure 5.2. Method for determining network-mediated activation (NMA_θ). (A) For each subject, Euclidean distances (left matrix) and functional connectivity (right matrix) are measured for all possible electrode pairs. Distances are linearized as $e^{-(distance)}$, with 1.0 representing no separation between two electrodes. Functional connectivity is the averaged 5-13 Hz multitaper coherence in 1-second windows extracted from a baseline period. **(B)** Pre- and post-stimulation theta power (Fig. 5.1C) is compared with a paired t-test to generate a *t*-statistic for each electrode. Electrodes are excluded from analysis if they exhibited significant post-stimulation artifact (red, see Methods for details) or were placed in the seizure onset zone or exhibit high inter-ictal spiking (orange). **(C)** Multiple linear regression is used to correlate the logit-transformed functional connectivity (between a recording electrode and the stimulation electrode) with the power *t*-statistic, independent of distance. To demonstrate this, the distance-residualized *t*-statistic ("Stim Effect") is plotted against functional connectivity in the example subject. The z-scored version of this correlation is referred to as the "network-mediated activation (θ)," or NMA_θ. **(D)** Rendering of the power *t*-statistic as color on each electrode in the example subject, plotted with the top 10% of functional connections to the stim electrode (red lines).

To account for the possibility that the theta response is sensitive to the pulse frequency or amplitude of stimulation, we asked whether NMA_θ differed in accordance with stimulation parameters. Across all stimulation sites, NMA_θ was marginally greater for trials delivered at a subject's maximum versus minimum amplitude (paired *t*-test, $t(71) = 1.91$, $P = 0.061$;

Figure 5.S2-A), but no difference was noted across pulse frequencies delivered at 10 Hz, 50 Hz, and 200 Hz (repeated measures ANOVA, F = 0.16, $P = 0.85$; Figure 5.S2-B). Additionally, raw evoked power was significantly greater for maximum amplitude stimulation ($t(71) = 3.52$, $P = 0.0008$), but did not reliably differ across pulse frequencies (F = 0.26, $P = 0.77$; Figure 5.S2-B). For the remainder of this study, all analyses consider stimulation events aggregated across amplitudes and frequencies.

Taken together, these results show that direct electrical stimulation of the MTL can induce spectral power changes across a distributed network of regions, particularly if stimulation occurs in or proximal to white matter. When this occurred, we discovered that functional low-frequency coherence is predictive of where stimulation-related modulations in theta power are observed.

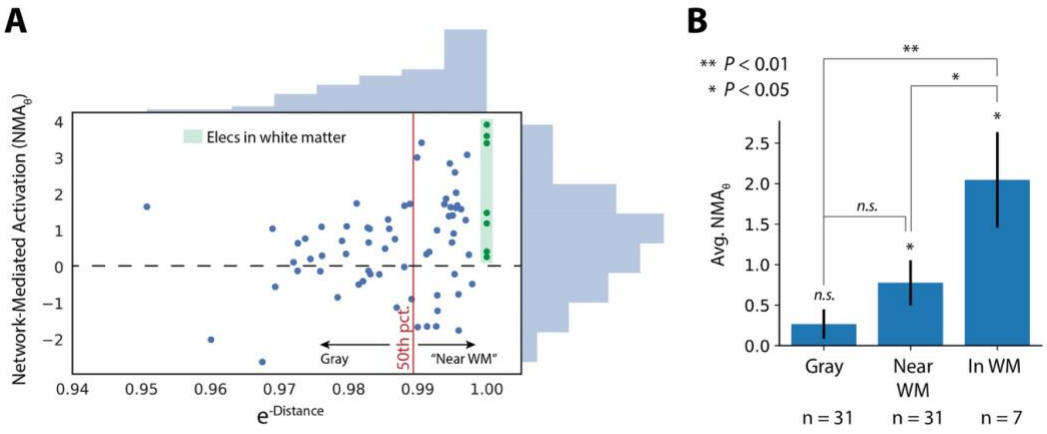

Figure 5.3. Proximity to white matter predicts NMA_θ**. (A)** Correlation between a stimulation site's distance from nearest white matter with the site's NMA_θ. The 50th percentile of white matter distances divides sites classified as "gray matter" versus "near white matter." Stimulated contacts in white matter are highlighted in green. See Figure 5.S3 for the Pearson correlation of these data ($r = 0.33$, $P = 0.005$). **(B)** NMA_θ increases with closeness to white matter, as determined by a permutation test ($P < 0.001$, see Methods) and by noting that NMA_θ for sites in or near white matter are significantly greater than zero (1-sample t-test, $P < 0.05$) while gray matter sites are not ($P = 0.15$). Electrodes placed in white matter have greater NMA_θ than electrodes near white matter (2-sample t-test, $P < 0.05$) or gray matter ($P < 0.01$). Error bars show +/- 1 SEM; * $P < 0.05$; ** $P < 0.01$.

Network properties of MTL stimulation

Having shown that stimulation in or near white matter sites induces distributed changes in theta power, we next sought to characterize the directionality of change. Specifically, high NMA_θ could be caused by increases in theta power at electrodes with strong functional connectivity to the stimulation target, or decreases in theta power at electrodes with weak connectivity to the stimulation target. To distinguish between these possibilities, we further examined theta power changes among the 16 stimulation sites that exhibited individually significant ($P < 0.05$) NMA_θ (see Table 5.T1 for statistics and anatomical placement of each significant site). In this subset, we measured the average pre- vs. post-stimulation theta power at the five electrodes with the strongest functional connectivity to the stimulation site (controlled for distance), and the five electrodes with the weakest functional connectivity. At strongly-connected sites, theta power change was significantly positive (1-sample *t*-test, $t(15) = 5.6$, $P = 4.0 \times 10^{-5}$) and significantly greater than power change at weakly-connected sites (paired *t*-test, $t(15) = 6.03$, $P = 1.7 \times 10^{-5}$; Figure 5.4B). No significant power change was observed at sites with weak functional connectivity (1-sample *t*-test, $t(15) = 1.5$, $P = 0.15$). Notably, we observed that of the 16 significant sites analyzed here, 15 were placed in or near white matter. We conclude that stimulation causes increased theta power at strongly-connected sites and little to no change in power at weakly-connected sites.

Principles of network control theory suggest a relation between the connectivity profile – or network topology – of a stimulation site and the ensuing change in brain activity. Network "hubs," or regions with strong connectivity to the rest of the brain, exert differential effects on overall brain activity versus non-hubs, or regions with strong connections to only a few areas[150,158]. To directly test whether stimulation propagates differently from hub regions, we asked whether stimulation-induced theta power correlated with the functional "hubness" of a stimulation site. We again took our measure of stimulation-induced activity to be the theta power change at the five recording sites with the strongest functional connectivity to the stimulation site, and tested this metric against the node strength of a stimulation site, an indicator of hubness. For this analysis, we considered all stimulation

sites in or near white matter, (n = 40) as these groups both exhibited significant NMA_θ (see Figure 5.3B). When weak hubs (lower tercile of hub scores; n = 13) were stimulated, power change at connected recording sites was significantly greater than zero (1-sample *t*-test, $t(12) = 3.6$, $P = 0.003$), but stimulation at strong hubs (upper tercile; n = 14) evoked no significant power modulation ($t(13) = 0.15$, $P = 0.87$; Figure 5.4D). While counterintuitive, this result could suggest that stimulation at a site with many connections may disperse or blunt the effect of perturbation, yielding lesser activation in downstream regions. Alternatively, hub stimulation does evoke widespread changes in brain activity, but these changes tend to be outside the theta band assessed here.

Our choice of low-frequency (5-13 Hz) functional connectivity as the basis for predicting distributed changes in theta power was motivated by prior studies that have shown strong, cognitively-relevant connectivity at low frequencies particularly the theta and alpha bands[73,100,154]. However, others have noted significant inter-regional connectivity in the beta and gamma bands[59]. As our study presented a unique opportunity to examine the causal nature of functional connectivity, we asked whether functional connectivity in other frequency bands is also predictive of downstream power modulations. Among all MTL electrodes placed in or near white matter (n = 40), we asked whether NMA was significant for networks constructed from any frequency to a maximum of 50 Hz. No frequencies outside the alpha/theta bands exhibited significant group-level NMA_θ, after correction for multiple comparisons (1-sample *t*-test, $P < 0.05$, Benjamini-Hochberg correction; Figure 5.4E). This demonstrates that functional networks constructed from high frequencies (> 13 Hz) are not predictive of stimulation-induced theta activity.

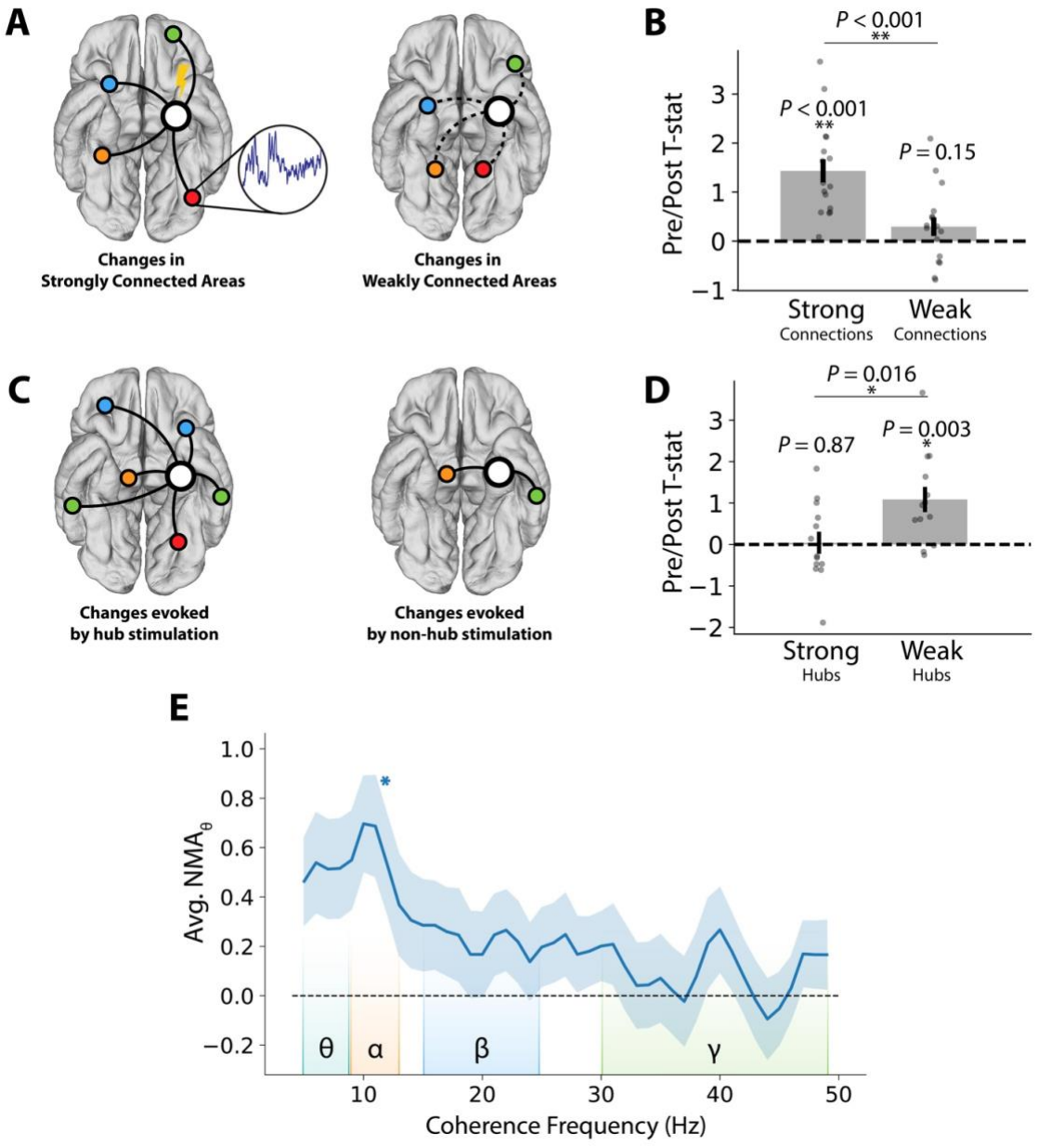

Figure 5.4. Network properties of stimulation-induced theta. (A) Schematic of a stimulation site and its most strongly-connected areas (left) or weakly-connected areas (right). **(B)** For each of 16 stimulation sites with significant NMA_θ ($P < 0.05$), the average post- vs. pre-stimulation theta T-statistic is computed for the five strongest-connected electrodes and the five weakest-connected electrodes (controlled for distance). Strongly-connected regions are typically areas of the lateral temporal, prefrontal, or inferior parietal cortices. Changes at strongly-connected recording sites are significantly greater than changes at weakly-connected sites (paired *t*-test, $t(15) = 6.03$, $P = 1.7 \times 10^{-}$

[5]). **(C)** Schematic of a hub-like stimulation site (left) and a non-hub stimulation site (right). Hub scores are calculated as the node strength, or average of all connection weights to a given electrode. **(D)** For each of 40 stimulation sites in or near white matter, the average post- vs. pre-stimulation theta T-statistic is computed for the five strongest-connected recording electrodes. Stimulation of a weak hub (lower tercile of hub scores, n = 13) yields significantly greater change in connected regions than stimulation of a strong hub (upper tercile of hub scores, n = 14) (2-sample *t*-test, $P = 0.016$). **(E)** Average NMA_θ across all in or near-white matter stimulation sites, as a function of functional connectivity frequency. NMA_θ is greatest for networks constructed from theta or alpha coherence (5-13 Hz). Corrected for multiple comparisons across all frequencies, NMA_θ is significantly greater than zero at 11 Hz. Error bars show +/- 1 SEM; * $P < 0.05$; ** $P < 0.01$.

Alternative measures of connectivity

Functional connectivity is a broad domain, generally referring to an array of measures that fundamentally reflect timeseries correlations. In addition to the phase-based measures (i.e. spectral coherence) used here, other correlations have also been shown to robustly capture inter-regional functional dynamics in the human brain. Of particular utility in iEEG investigations is the amplitude envelope of high-frequency broadband (HFB; 50-200 Hz), shown to reflect neuronal population spiking activity[27] and correlated with fMRI BOLD activation[28]. The slow (< 1 Hz) fluctuations of this signal have also been shown to correlate with resting-state functional connectivity (rsfMRI)[153,159,160]. It has recently been demonstrated that stimulation perturbs brain networks in accordance with measures of functional connectedness, including a modulation of remote cortical excitability[45,161].

We therefore sought to determine whether these established measures of intrinsic functional connectivity – HFB amplitude envelope correlation and rsfMRI connectivity – also predicted the location of evoked theta power. To do this, we replicated our procedure for computing NMA_θ, but used HFB amplitude envelope correlation or atlas-based rsfMRI connectivity as predictor variables (see Methods for details; see Figure 5.5A for example adjacency matrices). As with the low-frequency coherence networks, the result is a z-scored statistic (NMA_θ) that reflects the degree to which a functional network predicts remote changes in theta power. We emphasize that HFB envelope networks – though based on extracted high-frequency power – are wholly distinct from 30+ Hz coherence networks

assessed earlier; the former is a correlation of the slow variation in a power timeseries, while the latter is a measure of high-frequency phase consistency between two signals.

Though rsfMRI and HFB connectivity measures qualitatively recapitulated our earlier finding – NMA_θ increases with closeness to white matter – their ability to predict downstream changes in evoked theta power was not significant across all stimulation sites (HFB-connectivity, $t(71) = 1.07$, $P = 0.28$; atlas rsfMRI, $t(49) = 0.17$, $P = 0.87$; Figure 5.5B). We note that slightly fewer stimulation sites were available for the rsfMRI analysis (n = 50), due to subjects where atlas-based measures could not be estimated for a sufficient number of electrodes (see Methods for details).

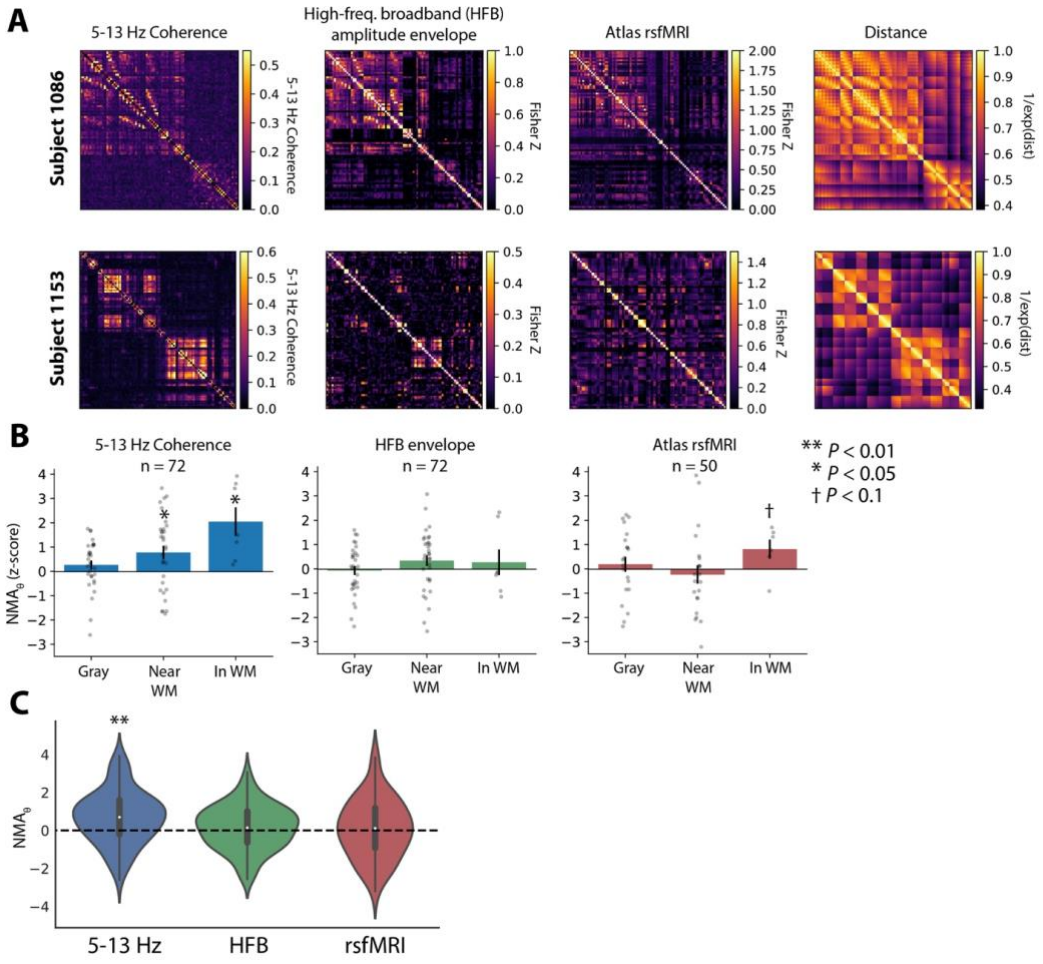

Figure 5.5. Alternative measures of connectivity. (A) Example adjacency matrices for two subjects, reflecting functional connectivity from low-frequency (5-13 Hz) coherence, correlated high-frequency broadband envelope (HFB; 50-200 Hz), and atlas-based resting state fMRI (rsfMRI). Matrices are organized as in Figure 5.2A. For reference, adjacency matrices of linearized Euclidean distance are shown at the far right. Colormap ranges are selected to visually emphasize network structure. Values in the HFB envelope and rsfMRI networks are Fisher z-transformed correlation coefficients. (**B)** NMA_θ is computed as in Figures 5.2-5.3, using adjacency matrices for each of the three measures. NMA_θ was binned by distance from white matter, organized as in Figure 5.3B. In addition to significant NMA_θ in and near white matter using 5-13 Hz coherence networks ($P < 0.05$), we noted marginally significant NMA_θ in white matter using atlas-based rsfMRI networks ($P < 0.1$). **(C)** Distribution of NMA_θ for all stimulation electrodes regardless of distance from white matter. NMA_θ is significantly greater than zero at the group level for 5-13 Hz coherence (1-sample *t*-test, $t(71) = 4.18$, $P = 8.2 \times 10^{-5}$). Note that the total count of stimulation electrodes is lower for rsfMRI connectivity (n = 50) analyses, due to subjects where atlas-based rsfMRI could not be extracted for a stimulation electrode; see Methods for details. Error bars show +/- 1 SEM; * $P < 0.05$; ** $P < 0.01$.

Though HFB envelope and rsfMRI connectivity did not strongly replicate our finding of significant NMA_θ using low-frequency coherence, several factors could account for this discrepancy. First, stimulation within the unique architecture of the MTL may propagate differently than the cortical surface stimulation used in many prior studies – it is possible that, at the cortical surface, HFB/rsfMRI connectivity is better predictive of stimulation effects than low-frequency coherence. Second, different measures of connectivity may differentially predict different kinds of evoked responses. Low-frequency coherence successfully predicts low-frequency power, but may fail to accurately predict modulations at higher frequencies.

Evoked responses at higher frequencies

While our choice to examine the effect of stimulation on theta frequencies was theoretically motivated by a vast literature implicating theta oscillations and cognition[124], activity in the HFB range is a useful marker of population neural activity[67], and cognitively-relevant oscillatory dynamics are also observed in the alpha, beta, gamma bands (9-13 Hz, 15-25 Hz, 30-60 Hz, respectively). To account for the possibility that stimulation evokes activity in these higher frequency bands, we extended our analysis to consider the correlation between low-frequency coherence and induced power in alpha/beta, gamma, and HFB ranges. Furthermore, to address the possibility that HFB-based connectivity networks (Figure 5.5A) better predict induced local HFB power, we asked about the correlation between HFB envelope connectivity and induced power across frequency ranges (see Methods for details).

We first assessed whether stimulation evoked any detectable modulation of power in the alpha/beta, gamma, and HFB bands, regardless of relationship to connectivity. To do this, we averaged the pre-versus-post stimulation T-statistic across all electrodes in each subject's brain, for each frequency band. The result is an average T-statistic reflecting the stimulation-evoked whole-brain change in power at each frequency band. Across all stimulation sites, stimulation significantly increased power in the theta, alpha/beta, and gamma bands, but significantly decreased power in the HFB range (1-sample T-test, FDR-corrected $P < 0.05$; Figure 5.6A-C). However, the power response to stimulation was not

uniform across electrodes within a subject; for electrodes that exhibited a strong theta response, evoked changes were weaker at higher frequencies (Figure 5.6D), indicating a theta-specific effect.

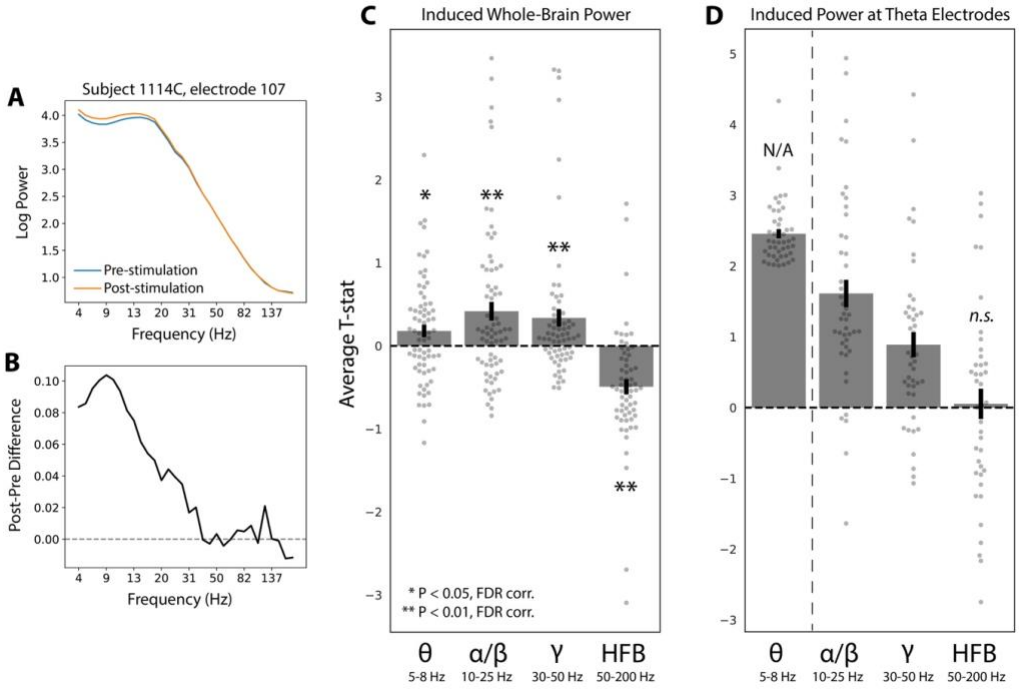

Figure 5.6. Stimulation-induced power across frequency bands. (A) Stimulation-induced power spectrogram for an example electrode from a single subject (stimulation in left MTL white matter, recording electrode in left inferior parietal cortex). **(B)** Post-minus-pre stimulation difference in power from the electrode in (A). **(C)** Whole-brain stimulation-induced power was measured by computing a T-statistic on the pre- vs. post-stimulation spectral power at each electrode in a subject, and then averaging across electrodes to get an estimate of whole-brain change in power. On average, stimulation elevated whole-brain power in the theta (5-8 Hz), alpha/beta (10-25 Hz), and gamma (30-50 Hz) bands (1-sample *t*-test, FDR-corrected $P < 0.05$). Stimulation decreased power in the HFB range (50-200 Hz). **(D)** For each subject/stimulation site, electrodes were classified by whether they exhibited a significant ($T > 2$) change in theta power induced by stimulation (at least 1 theta-responsive electrode was found for 47 of the 72 stimulation sites). The stimulation-induced change at higher frequencies was computed for this subset of electrodes, to determine whether the power response was specific to theta. Across all subjects/stimulation sites, increased power was observed in the alpha/beta and gamma range at theta-responsive electrodes, but no effect was observed in the HFB range (1-sample *t*-test, $t(46) = 0.25$). The bar for induced theta power is delineated by a dashed line and shown as a reference only, since theta power was the basis for selecting these electrodes for further analysis. Error bars show +/- 1 SEM; * corr. $P < 0.05$; ** corr. $P < 0.01$.

Given that stimulation evoked changes in spectral power beyond the theta range, we next asked whether functional connectivity networks predicted these changes (e.g. computing NMA_{HFB}. Corrected for multiple comparisons, low-frequency (5-13 Hz) coherence networks only correlated with evoked power in the theta range (1-sample T-test, $t(71) = 4.18$, FDR-corrected $P < 0.01$; Figure 5.7A). On average, HFB envelope connectivity did not significantly predict power modulation at any frequency band. However, given our earlier finding of decreases in power in the HFB band (Figure 5.6), we hypothesized that a null average effect was obscuring heterogenous – but individually significant – responses to stimulation. In other words, for specific subjects, HFB envelope networks could predict increases or decreases in HFB power and yield significant correlations in positive or negative directions. Indeed, HFB functional connectivity significantly predicted HFB power decreases for 7 stimulation sites and power increases for 3 stimulation sites, a total count that significantly exceeds the expected false positive rate (binomial test, FDR-corrected $P = 0.009$; Figure 5.7B).

Taken together, functional connectivity measured by low-frequency coherence significantly predicts stimulation-evoked power in the theta band, but not induced power at higher frequencies. On average, HFB envelope networks do not significantly correlate with evoked changes in any frequency band, even HFB power itself. However, the dynamics of stimulation appear to be more complex in this high-frequency band; HFB power is often decreased by stimulation – unlike the theta response – and for a significant number of stimulation sites, both low-frequency coherence and HFB functional connectivity predict where in the brain such decreases are observed.

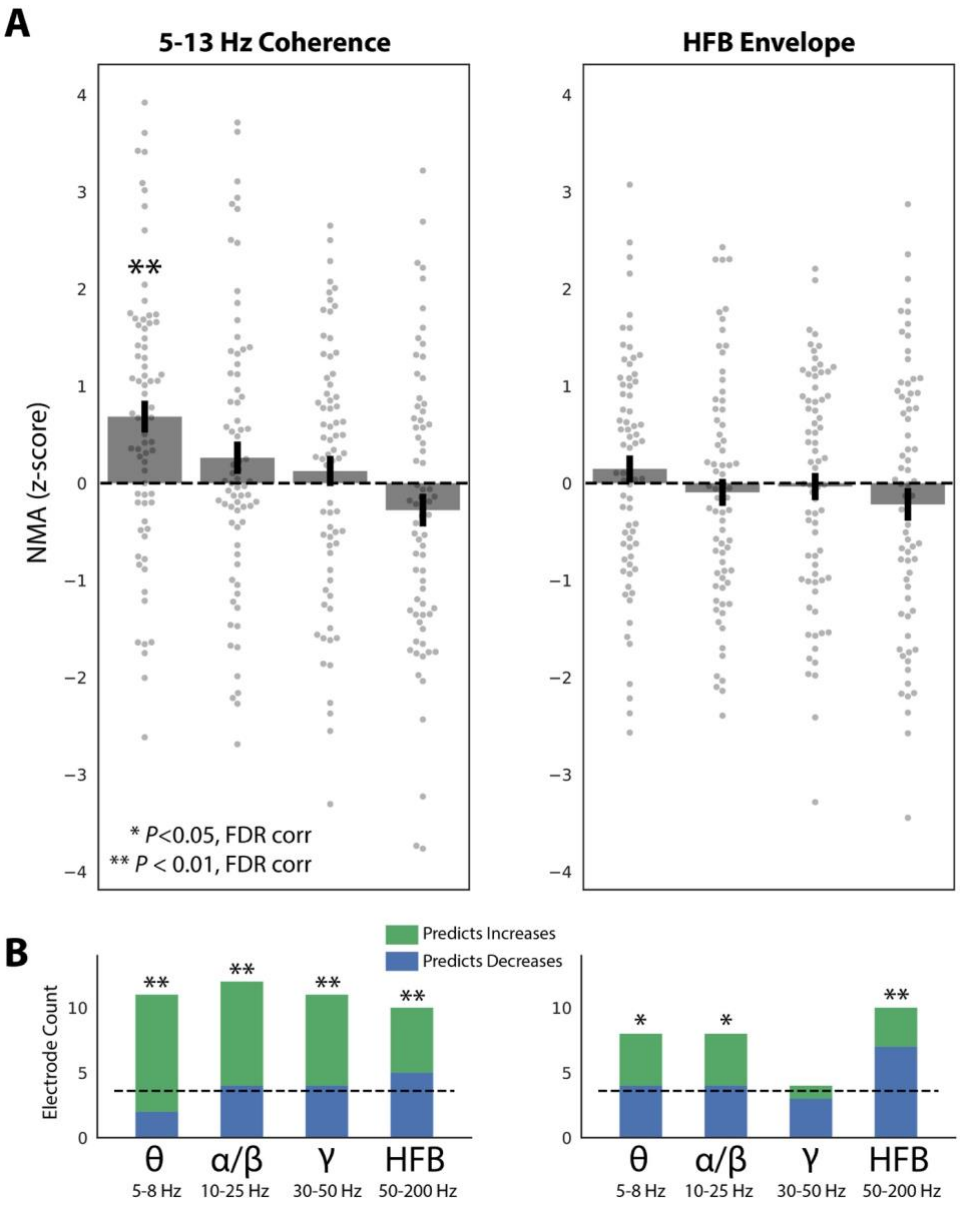

Figure 5.7. Power response at higher frequencies. (A) The average NMA – reflecting the degree to which functional connectivity predicts changes in spectral power – was computed for theta (5-8 Hz), alpha/beta (10-25 Hz), gamma (30-50 Hz), and HFB (50-200 Hz) bands for all 72 MTL stimulation sites. Functional connectivity was measured as 5-13 Hz coherence (left) and HFB amplitude correlation (right; see Methods for details). Across all stimulation sites, 5-13 Hz coherence significantly predicted changes in theta power, as demonstrated in Figure 5.2 (1-sample *t*-test, $t(71) = 4.18$, corrected $P < 0.01$). HFB amplitude correlations did not significantly predict power changes in any band. **(B)** To account for the fact that connectivity could predict decreases or increases in power,

each stimulation site was classified by whether its functional connectivity profile significantly predicted decreases (blue) or increases (green) power (two-tailed $P < 0.05$). The count of significant stimulation sites are depicted as stacked bars; the expected false positive rate ($P = 0.05$) is indicated as a dashed line. Note that though HFB amplitude correlations do not significantly predict changes in HFB power on average (panel A), the count of stimulation sites where connectivity significantly predicts changes in HFB power is significantly greater than chance (7 decreases, 3 increases; binomial test, corrected $P < 0.01$). Error bars show +/- 1 SEM; * corr. $P < 0.05$; ** corr. $P < 0.01$.

Discussion

We set out to test a fundamentally simple hypothesis: Do functional connections in the brain predict how focal electrical stimulation flows from one region to another? Though critical to the future of brain stimulation and therapeutic development, this hypothesis has not seen rigorous testing. Prior studies indicate that connectivity plays a role in how stimulation events perturb distant brain regions[44,45,149,157], but fundamental assumptions of graph-theoretic models remain untested[92]. More broadly, no prior studies have addressed whether iEEG-based functional connectivity indicates anything about causal relationships in the brain, or whether is it merely a correlative measure. Here we specifically tested a hypothesis about the effects of stimulation on theta power, given an especially rich literature showing the cognitive relevance of theta oscillations[115,121,123,162]. To account for possible dynamics outside this range, we extended several key analyses to alpha/beta, gamma, and high-frequency broadband power, and further considered whether functionally-derived measures of connectivity better capture the effects of stimulation-induced power.

We discovered that (1) modulation of theta power is correlated with functional connectivity, particularly if stimulation occurred in or near white matter, (2) stronger functional connections yield greater theta power increases, (3) low-frequency coherence better predicts downstream increases in theta power than HFB envelope or rsfMRI networks, and (4) in specific cases HFB envelope networks do succeed in predicting modulations in HFB power. These results suggest that stimulation evokes a heterogenous mixture of effects across frequencies, and that functional networks may best predict the frequency on which they were based.

The meaning of functional connectivity is a subject of considerable debate. Correlated activity between two parts of the brain may reflect direct connection between the two, an indirect connection through a third region, or the activity of a third region independently driving activity in each[36]. Though most neuroscientists are aware of such limitations, functional connectivity is often implicitly treated as a measure of causality nonetheless. Our use of targeted stimulation allowed us to test whether this implicit assumption is true. Our results generally support the idea that functional connectivity indicates causal relations in the brain; when stimulation occurs in or near white matter, we could predict where power changes would occur based on distance-independent measures of low-frequency functional connections. This finding aligns with observations that intrinsic functional connectivity in MRI is constrained by white matter anatomy[163]. However, substantial variance in power modulation remained unexplained by connectivity, and we also showed that propagation of gray matter stimulation – still rich with functional connections – cannot be predicted in the same way.

HFB amplitude envelope networks and atlas-based rsfMRI networks failed to strongly predict remote changes in theta power. However, earlier reports suggest that these functionally-relevant measures do correlate with CCEPs and changes in cortical excitability[45,161]. To explain this discrepancy, we note that there are several key differences between those reports and the present study. First, we solely examined the effect of medial temporal lobe stimulation, which has a distinct architecture that may affect how stimulation propagates to other regions – effects of stimulation at the cortical surface, as in prior studies, could differ markedly. Relatedly, we used stimulation amplitudes that are lower than those typically used at the cortical surface (< 2mA versus > 4mA). Finally, while HFB envelope networks did not successfully predict remote changes in theta power, they more accurately correlated with remote decreases in HFB power – it is possible that networks based on measures of cortical activation are better predictors of how stimulation affects those same measures.

In this study, we also assessed the relationship between stimulation and the network topology of a targeted region. Specifically, we asked whether the downstream effects of

stimulation differed between hubs and non-hubs, reflecting regions that are richly or sparsely connected. Counterintuitively, we found that stimulation of non-hubs yielded greater increases in theta power at downstream sites. It is possible that (1) hub stimulation does result in greater distributed power changes, but outside the theta band, or (2) hub stimulation results in a dispersal or blunting effect, causing widespread change but limiting the magnitude of the effect at any single downstream site. Such a result is plausible if there is an interaction between the underlying brain structure and the effect of stimulation – it has been demonstrated that stimulation less effectively activates large-diameter axons, for example[164]. Furthermore, principles of network control theory postulate that stimulation of sparsely connected regions can be efficacious for moving the brain to "difficult-to-reach" states, or states that require significant cognitive effort to achieve[92,150,158]. However, the mapping between spectral power and "brain states" in a cognitive sense remains unclear; further empirical and theoretical work should aim to clarify how control theoretic predictions can be tested with common intracranial techniques.

The findings from this study could be extended in several ways. A recent study by Keller, et al. (2018) asked whether a multivariate model could predict how direct brain stimulation alters remote cortical excitability[161]. A similar approach could be adopted with these data, wherein multimodal measures of connectivity – e.g. coherence, HFB-envelope, and white matter proximity – could be used to predict the stimulation response across locations and frequency ranges. Such an approach could reveal relationships that were obscured by the univariate methods in this manuscript; gray matter targets, for instance, may induce widespread, connectivity-related changes in specific frequencies that are predictable by a weighted combination of functional networks. Additionally, our study as designed was agnostic to the directionality of induced effects; especially in the setting of direct white matter stimulation, we expect that our results reflect a combination of prodromic and antidromic propagation. In other words, stimulation of MTL structures is potentially inducing activity in input and output regions, though the undirected measures of functional connectivity used here are unable to tease those effects apart.

We solely analyzed stimulation through the lens of changes in brain physiology. However, with an eye towards the eventual therapeutic use of stimulation, the results here begin to bridge prior studies of stimulation and behavior with underlying neural mechanisms. A recent study reported decreases in episodic memory performance during stimulation at certain times, associated with increases in cortical theta power[51]. Additionally, memory performance was noted to increase with theta-burst stimulation of the perforant path, a major white matter tract of the MTL[49]. Deep brain stimulation targeted to white matter tracts has also been shown to improve outcomes in treatment-resistant depression[144]. Collectively, these findings are supported by the results here – white matter stimulation appears to evoke remote increases in neural activity. Few studies have deeply examined stimulation-induced changes in physiology with behavioral enhancement, though our approach outlined here enables us to do exactly that in future work.

Here we demonstrated that functional connections in the human brain inform how stimulation evokes remote changes in neural activity. This is powerful new evidence that, even in the absence of knowledge about an individual's structural connectome, functional connectivity can reflect causality in the brain – a finding with significant implications for how neuroscientists interpret inter-regional correlations of neural activity. Furthermore, by showing that stimulation-evoked changes interact with the functional hubness of a targeted site, we provided a critical data point for the application of network control theory to real-world brain dynamics.

Methods

Participants

Twenty-six patients with medication-resistant epilepsy underwent a surgical procedure to implant subdural platinum recording contacts on the cortical surface and within brain parenchyma. Contacts were placed so as to best localize epileptic regions. Data reported were collected at 8 hospitals over 4 years (2015-2018): Thomas Jefferson University Hospital (Philadelphia, PA), University of Texas Southwestern Medical Center (Dallas, TX), Emory University Hospital (Atlanta, GA), Dartmouth-Hitchcock Medical Center (Lebanon,

NH), Hospital of the University of Pennsylvania (Philadelphia, PA), Mayo Clinic (Rochester, MN), National Institutes of Health (Bethesda, MD), and Columbia University Hospital (New York, NY). Prior to data collection, our research protocol was approved by the Institutional Review Board at participating hospitals, and informed consent was obtained from each participant.

Electrocorticographic recordings

iEEG signal was recorded using depth electrodes (contacts spaced 3.5-10 mm apart) using recording systems at each clinical site. iEEG systems included DeltaMed XlTek (Natus), Grass Telefactor, and Nihon-Kohden EEG systems. Signals were sampled at 500, 1000, or 1600 Hz, depending on hardware restrictions and considerations of clinical application. Signals recorded at individual electrodes were first referenced to a common contact placed intracranially, on the scalp, or mastoid process. To eliminate potentially confounding large-scale artifacts and noise on the reference channel, we next re-referenced the data using a bipolar montage. Channels exhibiting highly non-physiologic signal due to damage or misplacement were excluded prior to re-referencing. The resulting bipolar timeseries was treated as a virtual electrode and used in all subsequent analysis. Raw electrophysiogical data and analysis code used in this study is freely available at http://memory.psych.upenn.edu/Electrophysiological_Data.

Anatomical localization

To precisely localize MTL depth electrodes, hippocampal subfields and MTL cortices were automatically labeled in a pre-implant, T2-weighted MRI using the automatic segmentation of hippocampal subfields (ASHS) multi-atlas segmentation method[94]. Post-implant CT images were coregistered with presurgical T1 and T2 weighted structural scans with Advanced Normalization Tools[93]. MTL depth electrodes that were visible on CT scans were then localized within MTL subregions (including white matter) by neuroradiologists with expertise in MTL anatomy. All localizations in this manuscript refer to the bipolar midpoint of two recording contacts or the anode/cathode stimulation contacts.

Functional connectivity estimation

To obtain coherence values between electrode pairs, we used the MNE Python software package[140], a collection of tools and processing pipelines for analyzing EEG data. The coherence (C_{xy}) between two signals is the normalized cross-spectral density (Equation 1); this can be thought of as the consistency of phase differences between signals at two electrodes, weighted by the correlated change in spectral power at both sites.

$$C_{xy} = \left| \frac{S_{xy}}{S_{xx}S_{yy}} \right| \quad (1)$$

Where S_{xy} is the cross-spectral density between signals at electrodes x and y; S_{xx} and S_{yy} are the auto-spectral densities at each electrode. Consistent with other studies of EEG coherence[33,165], we used the multitaper method to estimate spectral density. We used a time-bandwidth product of 4 and a maximum of 8 tapers (tapers with spectral energy less than 0.9 were removed), computing coherence for frequencies between 4-50 Hz, avoiding the 60 Hz frequency range that may be contaminated by line noise. Inter-electrode coherences were computed for a series of 1-second windows extracted sequentially from 10-second baseline periods of a non-stimulation task, in which subjects wait passively before beginning a verbal free-recall task. Each subject typically had 24-72 such baseline periods, but all had a minimum of 10 (i.e. the minimum total number of windows used for network estimation was 100). To construct the low-frequency networks used in the majority of this paper, cross-spectra were first averaged across all baseline period windows, normalized by the average power spectra, and then averaged between 5-13 Hz. For the analysis in Figure 5.4E, networks are constructed for each frequency between 4-50 Hz with no averaging over bands.

Stimulation paradigm

At the start of each session, we determined the safe amplitude for stimulation using a mapping procedure in which stimulation was applied at 0.5 mA, while a neurologist monitored for afterdischarges. This procedure was repeated, incrementing the amplitude in steps of 0.5 mA, up to a maximum of 1.5 mA (chosen to be below the afterdischarge

threshold and below accepted safety limits for charge density[166]). For each stimulation session, we passed electrical current through a single pair of adjacent electrode contacts in the MTL. Stimulation was delivered using charge-balanced biphasic rectangular pulses (pulse width = 300 μs) at (10, 25, 50, 100, or 200) Hz frequency and (0.25 to 2.00) mA amplitude (0.25 mA steps) for 500 ms, with a minimum of 3 seconds between stimulation events. During a session, subjects were instructed to sit quietly and did not perform any task. An average of 2.7 stimulation sites were selected for each subject, with a minimum of 240 trials delivered for each. In a typical stimulation session, a given target would receive 360 total stimulation events, in blocks of 60 trials at each amplitude, with 12 randomly-spaced trials at each frequency within the block (Figure 5.1D). For all analyses in the main text, effects were aggregated across stimulation parameters; see Figure 5.S2 for consideration of stimulation frequency and amplitude.

In most subjects, a post-stimulation voltage deflection artifact briefly contaminates a subset of recording contacts. To identify and remove channels exhibiting this artifact, the average voltage in the 350 ms prior to stimulation is compared with a paired t-test to the average voltage in the 350 ms after stimulation, across all trials, for each channel. The same procedure is done with a levene test for different variances. Any electrode with a significantly different pre-vs.-post mean voltage or voltage variance ($P < 0.01$) is excluded from further analysis (see "Estimating theta modulation index"). On average, this procedure excludes 28% of channels. Regardless of stimulation artifact, any bipolar pair is excluded from analysis if it shares a common contact with the stimulated pair. See Figure 5.S4 for a representative example of this artifact.

Spectral power analysis

We used the multitaper method to assess spectral power in the pre- and post-stimulation intervals (-950 to -50 ms relative to stimulation onset, and +50 to +950 ms after stimulation offset; Figure 5.1B). We avoided the Morlet wavelet method to obviate the need for buffer periods that extend into the stimulation window. As in "Functional connectivity estimation," we used the MNE Python software package. For each trial, theta power was taken as the

average PSD from 5-8 Hz, using a time-bandwith product of 4 and excluding tapers with < 90% spectral concentration. To compute a T-statistic at each electrode, the pre- vs. post log-transformed power values were compared with a paired t-test (Fig. 5.1G, Fig. 5.2B). We avoid calculating significances for individual electrodes because sequential trials are non-independent events; T-statistics are only used for later correlation analysis (see "Estimating network-mediated activation").

For analyses that considered spectral power at higher frequencies (Figures 5.6-7), we used the following bands: alpha/beta (10-25 Hz), gamma (30-50 Hz), and high-frequency broadband (50-200 Hz). Power was otherwise computed exactly as described for theta. To measure whole-brain evoked power (Figure 5.6), we took the average T-statistic across all electrodes in each subject's brain, subject to the same exclusion criteria described in "Estimating network-mediated activation." Additionally, we excluded electrodes with T-statistics greater than 10 from the whole-brain average, to account for raw power values that are potentially corrupted by post-stimulation artifact which survives our exclusion procedure (their inclusion does not notably change the main results).

Estimating network-mediated activation

To examine the relationship between stimulation and functional connectivity, we developed an index that reflects the correlation between theta power modulation and connectivity, independent of distance. To do this, we first construct low-frequency (5-13 Hz) networks as described in "Functional connectivity estimation," and take the logit transform to linearize coherence values that fall between 0 and 1. We also construct adjacency matrices that reflect the normalized Euclidean distance between all possible pairs of electrodes (Fig. 5.2A), and linearize the distances by taking the reciprocal of their exponential (i.e. a Euclidean distance of zero would correspond to 1.0). For each stimulated electrode, we take that electrode's distance and connectivity to all other electrodes as predictors of the theta power t-statistic (see "Spectral power analysis) in a multiple linear regression. This controls for the effect of distance from a stimulation target, which is correlated with power and functional connectivity. Next, we permute the order of the predictors 1000 times and re-run

the regression for each. The true coefficient for functional connectivity is compared to the distribution of null coefficients to obtain a z-score and p-value for each stimulation site. The z-score is referred to as the network-mediated activation, or NMA.

Prior to computing NMA_θ, we excluded electrodes placed in the seizure onset zone or exhibiting significant inter-ictal spiking, as determined by a clinician. Electrodes with high post-stimulation artifact (see "Stimulation paradigm"), and stimulated electrodes themselves, were also excluded. Subjects were discarded if less than 10 electrodes remained after all exclusions.

To analyze the relationship between NMA_θ and white matter category (Fig. 5.3), we first binned electrodes according to their distance from nearest white matter. Distance were measured as the linearized Euclidean distance from a stimulation electrode (i.e. bipolar midpoint of the anode/cathode) to the nearest vertex of that subject's Freesurfer white matter segmentation[167] based on T1 MRI. The 50^{th} percentile of white matter distances marked the division between stimulation electrodes categorized as "near" white matter versus in gray matter. Seven stimulation electrodes were identified by expert neuroradiologists as being placed within white matter (see Figure 5.S1 for exact placements). To ask whether NMA_θ increases with white matter category, permuted the white matter labels for each electrode 1000 times and took the minimum T-statistic between gray vs. near and near vs. in categories at each permutation. We then compared the minimum T-statistic in the true data to the distribution of null statistics to generate a p-value.

Network properties of stimulation

To determine how the network structure of a stimulation site affected downstream alterations in theta power (Fig. 5.4), we first analyzed the relationship between pre- vs. post-stimulation theta power and the strength of functional connectivity to a stimulation site (Fig. 5.4A-B). For each stimulation site with a significant NMA_θ ($P < 0.05$), we ranked all other electrodes by the strength of their functional connectivity to that site, residualized on Euclidean distance (e^{-dist}). We then took the average power T-statistic (see "Spectral power

analysis") across the 5 strongest-connected sites and the 5 weakest-connected sites, to assess whether theta power changes correlated with the strength of a functional connection.

To assess whether the effects of stimulation differ between hubs and non-hubs (Fig. 5.4C-D), we measured the node strength[37] for each stimulation site in or near white matter (n=38), using our low-frequency coherence networks (see "Functional connectivity estimation"). The node strength reflects the sum of all connection strengths to a given node (for this paper, we normalized node strength by the total number of possible connections for a given site, yielding strengths in the range from 0 to 1). For all stimulation sites, we binned hub scores by tercile, and took the highest tercile as "strong hubs," the weakest tercile as "weak hubs" (n=13 for each). For stimulation at all strong and weak hubs, we took the average power T-statistic for the 5 strongest-connected electrodes. These values were used to assess whether hub stimulation tends to cause greater power changes in connected regions. The relationship between coherence frequency and theta modulation index (Figure 5.4E) was assessed by re-estimating the NMA_{θ} (see "Estimating network-mediated activation") using spectral coherence networks observed for each frequency between 4-50 Hz, spaced by 1Hz, for all stimulation electrodes placed within or near white matter. The average NMA_{θ} across sites/subjects was 1-sample *t*-tested against zero and p-values were FDR corrected for multiple comparisons (corrected $P < 0.05$). For visualization purposes only, the displayed NMA_{θ}/frequency curve was smoothed with a 3-point moving average window.

Alternative connectivity metrics

HFB amplitude envelope correlation: Networks of correlated high-frequency broadband (HFB; 50-200 Hz in this manuscript) amplitude envelopes were computed in a manner similar to Foster, et al. (2015)[153]. The general approach is to low-pass filter HFB spectral power during a resting period, and the resulting timeseries are correlated between recording electrodes to construct an adjacency matrix. Specifically, in a non-stimulation memory task, we extracted 240-second (4 minute) resting periods between any task events.

Resting periods were identified by searching for the maximum amount of time between task events; in some subjects, 240-second intervals were not available but timeseries were still extracted for that length in the best-possible period. Signals were bipolar re-referenced and notch filtered, sequentially band-passed in 10 Hz windows from 50-200 Hz, Hilbert transformed and normalized to the mean amplitude, and then averaged across bands. Finally, to estimate the slow variation in this signal as a basis for inter-regional correlation, we low-pass filtered the HFB amplitude (< 1 Hz), and computed the Pearson correlation coefficient between the resulting signals between all possible pairs of electrodes within a subject, yielding an adjacency matrix of correlations. The resulting correlations were Fisher z-transformed and then used as predictors of modulations in power (see "Estimating a theta modulation index").

Atlas-based rsfMRI: We used an independent dataset of resting state functional MRI from the Human Connectome Project (HCP)[168] to estimate functional connectivity between recording sites in each patient. For each patient, we mapped the location of subdural and depth electrodes to the HCP grayordinate space[169]. For subdural electrodes, we assigned vertices on the cortical surface mesh within 3mm (geodesic distance) of each recording site to a region of interest (ROI). The coordinates in the native space of each subject were then mapped to the standard fs_LR mesh (i.e., HCP surface space). The location of subcortical contacts in native space were transformed to MNI space using Advanced Normalizations Tools[170], with spherical ROIs centered at each bipolar midpoint. Adjacency matrices for each subject were constructed by computing the average connectivity (fisher-transformed timeseries correlations) between all grayordinates from each pairwise combination of ROIs, provided by the group-averaged (n=897 subjects) dense connectome. These adjacency matrices were subsequently used to determine whether fMRI defined networks provide a scaffold for the propagation of brain-wide theta power following direct electrical stimulation.

Supplemental Figures

Subject ID	Z	P	Region	Distance from WM
1096	3.016455	0	left ca1	0.989909
1101	3.411592	0.001	left fusiform gyrus wm	1
1113	1.72762	0.044	left sub	0.99386
1114	3.606953	0	left mtl wm	1
1114	1.659178	0.041	left amy	0.950779
1115	1.627038	0.045	left sub	0.99555
1120	3.919829	0	left mtl wm	1
1122	2.604052	0.003	right sub	0.995395
1125	1.737326	0.043	left prc	0.988886
1125	1.750235	0.027	left prc	0.981156
1125	3.090451	0.005	left phc	0.997158
1134	1.877686	0.034	left prc	0.994108
1144	1.647388	0.039	left phc	0.994771
1144	1.695835	0.048	left sub	0.995736
1144	2.851826	0.014	left sub	0.994648
1153	2.043864	0.021	left phc	0.995562
1163	3.423	0	left prc	0.990563

Table 5.T1. Stimulation sites with significant ($P < 0.05$) network-mediated activation. P-value were calculated relative to a null distribution; 0 indicates the true correlation exceeded all 1000 observed null correlations. Distances are reported as $e^{-(dist)}$, where 1 indicates electrodes placed in white matter. Legend: WM, white matter; sub, subiculum; amy, amygdala; prc, perirhinal cortex; phc, parahippocampal cortex. "mtl wm" refers to any white matter in the parahippocampal gyrus.

Stimulation region	Count
left amy	1
left ca1	10
left dg	3
left ec	2
left phc	5
left prc	12
left sub	6
left mtl wm	5
right amy	1
right ca1	13
right ca2	1
right dg	3
right ec	2
right prc	5
right sub	1
right mtl wm	2

Table 5.T2. Count of stimulation sites for each MTL subregion. Abbreviations are listed in legend for Table 5.T1.

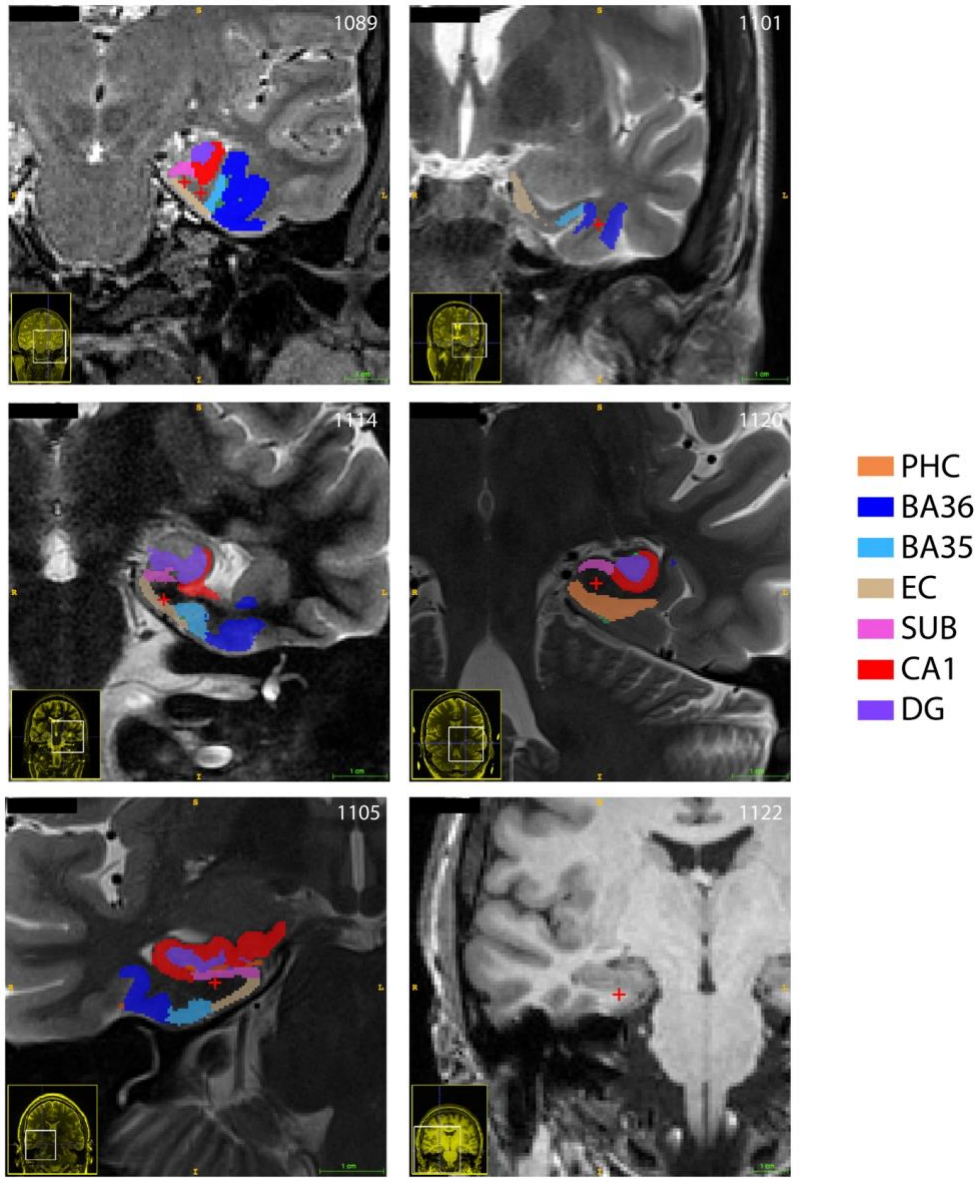

Figure 5.S1. MRI and electrode placements in white matter. In 6 subjects (7 distinct stimulation sites), bipolar stimulation electrode midpoints fell directly in MTL white matter, indicated by red crosses at the midpoint of the anode/cathode contacts. Overlaid segmentations show MTL subregions, according to the color legend above (no segmentation available for subject 1122). PHC, parahippocampal cortex; BA36, Broadmann area 36; BA35, Broadmann area 35/perirhinal cortex; EC, entorhinal cortex; SUB, subiculum; DG, dentate gyrus.

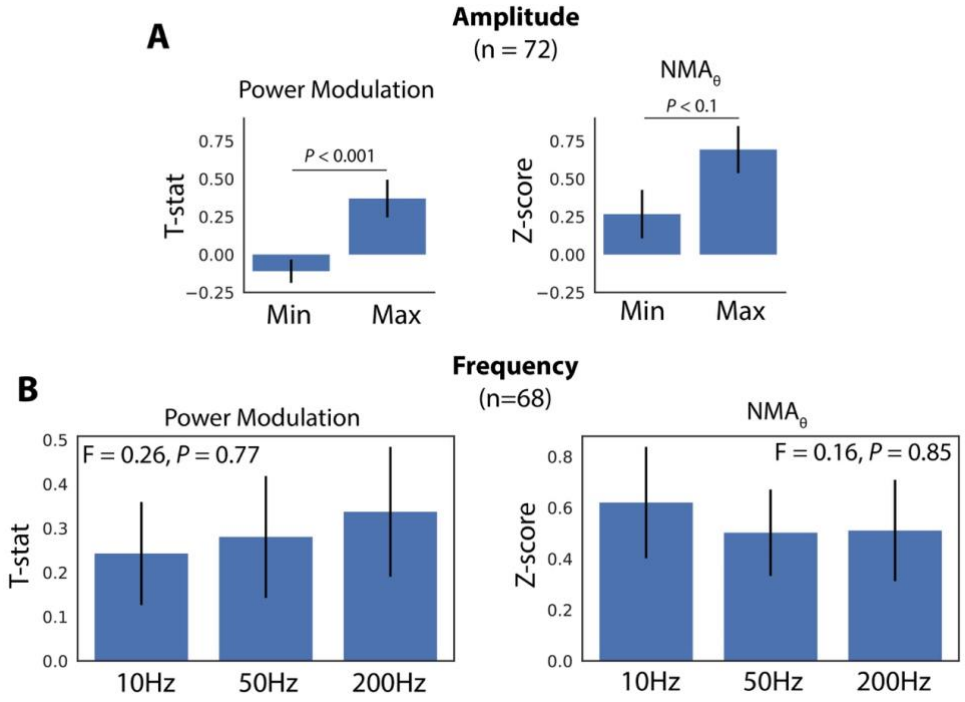

Figure 5.S2. Analysis of stimulation parameters on evoked power and theta network-mediated activation (NMA_θ). For each stimulation site, stimulation parameters were varied across amplitudes (three amplitudes, typically between 0.5-2 mA, 0.25 mA apart) and frequencies (10, 25, 50, 100, 200 Hz; see Methods for details). **(A)** The average theta (5-8 Hz) power evoked by stimulation (measured as the average pre-vs.-post T-statistic across the top 5 most strongly-connected electrodes to the stimulation target) is sensitive to stimulation amplitude, comparing the evoked power with the minimum delivered amplitude versus the maximum amplitude at each stimulation site (paired T-test, $P < 0.001$). The theta network-mediated activation (NMA_θ; see Figure 5.3 and Methods for details) is marginally sensitive to amplitude ($P < 0.1$). **(B)** Repeated measures ANOVA indicated no effect of sitmulation frequency (measured at 10 Hz, 50 Hz, 200 Hz) on evoked power or NMA_θ. Error bars show +/- 1 SEM.

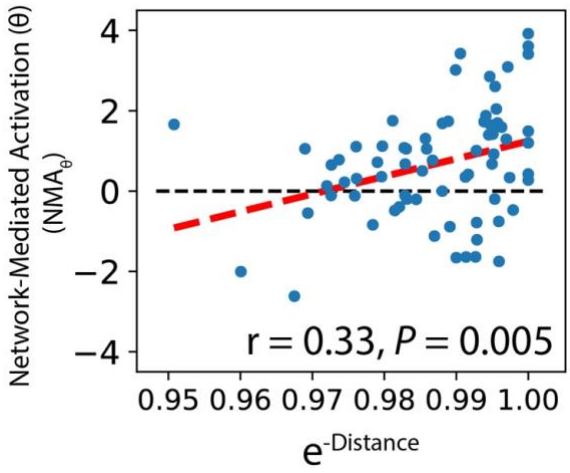

Figure 5.S3. Correlation of NMA_θ and distance to nearest white matter. There is a significant linear relationship (r = 0.33, *P* = 0.005) between an electrode's network-mediated activation in the theta band (NMA_θ) and distance to nearest white matter ($e^{-(dist)}$, where 1 indicates placement within white matter).

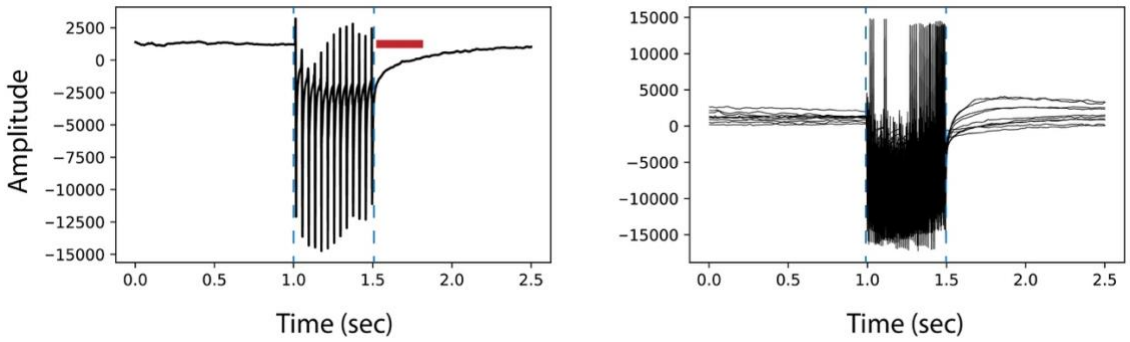

Figure 5.S4. Depiction of post-stimulation artifact. A subset of channels (average of 28% per subject) exhibited a non-physiologic post-stimulation artifact, characterized by a slowly decaying voltage offset immediately after the last stimulation pulse. A typical example of this artifact for one stimulation event, is shown on the left, and 10 representative examples are shown on the right, demonstrating their consistency across events. The red bar indicates the 350 ms post-stimulation period used to assess a channel for rejection (see Methods). Blue dashed lines indicate the 500 ms stimulation interval. For a representative artifact-free trace, see Figure 5.1E-F.

CHAPTER 6:
Conclusions

Developing an effective implantable memory therapeutic requires two key understandings: (1) what are the patterns of endogenous brain activity that define successful episodic memory, and (2) how does intracranial stimulation alter ongoing brain activity? Here we examined "brain activity" principally through the lens of iEEG-based network connectivity, to expand upon a more developed literature on purely local activity. To address these questions, this dissertation covered three core investigations. First, we assessed local activity and inter-regional connectivity at the whole-brain level during episodic memory performance, identifying widespread theta synchronization associated with increased local processing. Next, we assessed inter-regional coupling within the medial temporal lobe (MTL), a collection of structures specialized for episodic memory. We found that our findings at the whole-brain level recapitulated at the mesoscale level – MTL subregions tended to couple at theta frequencies during successful episodic encoding and retrieval, with a particular focus on the entorhinal cortex. Finally, we used intracranial stimulation to assess whether low-frequency connections suggest causal relations in the brain, confirming that stimulation-evoked activity propagates through low-frequency functional connections.

Taken together, these findings suggest a critical generality to low-frequency connectivity as a neural phenomenon. It is found at multiple spatial scales, across widespread regions, and likely reflects some level of causal interaction between brain regions. Additionally, the phenomenon is manifest during episodic memory encoding, retrieval, and during non-task

resting states. Until these studies were conducted, it was unclear as to whether or not low-frequency connectivity is specific to particular substructures (e.g. prefrontal cortex vs. hippocampus) in particular tasks. This new understanding directly informs the use of low-frequency connectivity as a biomarker for successful memory processing – if low-frequency connectivity is not observed, especially within the MTL, episodic encoding may not proceed properly. Furthermore, clinical interventions that can enhance low-frequency connections may prove to be effective memory therapeutics.

This work was exclusively conducted using intracranial EEG, which is both a strength and a weakness. By demonstrating that low-frequency connectivity is correlated with successful episodic memory, we provide a key link between findings from fMRI and the actual electrical activity in the brain; under both modalities, we observe coupling within the MTL, and between the MTL and cortical regions of the memory network (i.e. prefrontal cortex, lateral temporal cortex, and posterior parietal cortex)[7,10]. As the interpretation of fMRI BOLD correlations are a subject of perpetual debate, qualitative correlations with neurally-derived electrical networks supports the continued use of this powerful noninvasive modality. However, as with all iEEG studies, we note that all the data analyzed here was recorded from brains with severe epilepsy – limiting their generalizeability to neurotypical populations. Additionally, to the extent that this work informs eventual therapeutic devices, such devices must involve invasive neurosurgery; future investigations to ask whether noninvasive stimulation (see "Brain Stimulation," Chapter 1) can recapitulate these findings.

Though the findings in this dissertation unequivocally speak to the important of theta connectivity, it remains an open question as to how other frequencies may contribute to inter-regional communication. Notably, we observed strong inter-regional coupling in the alpha (9-13 Hz) band in the whole-brain analysis (Chapter 3), though this effect was less prominent within the medial temporal lobe (Chapter 4). Furthermore, though our data largely speak against a prominent role for high-frequency (e.g. gamma, 30+ Hz) inter-regional synchrony, there are a number of instances in the literature which do suggest transient gamma oscillations may be coordinated across space[55,59]. The studies done here were typically not powered to detect such effects; time-averaging across the encoding and

retrieval epochs, for example, could obscure such transient phenomena. Future studies could uncover to what extent different low-frequency bands support inter-regional communication (or different types of inter-regional communication), and whether high-frequency coupling has a mechanistically important role to play.

This thesis largely left unanswered how theta-band coupling supports memory encoding, even as it quantified the extent to which it exists. Current theories posit that coordinated oscillations support spike-timing dependent plasticity (STDP), effectively linking neurons that may represent different featural aspects of an item to be encoded in memory[55,171]. Relatedly, low-frequency synchronization may encourage more high-fidelity transmission of information from one region to another, by simultaneously optimizing the excitability of two regions[70]. Another possibility is that synchrony emerges as an epiphenomenon of another underlying process that causes similar patterns of activity across space, even as two regions are not explicitly linked.

Ultimately, determining the precise mechanistic role of theta in episodic memory processes will require a convergence across experimental modalities and integration over spatial scales: animal models, in which cellular-scale manipulations can uncover the way in which theta oscillations modulate synaptic plasticity; further human studies, in which more subtle behavioral contrasts can precisely localize theta oscillations to a particular cognitive function; and stimulation experiments in animals or humans to demonstrate the causal role of theta activity.

In these experiments, we convincingly demonstrated that intracranial stimulation could elicit theta activity across a distributed network of regions, in accordance with functional connections. However, this is not an explicit demonstration of induced theta connectivity itself. Though a single recent study started to ask whether targeted stimulation can induce theta coherence between brain regions[172], the space is largely unexplored. For example, a theoretical successful cognitive therapeutic must (1) induce characteristic signature of local activity (i.e. increases in HFA, and increases/decreases in theta for particular areas), and (2) induce inter-regional low-frequency connectivity between key memory structures. Though we now have some grasp on how local activity is modulated by stimulation, we do not know

what stimulation paradigms – if any – can evoke a desired pattern of inter-regional connectivity. Future studies should seek to rigorously explore how single-target stimulation alters ongoing patterns of functional connectivity, and whether multi-target simultaneous stimulation could be more efficacious.

Taken together, by applying principles of graph theory to a large intracranial dataset, the work in this dissertation extended the active frontiers of cognitive and network neuroscience. We uncovered, for the first time, a whole-brain network of *electrical* connections – previously unobservable with limited amounts of intracranial data. We also demonstrated that theta coupling generalizes to smaller scales, and provided a map of memory-related functional connections within the human medial temporal lobe. Finally, we demonstrated that intracranial stimulation can be used to probe the physiologic meaning of functional connectivity. Substantial work remains to build on these findings, but we hope this work lays a foundation that can be used by cognitive neuroscientists and clinicians alike.

Bibliography

1. Squire, L. R., Stark, C. E. L. & Clark, R. E. THE MEDIAL TEMPORAL LOBE. *Annu. Rev. Neurosci.* **27,** 279–306 (2004).
2. Alzheimer's Association. 2015 Alzheimer's disease facts and figures. *Alzheimers. Dement.* **11,** 332–84 (2015).
3. Burke, J. F., Merkow, M. B., Jacobs, J., Kahana, M. J. & Zaghloul, K. A. Brain computer interface to enhance episodic memory in human participants. *Front. Hum. Neurosci.* **8,** 1055 (2015).
4. Kim, K., Ekstrom, A. D. & Tandon, N. A network approach for modulating memory processes via direct and indirect brain stimulation: Toward a causal approach for the neural basis of memory. *Neurobiol. Learn. Mem.* **134,** 162–177 (2016).
5. Eichenbaum, H. A cortical-hippocampal system for declarative memory. *Nat. Rev. Neurosci.* **1,** 41–50 (2000).
6. Ranganath, C., Heller, A., Cohen, M. X., Brozinsky, C. J. & Rissman, J. Functional connectivity with the hippocampus during successful memory formation. *Hippocampus* **15,** 997–1005 (2005).
7. Schedlbauer, A. M. *et al.* Multiple interacting brain areas underlie successful spatiotemporal memory retrieval in humans. *Sci. Rep.* **4,** 6431 (2014).
8. van Kesteren, M. T. R., Fernández, G., Norris, D. G. & Hermans, E. J. Persistent schema-dependent hippocampal-neocortical connectivity during memory encoding and postencoding rest in humans. *Proc. Natl. Acad. Sci. U. S. A.* **107,** 7550–5 (2010).
9. Diana, R. A., Yonelinas, A. P. & Ranganath, C. Medial temporal lobe activity during source retrieval reflects information type, not memory strength. *J. Cogn. Neurosci.* **22,** 1808–18 (2010).
10. Vincent, J. L. *et al.* Coherent spontaneous activity identifies a hippocampal-parietal memory network. *J. Neurophysiol.* **96,** 3517–31 (2006).
11. Buzsáki, G., Anastassiou, C. A. & Koch, C. The origin of extracellular fields and currents — EEG, ECoG, LFP and spikes. *Nat. Rev. Neurosci.* **13,** 407–420 (2012).
12. Ebbinghaus, H. Memory: a contribution to experimental psychology. *Ann. Neurosci.* **20,** 155–6 (2013).
13. Howard, M. W. & Kahana, M. J. A Distributed Representation of Temporal Context. *J. Math. Psychol.* **46,** 269–299 (2002).
14. Kahana, M. *Foundations of human memory*. (2012).
15. Bellmund, J. L. S., Gärdenfors, P., Moser, E. I. & Doeller, C. F. Navigating cognition: Spatial codes for human thinking. *Science* **362,** eaat6766 (2018).
16. van den Heuvel, M. P. & Hulshoff Pol, H. E. Exploring the brain network: A review on resting-state fMRI functional connectivity. *Eur. Neuropsychopharmacol.* **20,** 519–534 (2010).
17. Ekstrom, A. D., Copara, M. S., Isham, E. A., Wang, W. & Yonelinas, A. P. Dissociable networks involved in spatial and temporal order source retrieval. *Neuroimage* **56,** 1803–13 (2011).
18. Strange, B. A., Otten, L. J., Josephs, O., Rugg, M. D. & Dolan, R. J. Dissociable Human

Perirhinal, Hippocampal, and Parahippocampal Roles during Verbal Encoding.
19. Pesaran, B. *et al.* Investigating large-scale brain dynamics using field potential recordings: analysis and interpretation. *Nat. Neurosci.* **21,** 903–919 (2018).
20. Başar, E., Başar-Eroglu, C., Karakaş, S. & Schürmann, M. Gamma, alpha, delta, and theta oscillations govern cognitive processes. *Int. J. Psychophysiol.* **39,** 241–248 (2001).
21. Buzsáki, G. & Draguhn, A. Neuronal Oscillations in Cortical Networks. *Science (80-.).* **304,** (2004).
22. Nyhus, E. & Curran, T. Functional role of gamma and theta oscillations in episodic memory. *Neurosci. Biobehav. Rev.* **34,** 1023–1035 (2010).
23. Klimesch, W. *et al.* Theta synchronization during episodic retrieval: neural correlates of conscious awareness. *Cogn. Brain Res.* **12,** 33–38 (2001).
24. Lisman, J. E. & Jensen, O. The Theta-Gamma Neural Code. *Neuron* **77,** 1002–1016 (2013).
25. Fries, P. Neuronal Gamma-Band Synchronization as a Fundamental Process in Cortical Computation. *Annu. Rev. Neurosci.* **32,** 209–224 (2009).
26. Colgin, L. L. & Moser, E. I. Gamma Oscillations in the Hippocampus. *Physiology* **25,** (2010).
27. Manning, J. R., Jacobs, J., Fried, I. & Kahana, M. J. Broadband shifts in local field potential power spectra are correlated with single-neuron spiking in humans. *J. Neurosci.* **29,** 13613–20 (2009).
28. Winawer, J. *et al.* Asynchronous broadband signals are the principal source of the BOLD response in human visual cortex. *Curr. Biol.* **23,** 1145–53 (2013).
29. Burke, J. F. *et al.* Human intracranial high-frequency activity during memory processing: neural oscillations or stochastic volatility? This review comes from a themed issue on Brain rhythms and dynamic coordination. *Curr. Opin. Neurobiol.* **31,** 104–110 (2015).
30. Chiang, S., Stern, J. M., Engel, J., Levin, H. S. & Haneef, Z. Differences in graph theory functional connectivity in left and right temporal lobe epilepsy. *Epilepsy Res.* **108,** 1770–1781 (2014).
31. Blume, W. T., Jones, D. C. & Pathak, P. Properties of after-discharges from cortical electrical stimulation in focal epilepsies. *Clin. Neurophysiol.* **115,** 982–989 (2004).
32. Gelinas, J. N., Khodagholy, D., Thesen, T., Devinsky, O. & Buzsáki, G. Interictal epileptiform discharges induce hippocampal–cortical coupling in temporal lobe epilepsy. *Nat. Med.* (2016). doi:10.1038/nm.4084
33. Khambhati, A. N. *et al.* Virtual Cortical Resection Reveals Push-Pull Network Control Preceding Seizure Evolution. *Neuron* **91,** 1170–1182 (2016).
34. Cajal, S. R. Y. The Croonian Lecture: La Fine Structure des Centres Nerveux. *Proc. R. Soc. London* **55,** 444–468 (1894).
35. Spaniol, J. *et al.* Event-related fMRI studies of episodic encoding and retrieval: meta-analyses using activation likelihood estimation. *Neuropsychologia* **47,** 1765–79 (2009).
36. Stevenson, I. H., Rebesco, J. M., Miller, L. E. & Körding, K. P. Inferring functional connections between neurons. *Curr. Opin. Neurobiol.* **18,** 582–588 (2008).
37. Bullmore, E. & Sporns, O. Complex brain networks: graph theoretical analysis of

structural and functional systems. *Nat. Rev. Neurosci.* **10,** 186–98 (2009).
38. Bassett, D. S. & Sporns, O. Network neuroscience. *Nat. Neurosci.* **20,** 353–364 (2017).
39. Rubinov, M. & Sporns, O. Complex network measures of brain connectivity: Uses and interpretations. *Neuroimage* **52,** 1059–1069 (2010).
40. Borchers, S., Himmelbach, M., Logothetis, N. & Karnath, H.-O. Direct electrical stimulation of human cortex — the gold standard for mapping brain functions? *Nat. Rev. Neurosci.* **13,** 63 (2011).
41. PENFIELD, W. & BOLDREY, E. SOMATIC MOTOR AND SENSORY REPRESENTATION IN THE CEREBRAL CORTEX OF MAN AS STUDIED BY ELECTRICAL STIMULATION. *Brain* **60,** 389–443 (1937).
42. Abrams, R. *Electroconvulsive therapy*. (2002).
43. Deuschl, G. *et al.* A Randomized Trial of Deep-Brain Stimulation for Parkinson's Disease. *N. Engl. J. Med.* **355,** 896–908 (2006).
44. Logothetis, N. K. *et al.* The effects of electrical microstimulation on cortical signal propagation. *Nat. Publ. Gr.* **13,** (2010).
45. Keller, C. J. *et al.* Intrinsic functional architecture predicts electrically evoked responses in the human brain. *Proc. Natl. Acad. Sci. U. S. A.* **108,** 10308–13 (2011).
46. Matsumoto, R. *et al.* Functional connectivity in human cortical motor system: a cortico-cortical evoked potential study. *Brain* **130,** 181–197 (2006).
47. Ezzyat, Y. *et al.* Closed-loop stimulation of temporal cortex rescues functional networks and improves memory. *Nat. Commun.* **9,** 365 (2018).
48. Rao, V. R. *et al.* Direct Electrical Stimulation of Lateral Orbitofrontal Cortex Acutely Improves Mood in Individuals with Symptoms of Depression. *Curr. Biol.* **28,** 3893–3902.e4 (2018).
49. Titiz, A. S. *et al.* Theta-burst microstimulation in the human entorhinal area improves memory specificity. *Elife* **6,** e29515 (2017).
50. Suthana, N. *et al.* Memory Enhancement and Deep-Brain Stimulation of the Entorhinal Area. *N. Engl. J. Med.* **366,** 502–510 (2012).
51. Ezzyat, Y. *et al.* Direct Brain Stimulation Modulates Encoding States and Memory Performance in Humans. *Curr. Biol.* **27,** 1251–1258 (2017).
52. Kim, K. *et al.* Network-based brain stimulation selectively impairs spatial retrieval. *Brain Stimul.* **11,** 213–221 (2018).
53. Jacobs, J. *et al.* Direct Electrical Stimulation of the Human Entorhinal Region and Hippocampus Impairs Memory. *Neuron* **92,** 983–990 (2016).
54. Harris, A. Z. & Gordon, J. A. Long-Range Neural Synchrony in Behavior. *Annu. Rev. Neurosci.* **38,** 171–194 (2015).
55. Axmacher, N., Mormann, F., Fernández, G., Elger, C. E. & Fell, J. Memory formation by neuronal synchronization. *Brain Res. Rev.* **52,** 170–182 (2006).
56. Singer, W. Neuronal Synchrony: A Versatile Code for the Definition of Relations? *Neuron* **24,** 49–65 (1999).
57. Yamamoto, J., Suh, J., Takeuchi, D. & Tonegawa, S. Successful Execution of Working Memory Linked to Synchronized High-Frequency Gamma Oscillations. *Cell* **157,** 845–857 (2014).
58. Gregoriou, G. G., Gotts, S. J., Zhou, H. & Desimone, R. High-frequency, long-range coupling between prefrontal and visual cortex during attention. *Science* **324,** 1207–

10 (2009).
59. Fell, J. *et al.* Human memory formation is accompanied by rhinal-hippocampal coupling and decoupling. *Nat. Neurosci.* **4,** 1259–64 (2001).
60. Rodriguez, E. *et al.* Perception's shadow: long-distance synchronization of human brain activity. *Nature* **397,** 430–3 (1999).
61. Miltner, W. H. R., Braun, C., a, M. A., Witte, H. & Taub, E. Coherence of gamma-band EEG activity as a basis for associative learning. *Nature* **397,** 434–436 (1999).
62. Shadlen, M. N. & Movshon, J. A. Synchrony Unbound: A Critical Evaluation of the Temporal Binding Hypothesis. *Neuron* **24,** 67–77 (1999).
63. Ray, S. & Maunsell, J. H. R. Differences in Gamma Frequencies across Visual Cortex Restrict Their Possible Use in Computation. *Neuron* **67,** 885–896 (2010).
64. Histed, M. H. & Maunsell, J. H. R. Cortical neural populations can guide behavior by integrating inputs linearly, independent of synchrony. *Proc. Natl. Acad. Sci. U. S. A.* **111,** E178-87 (2014).
65. Ray, S. & Maunsell, J. H. R. Do gamma oscillations play a role in cerebral cortex? *Trends Cogn. Sci.* **19,** 78–85 (2015).
66. Fell, J., Ludowig, E., Rosburg, T., Axmacher, N. & Elger, C. E. Phase-locking within human mediotemporal lobe predicts memory formation. *Neuroimage* **43,** 410–419 (2008).
67. Miller, K. J. *et al.* Broadband changes in the cortical surface potential track activation of functionally diverse neuronal populations. *Neuroimage* **85,** 711–720 (2014).
68. Kucewicz, M. T. *et al.* Dissecting gamma frequency activity during human memory processing. *Brain* **140,** 1337–1350 (2017).
69. Scheffer-Teixeira, R., Belchior, H., Leao, R. N., Ribeiro, S. & Tort, A. B. L. On High-Frequency Field Oscillations (>100 Hz) and the Spectral Leakage of Spiking Activity. *J. Neurosci.* **33,** 1535–1539 (2013).
70. Fell, J. & Axmacher, N. The role of phase synchronization in memory processes. *Nat. Rev. Neurosci.* **12,** 105–118 (2011).
71. Sarnthein, J., Petsche, H., Rappelsberger, P., Shaw, G. L. & von Stein, A. Synchronization between prefrontal and posterior association cortex during human working memory. *Proc. Natl. Acad. Sci. U. S. A.* **95,** 7092–6 (1998).
72. Molinaro, N., Barraza, P. & Carreiras, M. Long-range neural synchronization supports fast and efficient reading: EEG correlates of processing expected words in sentences. *Neuroimage* **72,** 120–132 (2013).
73. Watrous, A. J., Tandon, N., Conner, C. R., Pieters, T. & Ekstrom, A. D. Frequency-specific network connectivity increases underlie accurate spatiotemporal memory retrieval. *Nat. Neurosci.* **16,** 349–56 (2013).
74. Canolty, R. T. *et al.* High Gamma Power Is Phase-Locked to Theta Oscillations in Human Neocortex. *Science (80-.).* **313,** 1626–1628 (2006).
75. Lega, B., Burke, J., Jacobs, J. & Kahana, M. J. Slow-Theta-to-Gamma Phase-Amplitude Coupling in Human Hippocampus Supports the Formation of New Episodic Memories. *Cereb. Cortex* **26,** 268–78 (2016).
76. Lachaux, J. P., Rodriguez, E., Martinerie, J. & Varela, F. J. Measuring phase synchrony in brain signals. *Hum. Brain Mapp.* **8,** 194–208 (1999).
77. Lancaster, J. L. *et al.* Automated Talairach atlas labels for functional brain mapping.

Hum. Brain Mapp. **10,** 120–31 (2000).
78. Burke, J. F. *et al.* Human intracranial high-frequency activity maps episodic memory formation in space and time. *Neuroimage* **85,** 834–843 (2014).
79. Varela, F., Lachaux, J.-P., Rodriguez, E. & Martinerie, J. The brainweb: Phase synchronization and large-scale integration. *Nat. Rev. Neurosci.* **2,** 229–239 (2001).
80. Paller, K. A. & Wagner, A. D. Observing the transformation of experience into memory. *Trends Cogn. Sci.* **6,** 93–102 (2002).
81. Hughes, A. M., Whitten, T. A., Caplan, J. B. & Dickson, C. T. BOSC: A better oscillation detection method, extracts both sustained and transient rhythms from rat hippocampal recordings. *Hippocampus* **22,** 1417–1428 (2012).
82. Eichenbaum, H., Yonelinas, A. P. & Ranganath, C. The medial temporal lobe and recognition memory. *Annu. Rev. Neurosci.* **30,** 123–52 (2007).
83. Roberts, M. J. *et al.* Robust Gamma Coherence between Macaque V1 and V2 by Dynamic Frequency Matching. *Neuron* **78,** 523–536 (2013).
84. Burke, J. F. *et al.* Synchronous and asynchronous theta and gamma activity during episodic memory formation. *J. Neurosci.* **33,** 292–304 (2013).
85. Ward, A. M. *et al.* The parahippocampal gyrus links the default-mode cortical network with the medial temporal lobe memory system. *Hum. Brain Mapp.* **35,** 1061–1073 (2014).
86. King, D. R., de Chastelaine, M., Elward, R. L., Wang, T. H. & Rugg, M. D. Recollection-Related Increases in Functional Connectivity Predict Individual Differences in Memory Accuracy. *J. Neurosci.* **35,** (2015).
87. Igarashi, K. M., Lu, L., Colgin, L. L., Moser, M.-B. & Moser, E. I. Coordination of entorhinal–hippocampal ensemble activity during associative learning. *Nature* **510,** 143–147 (2014).
88. Hirabayashi, T. *et al.* Distinct Neuronal Interactions in Anterior Inferotemporal Areas of Macaque Monkeys during Retrieval of Object Association Memory. *J. Neurosci.* **34,** (2014).
89. Bosman, C. A. *et al.* Attentional Stimulus Selection through Selective Synchronization between Monkey Visual Areas. *Neuron* **75,** 875–888 (2012).
90. Buckner, R. L. *et al.* Cortical hubs revealed by intrinsic functional connectivity: mapping, assessment of stability, and relation to Alzheimer's disease. *J. Neurosci.* **29,** 1860–73 (2009).
91. Satterthwaite, T. D. *et al.* Connectome-wide network analysis of youth with Psychosis-Spectrum symptoms. *Mol. Psychiatry* **20,** 1508–1515 (2015).
92. Gu, S. *et al.* Controllability of structural brain networks. *Nat. Commun.* **6,** 8414 (2015).
93. Avants, B. B., Epstein, C. L., Grossman, M. & Gee, J. C. Symmetric diffeomorphic image registration with cross-correlation: Evaluating automated labeling of elderly and neurodegenerative brain. *Med. Image Anal.* **12,** 26–41 (2008).
94. Yushkevich, P. A. *et al.* Automated volumetry and regional thickness analysis of hippocampal subfields and medial temporal cortical structures in mild cognitive impairment. *Hum. Brain Mapp.* **36,** 258–87 (2015).
95. Fischl, B. *et al.* Automatically parcellating the human cerebral cortex. *Cereb. Cortex* **14,** 11–22 (2004).

96. Berens, P. CircStat : A *MATLAB* Toolbox for Circular Statistics. *J. Stat. Softw.* **31,** 1–21 (2009).
97. Sederberg, P. B. *et al.* Hippocampal and Neocortical Gamma Oscillations Predict Memory Formation in Humans. *Cereb. Cortex* **17,** 1190–1196 (2006).
98. van Vugt, M. K., Sederberg, P. B. & Kahana, M. J. Comparison of spectral analysis methods for characterizing brain oscillations. *J. Neurosci. Methods* **162,** 49–63 (2007).
99. Whitten, T. A., Hughes, A. M., Dickson, C. T. & Caplan, J. B. A better oscillation detection method robustly extracts EEG rhythms across brain state changes: The human alpha rhythm as a test case. *Neuroimage* **54,** 860–874 (2011).
100. Solomon, E. A. *et al.* Widespread theta synchrony and high-frequency desynchronization underlies enhanced cognition. *Nat. Commun.* **8,** 1704 (2017).
101. Vincent, J. L. *et al.* Coherent Spontaneous Activity Identifies a Hippocampal-Parietal Memory Network. *J. Neurophysiol.* **96,** 3517–3531 (2006).
102. Eichenbaum, H., Otto, T. & Cohen, N. J. The hippocampus--what does it do? *Behav. Neural Biol.* **57,** 2–36 (1992).
103. Wagner, A. D. *et al.* Building memories: remembering and forgetting of verbal experiences as predicted by brain activity. *Science* **281,** 1188–91 (1998).
104. Buzsáki, G. Theta Oscillations in the Hippocampus. *Neuron* **33,** 325–340 (2002).
105. Moser, E. I., Kropff, E. & Moser, M.-B. Place Cells, Grid Cells, and the Brain's Spatial Representation System. *Annu. Rev. Neurosci.* **31,** 69–89 (2008).
106. MacDonald, C. J., Lepage, K. Q., Eden, U. T. & Eichenbaum, H. Hippocampal 'time cells' bridge the gap in memory for discontiguous events. *Neuron* **71,** 737–749 (2011).
107. Montgomery, S. M. & Buzsáki, G. Gamma oscillations dynamically couple hippocampal CA3 and CA1 regions during memory task performance. *Proc. Natl. Acad. Sci. U. S. A.* **104,** 14495–500 (2007).
108. Schomburg, E. W. *et al.* Theta Phase Segregation of Input-Specific Gamma Patterns in Entorhinal-Hippocampal Networks. *Neuron* **84,** 470–485 (2014).
109. Seidenbecher, T., Laxmi, T. R., Stork, O. & Pape, H.-C. Amygdalar and hippocampal theta rhythm synchronization during fear memory retrieval. *Science* **301,** 846–50 (2003).
110. Colgin, L. L. Rhythms of the hippocampal network. *Nature Reviews Neuroscience* **17,** (2016).
111. Hasselmo, M. E. & Eichenbaum, H. Hippocampal mechanisms for the context-dependent retrieval of episodes. *Neural Netw.* **18,** 1172–90 (2005).
112. Diana, R. A., Yonelinas, A. P. & Ranganath, C. Imaging recollection and familiarity in the medial temporal lobe: a three-component model. *Trends Cogn. Sci.* **11,** 379–386 (2007).
113. Burgess, N., Maguire, E. A. & O'Keefe, J. The Human Hippocampus and Spatial and Episodic Memory. *Neuron* **35,** 625–641 (2002).
114. Fell, J. *et al.* Rhinal-hippocampal theta coherence during declarative memory formation: interaction with gamma synchronization? *Eur. J. Neurosci.* **17,** 1082–1088 (2003).
115. Lega, B. C., Jacobs, J. & Kahana, M. Human hippocampal theta oscillations and the formation of episodic memories. *Hippocampus* **22,** 748–761 (2012).

116. Kahana, M. J., Seelig, D. & Madsen, J. R. Theta returns. *Curr. Opin. Neurobiol.* **11,** 739–744 (2001).
117. Hasselmo, M. E. What is the function of hippocampal theta rhythm?--Linking behavioral data to phasic properties of field potential and unit recording data. *Hippocampus* **15,** 936–49 (2005).
118. Lin, J.-J. *et al.* Theta band power increases in the posterior hippocampus predict successful episodic memory encoding in humans. *Hippocampus* **27,** 1040–1053 (2017).
119. Greenberg, J. A., Burke, J. F., Haque, R., Kahana, M. J. & Zaghloul, K. A. Decreases in theta and increases in high frequency activity underlie associative memory encoding. *Neuroimage* **114,** 257–63 (2015).
120. Burke, J. F. *et al.* Theta and high-frequency activity mark spontaneous recall of episodic memories. *J. Neurosci.* **34,** 11355–65 (2014).
121. Buzsáki, G. & Moser, E. I. Memory, navigation and theta rhythm in the hippocampal-entorhinal system. *Nat. Neurosci.* **16,** 130–138 (2013).
122. Buzsáki, G. & Schomburg, E. W. What does gamma coherence tell us about inter-regional neural communication? *Nat. Neurosci.* **18,** 484–489 (2015).
123. Rutishauser, U., Ross, I. B., Mamelak, A. N. & Schuman, E. M. Human memory strength is predicted by theta-frequency phase-locking of single neurons. *Nature* **464,** 903–907 (2010).
124. Colgin, L. L. Mechanisms and Functions of Theta Rhythms. *Annu. Rev. Neurosci.* **36,** 295–312 (2013).
125. Clouter, A., Shapiro, K. L. & Hanslmayr, S. Theta Phase Synchronization Is the Glue that Binds Human Associative Memory. *Curr. Biol.* **27,** 3143–3148.e6 (2017).
126. Backus, A. R., Schoffelen, J. M., Szebényi, S., Hanslmayr, S. & Doeller, C. F. Hippocampal-prefrontal theta oscillations support memory integration. *Curr. Biol.* **26,** (2016).
127. Vinck, M., Oostenveld, R., van Wingerden, M., Battaglia, F. & Pennartz, C. M. A. An improved index of phase-synchronization for electrophysiological data in the presence of volume-conduction, noise and sample-size bias. *Neuroimage* **55,** 1548–1565 (2011).
128. Kragel, J. E. *et al.* Similar patterns of neural activity predict memory function during encoding and retrieval. *Neuroimage* **155,** 60–71 (2017).
129. Long, N. M. *et al.* Contextually Mediated Spontaneous Retrieval Is Specific to the Hippocampus. *Curr. Biol.* **27,** 1074–1079 (2017).
130. Davachi, L. Item, context and relational episodic encoding in humans. *Curr. Opin. Neurobiol.* **16,** 693–700 (2006).
131. Kloosterman, F., Witter, M. P. & Van Haeften, T. Topographical and laminar organization of subicular projections to the parahippocampal region of the rat. *J. Comp. Neurol.* **455,** 156–171 (2003).
132. Liang, J. C. & Preston, A. R. Medial Temporal Lobe Subregional Function in Human Episodic Memory. in *The Wiley Handbook on the Cognitive Neuroscience of Memory* 108–130 (John Wiley & Sons, Ltd, 2015). doi:10.1002/9781118332634.ch6
133. Holsheimer, J. & Feenstra, B. W. Volume conduction and EEG measurements within the brain: a quantitative approach to the influence of electrical spread on the linear

relationship of activity measured at different locations. *Electroencephalogr. Clin. Neurophysiol.* **43,** 52–8 (1977).
134. Merkow, M. B., Burke, J. F. & Kahana, M. J. The human hippocampus contributes to both the recollection and familiarity components of recognition memory. *Proc. Natl. Acad. Sci. U. S. A.* **112,** 14378–83 (2015).
135. Fell, J. *et al.* Human memory formation is accompanied by rhinal–hippocampal coupling and decoupling. (2001). doi:10.1038/nn759
136. Howard, M. W., Fotedar, M. S., Datey, A. V. & Hasselmo, M. E. The Temporal Context Model in Spatial Navigation and Relational Learning: Toward a Common Explanation of Medial Temporal Lobe Function Across Domains. *Psychol. Rev.* **112,** 75–116 (2005).
137. Hasselmo, M. E., Bodelón, C. & Wyble, B. P. A Proposed Function for Hippocampal Theta Rhythm: Separate Phases of Encoding and Retrieval Enhance Reversal of Prior Learning. *Neural Comput.* **14,** 793–817 (2002).
138. Cohen, M. X. Effects of time lag and frequency matching on phase-based connectivity. *J. Neurosci. Methods* **250,** 137–146 (2015).
139. Moore, M. *et al.* A comprehensive protocol for manual segmentation of the medial temporal lobe structures. *J. Vis. Exp.* (2014). doi:10.3791/50991
140. Gramfort, A. *et al.* MNE software for processing MEG and EEG data. *Neuroimage* **86,** 446–460 (2014).
141. Inman, C. S. *et al.* Direct electrical stimulation of the amygdala enhances declarative memory in humans. *Proc. Natl. Acad. Sci.* 201714058 (2017). doi:10.1073/PNAS.1714058114
142. Hampson, R. E. *et al.* Developing a hippocampal neural prosthetic to facilitate human memory encoding and recall. *J. Neural Eng.* **15,** 036014 (2018).
143. Sreekumar, V., Wittig, J. H., Sheehan, T. C. & Zaghloul, K. A. Principled Approaches to Direct Brain Stimulation for Cognitive Enhancement. *Front. Neurosci.* **11,** 650 (2017).
144. Riva-Posse, P. *et al.* A connectomic approach for subcallosal cingulate deep brain stimulation surgery: prospective targeting in treatment-resistant depression. *Mol. Psychiatry* **23,** 843–849 (2018).
145. Tehovnik, E. J. Electrical stimulation of neural tissue to evoke behavioral responses. *J. Neurosci. Methods* **65,** 1–17 (1996).
146. Yeomans, J. Electrically evoked behaviors: axons and synapses mapped with collision tests. *Behav. Brain Res.* **67,** 121–132 (1995).
147. Tolias, A. S. *et al.* Mapping Cortical Activity Elicited with Electrical Microstimulation Using fMRI in the Macaque. *Neuron* **48,** 901–911 (2005).
148. Matsumoto, R. *et al.* Functional connectivity in the human language system: a cortico-cortical evoked potential study. *Brain* **127,** 2316–2330 (2004).
149. Oya, H. *et al.* Mapping effective connectivity in the human brain with concurrent intracranial electrical stimulation and BOLD-fMRI. *J. Neurosci. Methods* **277,** 101–112 (2017).
150. Muldoon, S. F. *et al.* Stimulation-Based Control of Dynamic Brain Networks. *PLOS Comput. Biol.* **12,** e1005076 (2016).
151. Fox, K. C. R., Foster, B. L., Kucyi, A., Daitch, A. L. & Parvizi, J. Intracranial Electrophysiology of the Human Default Network. *Trends Cogn. Sci.* **22,** 307–324

(2018).
152. Greicius, M. D., Krasnow, B., Reiss, A. L. & Menon, V. Functional connectivity in the resting brain: a network analysis of the default mode hypothesis. *Proc. Natl. Acad. Sci. U. S. A.* **100,** 253–8 (2003).
153. Foster, B. L., Rangarajan, V., Shirer, W. R. & Parvizi, J. Intrinsic and task-dependent coupling of neuronal population activity in human parietal cortex. *Neuron* **86,** 578–90 (2015).
154. Betzel, R. F. *et al.* Inter-regional ECoG correlations predicted by communication dynamics, geometry, and correlated gene expression. *arXiv* (2017). doi:1706.06088
155. Solomon, E. A. *et al.* Functional wiring of the human medial temporal lobe. *bioRxiv* 257899 (2018). doi:10.1101/257899
156. Honey, C. J. *et al.* Predicting human resting-state functional connectivity from structural connectivity. *Proc. Natl. Acad. Sci. U. S. A.* **106,** 2035–40 (2009).
157. Kubota, Y. *et al.* In vivo human hippocampal cingulate connectivity: A corticocortical evoked potentials (CCEPs) study. *Clin. Neurophysiol.* **124,** 1547–1556 (2013).
158. Medaglia, J. D., Pasqualetti, F., Hamilton, R. H., Thompson-Schill, S. L. & Bassett, D. S. *Brain and Cognitive Reserve: Translation via Network Control Theory*. *Neuroscience & Biobehavioral Reviews* **75,** 53–64 (2016).
159. Kucyi, A. *et al.* Intracranial Electrophysiology Reveals Reproducible Intrinsic Functional Connectivity within Human Brain Networks. *J. Neurosci.* **38,** 4230–4242 (2018).
160. Keller, C. J. *et al.* Neurophysiological investigation of spontaneous correlated and anticorrelated fluctuations of the BOLD signal. *J. Neurosci.* **33,** 6333–42 (2013).
161. Keller, C. J. *et al.* Induction and quantification of excitability changes in human cortical networks. *J. Neurosci.* 1088–17 (2018). doi:10.1523/JNEUROSCI.1088-17.2018
162. Düzel, E., Penny, W. D. & Burgess, N. Brain oscillations and memory. *Curr. Opin. Neurobiol.* **20,** 143–149 (2010).
163. Van Dijk, K. R. A. *et al.* Intrinsic Functional Connectivity As a Tool For Human Connectomics: Theory, Properties, and Optimization. *J. Neurophysiol.* **103,** 297–321 (2010).
164. Ranck, J. B. Which elements are excited in electrical stimulation of mammalian central nervous system: a review. *Brain Res.* **98,** 417–40 (1975).
165. Scheeringa, R. *et al.* Neuronal Dynamics Underlying High- and Low-Frequency EEG Oscillations Contribute Independently to the Human BOLD Signal. *Neuron* **69,** 572–583 (2011).
166. Shannon, R. V. A model of safe levels for electrical stimulation. *IEEE Trans. Biomed. Eng.* **39,** 424–426 (1992).
167. Fischl, B. FreeSurfer. *Neuroimage* **62,** 774–781 (2012).
168. Van Essen, D. C. *et al.* The WU-Minn Human Connectome Project: An overview. *Neuroimage* **80,** 62–79 (2013).
169. Smith, S. M. *et al.* Resting-state fMRI in the Human Connectome Project. *Neuroimage* **80,** 144–168 (2013).
170. Avants, B. B. *et al.* A reproducible evaluation of ANTs similarity metric performance in brain image registration. *Neuroimage* **54,** 2033–2044 (2011).

171. Fries, P. A mechanism for cognitive dynamics: neuronal communication through neuronal coherence. *Trends Cogn. Sci.* **9,** 474–480 (2005).
172. Khambhati, A. N. *et al.* Predictive control of electrophysiological network architecture using direct, single-node neurostimulation in humans. *bioRxiv* 292748 (2018). doi:10.1101/292748